AN EXPERIMENTAL AND THEORETICAL INVESTIGATION OF THERMODYNAMIC EFFECTS ON DEVELOPED CAVITATION

Donald S. Weir

Pennsylvania State University

Prepared for:

Naval Sea Systems Command
National Aeronautics and Space Administration

21 February 1975

UNCLASSIFIED

SECURITY CLASSIFICATION OF THIS PAGE (When Data Entered)

REPORT DOCUMENTATION PAGE

READ INSTRUCTIONS BEFORE COMPLETING FORM

1. REPORT NUMBER: TM 75-34	2. GOVT ACCESSION NO.
3. RECIPIENT'S CATALOG NUMBER	
4. TITLE (and Subtitle): AN EXPERIMENTAL AND THEORETICAL INVESTIGATION OF THERMODYNAMIC EFFECTS ON DEVELOPED CAVITATION	5. TYPE OF REPORT & PERIOD COVERED: M.S. Thesis
	6. PERFORMING ORG. REPORT NUMBER: TM 75-34
7. AUTHOR(s): Donald S. Weir	8. CONTRACT OR GRANT NUMBER(s): N00017-73-C-1418
9. PERFORMING ORGANIZATION NAME AND ADDRESS: The Pennsylvania State University, Applied Research Laboratory, P. O. Box 30, State College, PA 16801	10. PROGRAM ELEMENT, PROJECT, TASK AREA & WORK UNIT NUMBERS
11. CONTROLLING OFFICE NAME AND ADDRESS: Naval Sea Systems Command, Department of the Navy, Washington, D. C. 20362	12. REPORT DATE: February 21, 1975
	13. NUMBER OF PAGES: 136
14. MONITORING AGENCY NAME & ADDRESS (if different from Controlling Office)	15. SECURITY CLASS. (of this report): Unclassified, Unlimited
	15a. DECLASSIFICATION/DOWNGRADING SCHEDULE

16. DISTRIBUTION STATEMENT (of this Report)

Approved for public release, distribution unlimited, per NSSC (Naval Sea Systems Command) 3/3/75

17. DISTRIBUTION STATEMENT (of the abstract entered in Block 20, if different from Report)

DISTRIBUTION OF THIS DOCUMENT IS UNLIMITED

18. SUPPLEMENTARY NOTES

PRICES SUBJECT TO CHANGE

19. KEY WORDS (Continue on reverse side if necessary and identify by block number)

CAVITATION
CAVITY LENGTH
HEAT TRANSFER
JAKOB NO.
LAMINAR BOUNDARY LAYER
SEMI-EMPIRICAL ENTRAINMENT THEORY
TEMPERATURE DEPRESSION
THERMODYNAMIC EFFECTS
TUNNEL BLOCKAGE
TURBULENT BOUNDARY LAYER
VELOCITY

20. ABSTRACT (Continue on reverse side if necessary and identify by block number)

The results of an experimental and theoretical investigation of thermodynamic effects on developed cavitation are presented. Distributions of temperature and pressure were measured for zero- and quarter-caliber ogives over a wide range of velocities, temperatures and cavity lengths.

The semi-empirical entrainment theory is used to correlate the measured temperature depressions in the cavity. This theory relates the maximum temperature depression expressed in dimensionless form as the Jakob number

DD FORM 1 JAN 73 1473 EDITION OF 1 NOV 65 IS OBSOLETE

UNCLASSIFIED

SECURITY CLASSIFICATION OF THIS PAGE (When Data Entered)

20. ABSTRACT (Continued)

in terms of the dimensionless numbers of Nusselt, Reynolds, Froude, and Peclet, and dimensionless cavity length. The results show that, in general, the temperature depression increases with cavity lengths and temperature.

The cavitation number based on cavity pressure was found to be independent of velocity and temperature, and is expressed as a function of the cavity length-to-model diameter ratio for a given model contour. Tunnel blockage was shown to have a significant effect on the cavitation number.

Two theories of the cavity heat transfer characteristics are presented. The first, based on a two-phase laminar boundary layer analysis, produces an expression for the cavity temperature depression which agrees with the entrainment theory results. The second, based on a turbulent boundary layer analysis proposed by Brennen, yields an expression for the cavity Nusselt number which agrees in part with the empirical correlation.

FG

AN EXPERIMENTAL AND THEORETICAL INVESTIGATION OF THERMODYNAMIC EFFECTS ON DEVELOPED CAVITATION

Donald S. Weir

Technical Memorandum
File No. TM 75-34
February 21, 1975
Contract No. N00017-73-C-1418

Copy No. 5

The Pennsylvania State University
Institute for Science and Engineering
APPLIED RESEARCH LABORATORY
Post Office Box 30
State College, PA 16801

NAVY DEPARTMENT

NAVAL SEA SYSTEMS COMMAND

ACKNOWLEDGMENTS

The author expresses appreciation for the guidance and counseling of his advisor, Dr. J. William Holl, while conducting this investigation.

The investigation was conducted at the Garfield Thomas Water Tunnel of the Applied Research Laboratory at The Pennsylvania State University under the sponsorship of the National Aeronautics and Space Administration (Grant No. NGL 39-009-001) whose support is appreciated. Mr. Werner R. Britsch of NASA has been technical monitor of this grant.

Further appreciation is expressed to the Garfield Thomas Water Tunnel staff, and in particular, Mr. Michael L. Billet, whose assistance was invaluable in the experimental portion of this investigation. In addition, the author wishes to acknowledge the helpful suggestions of Drs. B. R. Parkin and J. H. Kim in the theoretical portion of this investigation.

TABLE OF CONTENTS

TABLE OF CONTENTS

TABLE OF CONTENTS (Cont.)

LIST OF TABLES

LIST OF FIGURES

LIST OF FIGURES (Cont.)

LIST OF FIGURES (Cont.)

LIST OF FIGURES (Cont.)

NOMENCLATURE

a, b, ..., m, n	-	Empirical exponents in entrainment theory correlations
A	-	Cavity half length
A_W	-	Surface area of cavity
B	-	B-factor = ratio of volume of vapor to volume of liquid involved in the cavitation process = V_V/V_L
C, C_1, ..., C_5	-	Constants, integration functions
C_A	-	Area coefficient = A_W/D^2
C_D	-	Drag coefficient
C_{P_L}	-	Specific heat of liquid
C_Q	-	Flow coefficient = $Q/V_\infty D^2$
D	-	Model diameter, characteristic dimension
D_M	-	Maximum cavity diameter
D_T	-	Test section diameter
F, $\tilde{F}$	-	General expressions for correlating and experimental values
Fr	-	Froude number = $V_\infty/\sqrt{gD}$
f(y)	-	Dimensionless velocity and temperature similarity profile
G, H, ...	-	General correlating parameters
g	-	Acceleration due to gravity
h	-	Local heat transfer coefficient
$\overline{h}$	-	Average heat transfer coefficient

NOMENCLATURE (Cont.)

Δh_L	-	Change in specific enthalpy of liquid
Δh_V	-	Change in specific enthalpy of vapor
ΔH_V	-	Vapor pressure depression head
k_L	-	Thermal conductivity of liquid
K_1, K_2, K_3	-	Integration functions
L	-	Cavity length
L/D	-	Dimensionless cavity length
M_L	-	Mass of liquid
M_V	-	Mass of vapor
$\dot{M}_V$	-	Mass flow rate of vapor
n_1, ..., n_4	-	Exponents in B-factor correlation
N	-	Number of data points
N_B	-	Blockage correction factor = $\frac{\text{cavitation number}}{\text{unblocked cavitation number}}$
Nu	-	Nusselt number = $\bar{h}D/k_L$
Nu_x	-	Local Nusselt number = hD/k_L
P	-	Pressure
P_C	-	Cavity pressure
P_G	-	Gas pressure
P_V	-	Vapor pressure
P_∞	-	Free stream static pressure
ΔP_V	-	Vapor pressure depression

NOMENCLATURE (Cont.)

Pe	-	Péclêt number = $V_\infty D/\alpha_L$
Pr	-	Prandtl number = ν_L/α_L
$\dot{q}$	-	Heat transfer rate
Q	-	Volume flow rate
Re	-	Reynolds number = $V_\infty D/\nu_L$
R_L	-	Reynolds number of liquid = $U_\infty D/\nu_L$
R_V	-	Reynolds number of vapor = $U_\infty D/\nu_V$
R_I'	-	Constant characteristic of large eddy structure
s_L	-	Liquid specific entropy
s_V	-	Vapor specific entropy
T	-	Temperature
T_C	-	Cavity temperature
$T_{C_{min}}$	-	Minimum cavity temperature
T_∞	-	Free stream temperature
ΔT	-	Temperature depression
ΔT_{max}	-	Maximum temperature depression
$\tilde{u}$, $\tilde{v}$	-	Velocity components in $\tilde{x}$, $\tilde{y}$ direction
u, v	-	Dimensionless velocity components = $\frac{\tilde{u}}{U_x}$, $\frac{\tilde{v}}{U_\infty}$
U_C	-	Velocity at cavity surface
U_∞	-	Velocity outside liquid boundary layer
$\forall_L$	-	Volume of liquid involved in the cavitation process

NOMENCLATURE (Cont.)

$\forall_V$	-	Volume of vapor involved in the cavitation process
V_∞	-	Free stream velocity
$\tilde{x}$, $\tilde{y}$	-	Cartesian coordinates
x, y	-	Dimensionless coordinates = $\frac{\tilde{x}}{D}$, $\frac{\tilde{y}}{D}$
$\tilde{x}_o$	-	Virtual origin of turbulent boundary layer
x/L	-	Dimensionless axial position
α, β,	-	General exponents in correlations
α_L	-	Thermal diffusivity of liquid
δ	-	Vapor layer thickness
δ_L	-	Liquid thermal boundary layer thickness
Δ	-	Sum of the squared error between experimental and correlation values
n_δ	-	Dimensionless vapor layer thickness = δ/D
θ	-	Dimensionless temperature profile = $\frac{T - T_\infty}{T_C - T_\infty}$
ϑ_m	-	Momentum thickness
κ	-	Constant
λ	-	Latent heat of vaporization
μ_L	-	Dynamic viscosity of liquid
μ_V	-	Dynamic viscosity of vapor
ν_L	-	Kinematic viscosity of liquid
ν_V	-	Kinematic viscosity of vapor
ρ_L	-	Mass density of liquid

NOMENCLATURE (Cont.)

ρ_V - Mass density of vapor

σ - Cavitation number = $\dfrac{P_\infty - P_C}{1/2\rho V_\infty^2}$

ϕ - Dimensionless stream function in liquid

ψ - Dimensionless stream function in vapor

CHAPTER I

INTRODUCTION

1.1 Origin and Importance of this Investigation

Cavitation is an important consideration in the design and analysis of liquid handling machinery. Cavitation will occur in any liquid flow whenever the local pressure is reduced below some critical value It is generally assumed that cavitation will occur when the minimum pressure in a flow reaches the vapor pressure based on the free stream temperature of the liquid. However, this assumption is invalid if significant thermodynamic effects are present.

A continuous supply of vapor is required to sustain a developed cavity This vaporization process requires a transfer of heat to the cavity, so that the temperature of the cavity will always be less than the free stream temperature of the liquid. This localized cooling phenomenon is referred to as the thermodynamic effect.

The determination of the cavity pressure is of primary importance in developed cavity flows. The thermodynamic effect can significantly influence the cavity pressure when the liquid temperature (T) is close to the critical temperature where the magnitude of the vapor pressure (P_V) and its derivative dP_V/dT are large.

In recent years, thermodynamic effects have become increasingly important due to the need to design turbomachines for operation in cryogens such as liquid hydrogen and liquid oxygen. For these liquids, the operating temperature is closer to the critical temperature, and thermodynamic effects can be significant.

A significant thermodynamic effect can occur in any cavitating liquid Due to the complex nature of a developed cavity, prediction of cavity temperature depressions is a difficult task, and extensive study of this subject is needed.

1.2 Previous Investigations

Stahl and Stepanoff [1]* were two of the first investigators who studied the thermodynamic effect on developed cavities. In that paper, the B-factor method based on a quasi-static theory was developed for predicting thermodynamic effects with particular emphasis on pump applications. Fisher [2], Jacobs [3], and Acosta and Hollander [4] also considered the B-factor approach and its application Later, other investigators such as Salemann [5], Spraker [6], and Hammitt [7] experimentally determined the effect of fluid property variations on the performance characteristics of pumps

NASA has undertaken a program to extend the previous work in an effort to obtain improved design criteria to aid in the

*Numbers in brackets refer to the List of References at the end of this thesis.

prediction of cavitating pump performance. Ruggeri, et. al. [8-10] and Hord, et al. [11-16] have obtained extensive experimental data of cavity pressure and temperature depressions for a variety of model shapes and fluids, and have correlated the results using the B-factor theory.

Recently, Billet [17] has proposed an alternative to the B-factor approach. This method, called the entrainment theory, is a dynamic approach based on an energy balance for the cavity. The entrainment theory appears to be a better physical model than the B-factor theory, although both theories are quasi-empirical in nature.

1.3 Purpose of this Investigation

The purpose of this investigation is twofold. First, the entrainment theory concepts are extended by additional experimental and theoretical analyses to show that it is a favorable alternative to the B-factor theory. Second, a detailed summary of other investigations is given to establish the current state of knowledge for predicting the thermodynamic effect on developed cavitation. The principal theoretical and experimental results are presented for comparison with results obtained in this study.

CHAPTER II

EXPERIMENTAL INVESTIGATIONS

2.1 Introduction

Due to the complex nature of a developed cavity flow, experimental determination of the cavity characteristics is probably the most important phase of this investigation. Knowledge of the cavity pressure, temperature, geometry, and vapor mass flow rate is necessary to treat problems concerning thermodynamic effects as well as other developed cavity phenomenon. In this chapter, experimental procedures used in this study are presented and the characteristics of the resulting data discussed.

2.2 Facilities and Models

Two facilities were used to conduct the experimental investigation, both of which are located at the Applied Research Laboratory of The Pennsylvania State University. The primary facility used is the NASA-sponsored ultra-high-speed cavitation tunnel as shown in Figure 1. The tunnel is a recirculating system having a circular 3.8 cm internal diameter test section, and has the capability of operating over a wide range of velocities, pressures, and temperatures in various liquids. The working fluids used in this study are water and Freon 113. A detailed description

of the facility and data acquisition system is given in References [17-22]. A second facility, a 30.5 cm diameter test section water tunnel with a more limited operating range was used for the ventilated cavity tests. A detailed description of this facility is given in References [22-23].

A total of fourteen sting-mounted ogive test models having two basic nose contours were employed in the experiments. The zero-caliber ogives have a blunt nose, whereas the quarter-caliber ogives have a rounded nose with a radius of curvature equal to one quarter of the model diameter. A description of the two basic nose contours is given in Figure 2, and a summary of the test models used is given in Table I.

The six models that were used for the ventilated cavity tests were three zero-caliber ogives with model diameters of 0.318, 0.635, and 1.27 cm, and three quarter-caliber ogives with model diameters of 0.318, 0.635, and 1.27 cm. These models have a hollow center from which air is injected through holes near the leading edge to form the ventilated cavities, and a tube along the surface of the model with a pressure port close to the leading edge to measure the cavity pressure.

Four models were used to measure the cavity pressure of natural developed cavities: two zero-caliber ogives having model diameters of 0.318 and 0.635 cm, and two quarter-caliber ogives having model diameters of 0.318 and 0.635 cm. These models have three tubes along the surface of the model with each tube having a pressure

port located at a different axial position on the model, allowing the axial variation in cavity pressure to be determined. A photograph of the four cavity pressure models is given in Figure 3.

Four models were used to measure the cavity temperature for natural developed cavities as shown in Figure 4. The two zero-caliber ogives have model diameters of 0.318 and 0.635 cm and the two quarter-caliber ogives also have model diameters of 0.318 and 0.635 cm. These models have three ports in which thermocouple beads are cemented, and the thermocouple leads exit the tunnel through the hollow center of the model and the sting mount. The thermocouples are mounted at three different axial positions on the model so that the axial distribution of temperature within the cavity could be determined. Details of the thermocouple fabrication and installation procedure are given in Appendix A. In addition, the two larger diameter models have one tube along the surface of the model to monitor the cavity pressure.

2.3 Cavity Geometry

The geometric characteristics of developed cavities were determined from photographs of developed cavity profiles taken in both the 30.5 cm and 3.8 cm tunnels for both model contours. Typical photographs of developed cavities for the two model contours are shown in Figures 5 and 6 for water and Figures 7 and 8 for Freon 113. From measurements of the cavity profile taken from the photographs, the maximum cavity diameter (D_M), cavity half length

(A), and cavity surface area (A_W) were determined for both natural and ventilated cavities at various velocities, dimensionless cavity lengths, and model diameters. Details of the procedure and resulting data are given by Billet [17] and Billet, Holl, and Weir [24].

The data show that for a given model geometry and cavitation number, ventilated and natural cavities have the same profile, within experimental error, independent of the free stream velocity, and that the cavity dimensions are directly proportional to the model diameter. This is in agreement with Waid [25], who measured developed cavity profiles behind a circular disk. In addition, for the same flow conditions, the surface area of a cavity on a zero-caliber ogive is about twice that of a quarter-caliber ogive. The resulting data for the area coefficient (A_W/D^2) as a function of dimensionless cavity length (L/D) for the two model contours are given in Figures 9 and 10.

2.4 Cavity Flow Coefficients

The cavity flow coefficient (C_Q) is a dimensionless representation of the volume flow rate of gas required to sustain a ventilated cavity and is defined as

$$C_Q = \frac{Q}{V_\infty D^2} \tag{1}$$

In general, the flow coefficient is a function of model geometry, free stream velocity, and cavitation number.

Measurements were made in the 30.5 cm water tunnel of the volume flow rate of gas and the cavitation number at various velocities and dimensionless cavity lengths for the six ventilated cavity models. The gas flow rate was measured using a Gilmont float-type flowmeter. The free stream pressure was adjusted so that the cavity pressure was equal to the partial pressure of gas in the free stream to ensure that minimal gas diffusion occurred across the cavity wall. From the data, the flow coefficient (C_Q) as a function of cavitation number (σ), and the cavitation number as a function of dimensionless cavity length (L/D) were determined for various flow conditions. Details of the experimental procedure are given by Billet and Weir [26-27].

The resulting data of the flow coefficient as a function of cavitation number is presented in Figures 11 to 13 for the three zero-caliber ogive test models and in Figures 14 to 16 for the three quarter-caliber ogive test models. In addition, Figures 17 and 18 give the cavitation number as a function of dimensionless cavity length for the two model contours.

The results demonstrate that for a given model geometry, the flow coefficient increases with increasing velocity and model diameter and increases with decreasing cavitation number. The cavitation number for a given model contour is a function of dimensionless cavity length only. Finally, for the same flow conditions, the flow coefficient for the zero-caliber ogive is about five times that for the quarter-caliber ogive.

2.5 Cavity Pressure Measurements

Measurements of cavity pressures were made in the 3.8 cm tunnel for natural developed cavities in Freon 113 and water. Pressures were measured using Pace variable reluctance transducers with an accuracy of ± 0.07 N/cm^2 and an integrating digital voltmeter to obtain time averaged data. The cavity lengths were determined by aligning the cavity closure point with lines scribed on the models. Cavitation numbers based on local cavity pressure at three different axial positions within the cavity were obtained in Freon 113 for the four cavity pressure models over a velocity range of 19.5 to 36.6 m/sec., temperature range of 20 to 93°C, and dimensionless cavity length range of 2.0 to 7.0. In addition, measurements of cavitation numbers were made in water during the cavity temperature tests with the single cavity pressure port on the two 0.635 cm diameter cavity temperature models for a velocity range of 19.5 to 36.6 m/sec., temperature range of 60 to 120°C, and dimensionless cavity length range of 2.0 to 5.0.

To determine the variation of cavitation number with temperature, the cavitation number measured at the pressure port located closest to the leading edge of the model was determined as a function of free stream temperature, velocity, and dimensionless cavity length. Results for the zero-caliber ogives are given in Figures 19 and 20 and results for the quarter-caliber ogives are given in Figures 21 and 22. Each data point shown is an average of at least five test runs. Data obtained by Billet [17] and

Buddenbaum [28] for the 0.635 cm zero-caliber ogive are presented for comparison. Referring to the figures, it can be seen that the cavitation number is independent of velocity and free stream temperature within experimental error, and depends only on dimensionless cavity length for a given model contour and diameter. The cavitation numbers are referred to as uncorrected since the effect of blockage has not been taken into account. This effect will be discussed in detail in Chapter IV.

Cavitation numbers measured at the other axial pressure ports were also independent of free stream temperature and velocity. Figures 23 to 26 show the cavitation number as a function of dimensionless axial position (x/L) and dimensionless cavity length in Freon 113 for the two model contours. Each data point is an average over all temperatures and represents at least 40 test runs. It can be seen from the figures that the cavitation number, and the corresponding cavity pressure, remains roughly constant over the first 60 percent of the cavity, then the cavity pressure begins to increase. The measurements were made with the Freon 113 nearly saturated with air, therefore the data is affected by both thermodynamic and diffused air effects. Since these effects cannot be separated, direct comparisons of measured cavity pressures and vapor pressures based on measured cavity temperatures were not made

2.6 Cavity Temperature Measurements

Measurements of cavity temperatures were made in the 3.8 cm tunnel for natural developed cavities in Freon 113 and water with the four cavity temperature models. Cavity temperatures were measured at three different axial positions within the cavity with 0.010 cm diameter copper-constantan thermocouples with an accuracy of ± 0.28°C. The cavity thermocouples were each connected in series with a downstream thermocouple so that the temperature depression (ΔT) could be measured directly. The free stream temperature was measured independently with a thermocouple referenced to a 0°C ice bath.

All temperature readings were taken with an integrating digital voltmeter to time average any temperature fluctuations. This differs from the procedure of Billet [17], who used a galvanometer to take instantaneous readings, and then only considered the minimum measured cavity temperatures. The time averaging technique therefore produces temperature depressions which are smaller than those obtained by Billet but which are more consistent with the steady-state entrainment analysis.

In order to minimize the effects of variations in the amount of noncondensable gas dissolved in the liquids, all cavity temperature tests were run at nominal air contents of 14 ppm by moles in water and 1200 ppm by moles in Freon 113. However, it has been shown by Fricks [18] that the gas content of the liquid

has little effect on measured cavity temperature depressions for the models and test conditions employed in this investigation.

Figures 27 to 29 show typical results of the measured temperature depression as a function of dimensionless axial position (x/L). Data obtained by Fricks [18] in Freon 113 for the two 0.318 cm models are presented for comparison. As can be seen from the figures, the axial variation of the temperature depression along the cavity was found to be roughly linear, with the maximum temperature depression occurring near the leading edge of the cavity. This is in agreement with other investigators [8-11, 13-18]. Therefore, to consistently determine the maximum temperature depression ($\Delta T_{max} = T_{\infty} - T_{C_{min}}$), the axial temperature depression distribution was extrapolated to the cavity leading edge as shown in Figures 27 to 29, and the resulting ΔT_{max} was considered in all cases to be the maximum temperature depression.

The maximum temperature depression was determined as a function of free stream temperature for various flow conditions. Data were obtained in Freon 113 over a velocity range of 19.5 to 36.6 m/sec., temperature range of 35 to 95°C, and dimensionless cavity length range of 2.0 to 7.0. In addition, data were obtained in water for the two 0.635 cm diameter models over a velocity range of 19.5 to 36.6 m/sec., temperature range of 60 to 125°C, and dimensionless cavity length range of 2.0 to 5.0. The results are given in Figures 30 to 35, where each data point is the average of at least 10 test runs.

It can be seen from the figures that the maximum temperature depressions are about an order of magnitude larger in Freon 113 than in water over the temperature ranges tested. This can be attributed to the fact that since the critical temperature of Freon 113 is 214.1°C compared to 374.1°C for water, the Freon 113 data were taken at temperatures closer to its critical temperature. The largest maximum temperature depression observed was 9.0°C for the 0.635 cm quarter-caliber ogive in Freon 113.

As demonstrated by Figures 30 to 35, the maximum temperature depression increases with increasing free stream temperature and dimensionless cavity length for both model contours. However, the maximum temperature depression increases with increasing velocity and model diameter for the quarter-caliber ogives, but decreases with increasing velocity and model diameter for the zero-caliber ogives. These results suggest fundamental differences in the thermodynamic characteristics for the two model contours, but this will be clarified by examining the data within the context of the entrainment theory in Chapter IV.

2.7 Other Experimental Investigations

Measurements of cavity pressures and temperatures have been made by other investigators for a variety of model geometries and liquids. These investigations are summarized in Table II, which gives the models and fluids tested as well as the range of flow parameters. The measured ΔT at the leading edge thermocouple is

considered in all cases. The data for the ΔT_{max} obtained in this study are presented for comparison.

The geometries of the zero- and quarter-caliber ogives have already been discussed. The venturi models are axisymmetric and have a quarter-round ridge at the minimum area point to ensure that a well defined cavity leading edge is formed. The hydrofoil model is two-dimensional with a leading edge having a semi-circular cross-section and a streamlined trailing edge section. For a detailed description of the models, refer to the references cited in Table II.

CHAPTER III

THEORETICAL CONSIDERATIONS

3.1 Introduction

A direct theoretical description of the thermodynamic processes involved in the maintenance of a natural developed cavity is an extremely complex problem. It would include a detailed knowledge of the vaporization, condensation, convection, and diffusion processes occurring. Since the flow field is two-phase, nonisentropic, and in most cases turbulent, an analytical determination of the velocity and temperature profiles within the cavity and surrounding liquid, the heat required to form the cavity, and the magnitude of any thermodynamic effects is beyond the current state of knowledge.

Several simplified theories have been developed to model the thermodynamic aspects of a natural developed cavity, and are presented in the following sections. First, some preliminary considerations will be discussed.

A developed cavity is described by the cavitation number (σ) defined as

$$\sigma = \frac{P_\infty - P_C}{1/2\rho_L V_\infty^2} \qquad (2)$$

In general, the cavity pressure (P_C) is given by

$$P_C = P_V + P_G - \Delta P_V \quad , \tag{3}$$

where

P_V = vapor pressure based on the free stream temperature of the liquid (T_∞),

P_G = partial pressure of noncondensable gas in the cavity, and

ΔP_V = vapor pressure depression due to the thermodynamic effect.

Substitution of Equation (3) into Equation (2) expresses the cavitation number as

$$\sigma = \frac{P_\infty - P_V}{1/2\rho_L V_\infty^2} - \frac{P_G}{1/2\rho_L V_\infty^2} + \frac{\Delta P_V}{1/2\rho_L V_\infty^2} \quad . \tag{4}$$

Several investigators [29-31] have shown that the contribution of noncondensable gas in Equation (4) can be significant, and as the bulk temperature of the liquid increases toward the critical temperature, the vapor pressure depression term will also become important. In addition, the vapor pressure depression can, in general, be affected by the gas content of the cavity.

The vapor pressure depression can be expressed in terms of the difference between the free stream and cavity temperatures.

The vapor pressure depression can be expanded in a Taylor series as

$$\Delta P_V = \left.\frac{dP_V}{dT}\right|_{T_\infty} \Delta T + \left.\frac{d^2P_V}{dT^2}\right|_{T_\infty} \frac{\Delta T^2}{2} + \ldots \quad , \tag{5}$$

where $\Delta T = T_\infty - T_C$ is the temperature depression. Now, retaining only the first term of the series and using the Clausius-Clapeyron relationship for $\frac{dP_V}{dT}$ yields

$$\Delta P_V = \frac{\rho_V \lambda \Delta T}{T_\infty\left(1 - \frac{\rho_V}{\rho_L}\right)} \quad . \tag{6}$$

One can estimate the vapor pressure depression by Equation (6) once the temperature depression is known, provided the vapor pressure depression is small.

3.2 Entrainment Theory

The entrainment theory is a semi-empirical method for predicting thermodynamic effects on developed natural cavities. The theory, based on a simple energy balance, correlates the temperature depression (ΔT) in terms of the relevant nondimensional parameters and fluid property terms. The foundations to the theory are presented by Holl and Wislicenus [32] and in a discussion by Acosta and Parkin [33] of that paper. Billet [17] and Fricks [18] successfully correlated temperature depression data using this method

Consider a vapor region in an otherwise liquid flow. If this cavity is assumed to be steady, then it requires a constant mass flow rate of vapor to sustain it. The vaporization is assumed to occur near the leading edge of the cavity at the cavity wall, with condensation occurring in the cavity closure region. Thus, the heat required to produce this mass flow rate of vapor is given by

$$\dot{q} = \lambda \dot{M}_V \tag{7}$$

or, expressing it in terms of the volume flow rate (Q),

$$\dot{q} = \lambda \rho_V Q \quad . \tag{8}$$

Now, defining a flow coefficient (C_Q) as

$$C_Q = \frac{Q}{V_\infty D^2} \quad . \tag{9}$$

The heat required for vaporization becomes

$$\dot{q} = \rho_V \lambda C_Q V_\infty D^2 \quad . \tag{10}$$

Following the convention of convective heat transfer, an average heat transfer coefficient ($\bar{h}$) can be defined as

$$\bar{h} = \frac{\dot{q}}{A_W(T_\infty - T_C)} \quad , \tag{11}$$

where A_W is the characteristic cavity surface area. Substitution of Equation (10) into Equation (11) and rearranging yields

$$\Delta T = \frac{C_Q}{\bar{h}} \frac{D^2}{A_W} \cdot V_\infty \cdot \lambda \cdot \rho_V \tag{12}$$

or, rearranging in terms of nondimensional parameters

$$\Delta T = \frac{C_Q}{C_A} \frac{Pe}{Nu} \frac{\rho_V}{\rho_L} \frac{\lambda}{C_{P_L}} \quad , \tag{13}$$

where

$$C_A = \frac{A_W}{D^2} = \text{area coefficient,}$$

$$Pe = \frac{V_\infty D}{\alpha_L} = \text{Péclét number,}$$

and

$$Nu = \frac{\bar{h} \cdot D}{k_L} = \text{Nusselt number,}$$

and the fluid property terms are evaluated at the bulk temperature of the liquid. Division of ΔT in Equation (13) by the fluid property terms $(\rho_V/\rho_L)(\lambda/C_{P_L})$ produces the Jacob number on the left hand side of this equation.

The Péclét number and fluid property terms on the right hand side of Equation (13) are known from the free stream conditions (T_∞ and V_∞) and characteristic model dimension (D). However, C_A, C_Q, and Nu are characteristic of the cavity flow and are to be determined empirically.

The flow coefficient (C_Q) is determined from ventilated cavity tests. Ventilated cavities have been used to model natural cavities since the work of Reichardt [34] showed that the drag and geometry of ventilated and natural cavities were the same for a given cavitation number and flow geometry. Based on this result, it is assumed that the flow rate of vapor required to sustain a natural developed cavity can be estimated by measuring the volume flow rate of gas needed to sustain the corresponding ventilated cavity. This flow rate of gas is expressed as a nondimensional flow coefficient.

Billet and Weir [26-27] correlate flow coefficient data with the relation

$$C_Q = C_1 \, Re^a \, Fr^b \left(\frac{L}{D}\right)^c \tag{14}$$

where

$$Re = \frac{V_\infty \cdot D}{\nu_L} = \text{Reynolds number},$$

$$Fr = \frac{V_\infty}{\sqrt{gD}} = \text{Froude number},$$

and

$$\frac{L}{D} = \text{dimensionless cavity length}$$

This is similar to the correlation made by Reichardt [34], using the Froude number and maximum cavity diameter.

The area coefficient was determined from photographs of the developed cavity contour. Data by Waid [25], and Billet, Holl, and Weir [24] show that the cavity geometry depends only on

dimensionless cavity length. Therefore, the area coefficient data can be correlated by

$$C_A = C_2 \left(\frac{L}{D}\right)^d \quad . \tag{15}$$

Finally, the Nusselt number is determined from Equation (13) using the correlations for C_A and C_Q and measured values of ΔT. The Nusselt number (Nu) is assumed to be of the form

$$Nu = C_3 \, Re^e \, Pr^f \, Fr^h \left(\frac{L}{D}\right)^i \quad , \tag{16}$$

where

$$Pr = \frac{\nu_L}{\alpha_L} = \text{Prandtl number.}$$

Equation (16) employs the standard heat transfer parameters, Reynolds number and Prandtl number, plus the important cavity flow parameters, Froude number and dimensionless cavity length.

Once the C_A, C_Q, and Nu expressions have been obtained, temperature depressions may be calculated from Equation (13). Or, by combining Equations (13) to (16), ΔT can be correlated directly as

$$\Delta T = C_4 \cdot Pe \cdot \left(\frac{L}{D}\right)^j Re^k \, Fr^\ell \, Pr^m \, \frac{\rho_V}{\rho_L} \, \frac{\lambda}{C_{P_L}} \quad . \tag{17}$$

The entrainment theory is certainly not lacking in assumptions or empirical constants. However, it is derived from basic concepts

and gives a sound physical basis to the problem. It can be used successfully to correlate temperature depression data as shown in Chapter IV.

3.3 B-Factor Theory

The B-factor theory is a quasi-static model for the thermodynamic aspects of a developed cavity. It is assumed that the flow is steady, irrotational, and frictionless, that the vaporization process is one-dimensional and adiabatic, and that the fluid is continuously in stable thermodynamic equilibrium. Acosta and Hollander [4] state that the B-factor theory is analogous to the problem of an insulated cylinder with a tightly fitted piston. The cylinder is initially filled with a saturated liquid. Then, as the piston is withdrawn, a certain volume of vapor is formed. The B-factor is defined as the ratio of the volume of vapor to the volume of liquid involved in the vaporization process.

The classic derivation of the B-factor theory is usually attributed to Stahl and Stepanoff [1]; however, Jacobs [3] and Fisher [2] have also obtained similar results. Assuming constant fluid properties, the change in specific enthalpy of the liquid phase is given by

$$\Delta h_L = C_{P_L} \Delta T \quad . \tag{18}$$

If thermodynamic equilibrium is reached after vaporization, then the

energy balance per unit mass of liquid is

$$\Delta h_L = M_V \lambda \quad . \tag{19}$$

But, from the definition of the B-factor

$$B = \frac{\forall_V}{\forall_L} = \frac{\rho_L}{\rho_V} M_V = \frac{\rho_L}{\rho_V} \frac{\Delta h_L}{\lambda} \tag{20}$$

or substituting Equation (18) into Equation (20)

$$B = \frac{\rho_L}{\rho_V} \frac{C_{P_L}}{\lambda} \Delta T \quad . \tag{21}$$

Equation (21) relates the B-factor to the cavity temperature depression. Applying the Clausius-Clapeyron relation for ΔT and assuming that $\frac{\rho_V}{\rho_L} << 1$ gives an alternate expression for the B-factor

$$B = \left(\frac{\rho_L}{\rho_V \lambda}\right)^2 C_{P_L} T_\infty \Delta H_V \quad , \tag{22}$$

where $\Delta H_V = \Delta P_V / \rho_L$ is the cavity pressure depression expressed as a change in head.

Gelder, Ruggeri, and Moore [9] refined the calculation of the B-factor to account for changes in fluid properties with temperature and changes in enthalpy of the vapor. Again, considering the quasi-static model of Acosta and Hollander [4], the piston is

withdrawn in small incremental steps such that the system remains in thermodynamic equilibrium. The energy balance (19) per unit mass of liquid at some step n is given by

$$M_{V_n} \lambda_n = \left[1 - M_{V_n} - \sum_{i=1}^{n-1} M_{V_i}\right] \Delta h_{L_n} + \sum_{i=1}^{n-1} M_{V_n} \Delta h_{V_n} \qquad (23)$$

where the effect of the change in enthalpy of the vapor has been added, and the summation accounts for the vapor created in previous steps. The volumes of liquid and vapor are given by

$$\mathcal{V}_V = \sum_{i=1}^{n} \frac{M_{V_i}}{\rho_{V_n}} \qquad (24)$$

and

$$\mathcal{V}_L = \frac{1 - \sum_{i=1}^{n} M_{V_i}}{\rho_{L_n}} \qquad (25)$$

so that the B-factor becomes

$$B = \frac{\mathcal{V}_V}{\mathcal{V}_L} = \frac{\sum_{i=1}^{n} M_{V_i}}{\left(1 - \sum_{i=1}^{n} M_{V_i}\right)\left[\frac{\rho_V}{\rho_L}\right]_n} , \qquad (26)$$

where n is the number of incremental steps and the M_{V_i} are calculated from Equation (23). Note that if n = 1, Equation (26) reduces to Equation (20).

Due to the lengthy calculations required for the Gelder, Ruggeri, and Moore [9] method, Hord and Voth [12] devised a

simpler method based on entropy considerations to account for fluid property variations in the calculation of the B-factor. Since, from the assumptions of the quasi-static model, the vaporization process is isentropic, then, as shown in Figure 36, the initial (i) and final (f) entropies can be equated as

$$M_{L_i} s_{L_i} = M_{L_f} s_{L_f} + M_{V_f} s_{V_f} \tag{27}$$

and conservation of mass gives that

$$M_{L_i} = M_{L_f} + M_{V_f} \tag{28}$$

Combining Equations (27) and (28) with the definition of the B-factor yields

$$B = \left(\frac{\rho_L}{\rho_V}\right)_f \frac{s_{L_i} - s_{L_f}}{s_{V_f} - s_{L_i}} \tag{29}$$

The B-factor may be calculated from Equations (21), (26), or (29), once the temperature depression is known. However, none of these equations account for the dynamics of the cavity flow. Gelder, Ruggeri, and Moore [9] show that the B-factor should be proportional to the maximum cavity diameter (D_M) and inversely proportional to the thickness of the liquid thermal boundary layer

(δ_L) Since, in general

$$D_M = f_1(L/D) \tag{30}$$

and

$$\delta_L = f_2\left(\frac{V_\infty \cdot D}{\alpha_L}\right) \tag{31}$$

the B-factor is correlated by the relation

$$B = B_R \left(\frac{(\alpha_L)_R}{\alpha_L}\right)^{n_1} \left(\frac{L/D}{(L/D)_R}\right)^{n_2} \left(\frac{D}{D_R}\right)^{n_3} \left(\frac{V_\infty}{V_{\infty_R}}\right)^{n_4} , \tag{32}$$

where the subscript R indicates a reference value Hord [14-16] has introduced additional scaling parameters such as surface tension, kinematic viscosity, and two phase sonic velocity.

Thus the procedure used in applying the B-factor theory is to calculate the B-factor for a measured ΔT from an equation such as Equation (29), and correlate the results in a form such as Equation (32) where one data point is used for the reference values Then, temperature depressions may be estimated by working backwards through the procedure.

The B-factor theory and the entrainment theory are both semi-empirical in nature. The entrainment theory, based on a dynamic model, is more closely related to the actual flow field than the quasi-static B-factor model. However, by comparing Equations (13) and (21) it can be seen that the B-factor theory and the entrainment theory correspond if

$$B = \frac{C_Q}{C_A} \frac{Pe}{Nu} \tag{33}$$

Thus, employment of the entrainment theory enables the B-factor to be expressed in terms of the four dimensionless parameters which describe the geometric, entrainment, and heat transfer characteristics of the cavity.

3.4 Two-Phase Laminar Boundary Layer

In many cavity flows the length of a developed cavity is much greater than its thickness, and the flow resembles that of a boundary layer or wake. The solutions for such flows are well known. In this section, methods developed for the solution of one phase boundary layer problems will be applied to a two-phase flow.

Consider a heated, two dimensional, infinite flat plate as shown in Figure 37 with an incoming flow velocity U_∞ and temperature T_∞. The plate heats the liquid so that a vapor layer is formed on the plate. The saturation temperature of the liquid is assumed to be the same as the plate temperature T_C, so that the vapor is isothermal. The flow is assumed laminar with constant fluid properties, and the boundary layer approximations are assumed to be valid in the vapor and liquid region near the plate. This model corresponds to an infinite cavity with zero cavitation number. However, heat is convected away from the "cavity" in this problem ($T_\infty - T_C < 0$), whereas in the natural cavity case, heat is

convected to the cavity ($T_\infty - T_C > 0$), but the heat transfer mechanisms should be similar.

Refer to the coordinate system in Figure 37 The conservation equations in boundary layer approximation for the liquid are

$$\text{Continuity:} \quad \frac{\partial \tilde{u}}{\partial \tilde{x}} + \frac{\partial \tilde{v}}{\partial \tilde{y}} = 0 \quad , \tag{34}$$

$$\text{Momentum:} \quad \rho_L \left(\tilde{u} \frac{\partial \tilde{u}}{\partial \tilde{x}} + \tilde{v} \frac{\partial \tilde{u}}{\partial \tilde{y}} \right) = \mu_L \frac{\partial^2 \tilde{u}}{\partial \tilde{y}^2} \quad , \tag{35}$$

$$\text{Energy:} \quad \rho_L C_{P_L} \left(\tilde{u} \frac{\partial T}{\partial \tilde{x}} + \tilde{v} \frac{\partial T}{\partial \tilde{y}} \right) = k_L \frac{\partial^2 T}{\partial \tilde{y}^2} + \mu_L \left(\frac{\partial \tilde{u}}{\partial \tilde{y}} \right)^2 \tag{36}$$

and for the vapor are

$$\text{Continuity:} \quad \frac{\partial \tilde{u}}{\partial \tilde{x}} + \frac{\partial \tilde{v}}{\partial \tilde{y}} = 0 \quad , \tag{37}$$

$$\text{Momentum:} \quad \rho_V \left(\tilde{u} \frac{\partial \tilde{u}}{\partial \tilde{x}} + \tilde{v} \frac{\partial \tilde{u}}{\partial \tilde{y}} \right) = \mu_V \frac{\partial^2 \tilde{u}}{\partial \tilde{y}^2} \quad , \tag{38}$$

and

$$\text{Energy:} \quad T = T_C = \text{constant} \quad , \tag{39}$$

where the tilda indicates dimensional variables. The boundary conditions for the problem are

$$\tilde{u}(\tilde{x},0) = \tilde{v}(\tilde{x},0) = 0 \quad , \tag{40}$$

$$T(\tilde{x},\delta) = T_C \quad , \tag{41}$$

$$\tilde{u}(\tilde{x},\tilde{y}) = U_\infty \text{ as } y \to \infty \tag{42}$$

and

$$T(\tilde{x},\tilde{y}) = T_\infty \text{ as } y \to \infty \tag{43}$$

Three conditions are also required at the liquid-vapor interface ($\tilde{y} = \delta$). Velocity continuity states that

$$\tilde{u}_{LIQ} = \tilde{u}_{VAP} \text{ at } \tilde{y} = \delta \tag{44}$$

and stress continuity requires that

$$\mu_L \left(\frac{\partial \tilde{u}}{\partial \tilde{y}}\right)_{LIQ} = \mu_V \left(\frac{\partial \tilde{u}}{\partial \tilde{y}}\right)_{VAP} \text{ at } \tilde{y} = \delta \quad . \tag{45}$$

A third interface condition can be derived from mass continuity. For a control volume as shown in Figure 38,

$$\dot{M}_{AB} + \dot{M}_{BD} = \dot{M}_{AC} + \dot{M}_{CD} \quad , \tag{46}$$

since the flow is steady. These mass flow rates can be expressed in terms of velocities as

$$\dot{M}_{AB} = \rho_L \, \tilde{u} \, \frac{d\delta}{d\tilde{x}} \, d\tilde{x} \quad , \tag{47}$$

$$\dot{M}_{BD} = \rho_V \, \tilde{v} \, d\tilde{x} \quad , \tag{48}$$

$$\dot{M}_{AC} = \rho_L \left(\tilde{v} + \frac{\partial \tilde{v}}{\partial \tilde{y}} \, d\tilde{y} \right) d\tilde{x} \quad , \tag{49}$$

and

$$\dot{M}_{CD} = \rho_V \left(\tilde{u} + \frac{\partial \tilde{u}}{\partial \tilde{x}} \, d\tilde{x} \right) \frac{d\delta}{d\tilde{x}} \, d\tilde{x} \tag{50}$$

Therefore, neglecting terms of order $(d\tilde{x})^2$, the mass continuity relationship is

$$\rho_L \left(u \, \frac{d\delta}{d\tilde{x}} - \tilde{v} \right)_{LIQ} = \rho_V \left(\tilde{u} \, \frac{d\delta}{d\tilde{x}} - \tilde{v} \right)_{VAP} \quad \text{at } \tilde{y} = \delta \tag{51}$$

The problem can be simplified by introducing the dimensionless variables

$$u = \frac{\tilde{u}}{U_\infty} \quad , \qquad v = \frac{\tilde{v}}{U_\infty} \quad , \tag{52}$$

$$x = \frac{\tilde{x}}{D} \quad , \qquad y = \frac{\tilde{y}}{D} \quad , \tag{53}$$

and

$$\theta = \frac{T - T_\infty}{T_C - T_\infty} \quad , \tag{54}$$

where U_∞ is the characteristic velocity scale and D is a characteristic length scale Also, to satisfy the continuity relations Equations (34) and (37), stream functions ϕ and ψ can be introduced such that

$$u = \frac{\partial \phi}{\partial y} \quad , \qquad v = - \frac{\partial \phi}{\partial x} \qquad \text{in the liquid} \quad , \tag{55}$$

$$u = \frac{\partial \psi}{\partial y} \qquad \text{and} \qquad v = - \frac{\partial \psi}{\partial x} \qquad \text{in the vapor} \tag{56}$$

Therefore, the governing equations become

$$\left(\frac{\partial \psi}{\partial y} \frac{\partial}{\partial x} - \frac{\partial \psi}{\partial x} \frac{\partial}{\partial y} - \frac{1}{R_V} \frac{\partial^2}{\partial y^2} \right) \frac{\partial \psi}{\partial y} = 0 \quad , \tag{57}$$

$$\left(\frac{\partial \phi}{\partial y} \frac{\partial}{\partial x} - \frac{\partial \phi}{\partial x} \frac{\partial}{\partial y} - \frac{1}{R_L} \frac{\partial^2}{\partial y^2} \right) \frac{\partial \phi}{\partial y} = 0 \quad , \tag{58}$$

and

$$\frac{\partial \phi}{\partial y} \frac{\partial \theta}{\partial x} - \frac{\partial \phi}{\partial x} \frac{\partial \theta}{\partial y} = \frac{1}{Pe} \left(\frac{\partial^2 \theta}{\partial y^2} - \frac{Pr U_\infty^2}{C_{P_L} \Delta T} \left(\frac{\partial^2 \phi}{\partial y^2} \right)^2 \right) \quad , \tag{59}$$

where

$$R_V = \frac{U_\infty D}{\nu_V} \quad , \qquad R_L = \frac{U_\infty D}{\nu_L} \quad , \tag{60}$$

$$Pe = \frac{U_\infty D}{\alpha_L} \quad , \qquad Pr = \frac{\nu_L}{\alpha_L} \quad , \tag{61}$$

and $\Delta T = T_C - T_\infty$. The boundary conditions become

$$\psi(x,0) = 0 \quad , \tag{62}$$

$$\frac{\partial \psi}{\partial x}(x,0) = \frac{\partial \psi}{\partial y}(x,0) = 0 \quad , \tag{63}$$

$$\frac{\partial \phi}{\partial y}(x,y) = 1 \text{ as } y \to \infty \quad , \tag{64}$$

$$\theta(x,\eta_\delta) = 1 \quad , \tag{65}$$

and

$$\theta(x,y) = 0 \text{ as } y \to \infty \quad , \tag{66}$$

where (62) introduces the arbitrary origin of the stream function ψ and $\eta_\delta = \delta/D$ The interface conditions become

$$\frac{\partial \psi}{\partial y} = \frac{\partial \phi}{\partial y} \text{ at } y = \eta_\delta \quad , \tag{67}$$

$$\mu_V \frac{\partial^2 \psi}{\partial y^2} = \mu_L \frac{\partial^2 \phi}{\partial y^2} \text{ at } y = \eta_\delta \quad , \tag{68}$$

and

$$\rho_V\left[\frac{\partial \psi}{\partial y}\frac{d\eta_\delta}{dx} + \frac{\partial \psi}{\partial x}\right] = \rho_L\left[\frac{\partial \phi}{\partial y}\frac{d\eta_\delta}{dx} + \frac{\partial \phi}{\partial x}\right] \text{ at } y = \eta_\delta \tag{69}$$

Equations (57) to (59) are a system of three simultaneous nonlinear partial differential equations. The following solution requires nine boundary conditions, provided by Equations (62) to (69) However, since $\eta_\delta(x)$ is not known, one more condition is needed From the energy balance at the interface, the total heat per unit area transferred from the plate must equal the heat required for vaporization plus the heat conducted away from the liquid, which can be expressed as

$$\dot{q}_{TOT} = \dot{q}_{VAP} + \dot{q}_{COND} \tag{70}$$

Expressing the total heat transferred ($\dot{q}_{TOT}$) in terms of a local heat transfer coefficient (h) and using known expressions for $\dot{q}_{VAP}$ and $\dot{q}_{COND}$, the energy balance is

$$h \cdot \Delta T = \dot{M}_V \lambda - k_L \left.\frac{\partial T}{\partial \tilde{y}}\right|_{\tilde{y}=\delta} \quad . \tag{71}$$

From the right hand side of Equation (51),

$$\dot{M}_V = \rho_V \left(\tilde{u} \frac{d\delta}{d\tilde{x}} - \tilde{v}\right) \quad ,$$

which, expressed in terms of the stream function in dimensionless form, is

$$\dot{M}_V = \rho_V U_\infty \left(\frac{\partial \psi}{\partial y} \frac{d\eta_\delta}{dx} + \frac{\partial \psi}{\partial x}\right) \tag{72}$$

Substituting into Equation (71) and expressing the results in dimensionless form, the interface energy balance is

$$\frac{hD}{k_L} = Nu_x = \frac{Pe}{\Delta T} \frac{\rho_V}{\rho_L} \frac{\lambda}{C_{P_L}} \left(\frac{\partial \psi}{\partial y} \frac{d\eta_\delta}{dx} + \frac{\partial \psi}{\partial x}\right) - \left.\frac{\partial \theta}{\partial y}\right|_{y=\eta_\delta} \quad , \tag{73}$$

where Nu_x is the local Nusselt number. This completes the closure to the problem

Determination of an exact solution to this problem is a formidable task. However, an approximate solution can be obtained in the limit as ρ_V/ρ_L approaches zero. For most fluids at a

temperature well below the critical temperature, the ratio of vapor density to liquid density is small. For example, in water at 38°C, the saturation density ratio (ρ_V/ρ_L) is 0.461×10^{-4}. This limit is equivalent to taking the limit as the vapor Reynolds number (R_V) goes to zero and the liquid Reynolds number (R_L) goes to infinity. For example, consider water at 38°C with U_∞ = 30.5 m/sec., and D = 0.635 cm. Then $R_L = 2.78 \times 10^5$ and R_V = 89.1. Thus, it can be seen that this approximation is fairly good.

The approximate solution for the stream function in the vapor phase will now be determined. Equation (57) can be rearranged in the form

$$\left\{ R_V \frac{\partial \psi}{\partial y} \frac{\partial}{\partial x} - R_V \frac{\partial \psi}{\partial x} \frac{\partial}{\partial y} - \frac{\partial^2}{\partial y^2} \right\} \frac{\partial \psi}{\partial y} = 0 \quad . \tag{74}$$

In the limit as R_V approaches zero, Equation (74) becomes

$$\frac{\partial^3 \psi}{\partial y^3} = 0 \quad , \tag{75}$$

or upon integrating three times,

$$\psi = C_1 y^2 + C_2 y + C_3 \quad , \tag{76}$$

where C_1, C_2, and C_3 are functions of x only. Then, applying the boundary conditions Equations (62) and (63), Equation (76) is reduced to

$$\psi = C_1(x)\, y^2 \quad , \tag{77}$$

where $C_1(x)$ must be determined from a matching condition at the interface

Similarly, the approximate solution for the stream function in the liquid phase can be determined. By taking the curl of Equation (58), it can be converted to the vorticity transport equation, which in boundary layer approximation is

$$\left(\frac{\partial\psi}{\partial y}\frac{\partial}{\partial x} - \frac{\partial\phi}{\partial x}\frac{\partial}{\partial y} - \frac{1}{R_L}\frac{\partial^2}{\partial y^2}\right)\frac{\partial^2\phi}{\partial y^2} = 0 \quad . \tag{78}$$

In the limit as R_L approaches infinity,

$$\left(\frac{\partial\phi}{\partial y}\frac{\partial}{\partial x} - \frac{\partial\phi}{\partial x}\frac{\partial}{\partial y}\right)\frac{\partial^2\phi}{\partial y^2} = 0 \quad . \tag{79}$$

A first integral of Equation (79) shows that the vorticity is constant along a streamline. Since the flow upstream of the plate is irrotational, then the vorticity is zero everywhere in the liquid and

$$\frac{\partial^2\phi}{\partial y^2} = 0 \tag{80}$$

Equation (80) can be integrated twice to yield

$$\phi = K_1 y + K_2 \quad . \tag{81}$$

As a result of Equation (64) $K_1 = 1$. The function K_2 must be determined from the matching conditions at the interface. Therefore

$$\phi = y + K_2(x) \quad . \tag{82}$$

There are two unknowns in Equations (77) and (82) and three matching conditions. The problem is over-constrained since the order of Equation (78) was reduced when the limit as R_L approaches infinity was taken. Equation (68) leads to a trivial solution for ψ ($C_1(x) = 0$) and therefore this matching condition will be discarded. Physically, this decision neglects the condition of stress continuity, which determines the jump in slope of the velocity profile at the interface (see Figure 37), in favor of the more important requirement of velocity continuity across the interface. The remaining interface conditions are

$$\frac{\partial \psi}{\partial y} = \frac{\partial \phi}{\partial y} \tag{83}$$

and

$$\rho_V \left(\frac{\partial \psi}{\partial y} \frac{d\eta_\delta}{dx} + \frac{\partial \psi}{\partial x} \right) = \rho_L \left(\frac{\partial \phi}{\partial y} \frac{d\eta_\delta}{dx} + \frac{\partial \phi}{\partial x} \right) \tag{84}$$

at the interface ($y = \eta_\delta$). The final form for the vapor stream function is determined by substituting Equations (77) and (82) into Equation (83) and evaluating them at $y = \eta_\delta$. Therefore

$$\psi = \frac{y^2}{2\eta_\delta} \quad , \tag{85}$$

Similarly, the final form of the liquid stream function can be determined by substituting ψ and ϕ into Equation (84) and taking the limit as ρ_V/ρ_L approaches zero. The resulting expression for $K_2(x)$ is

$$\frac{d\eta_\delta}{dx} + \frac{dK_2}{dx} = 0 \quad , \tag{86}$$

or,

$$K_2 = -\eta_\delta + K_3 \quad . \tag{87}$$

The constant K_3 can be arbitrarily taken as zero, so finally

$$\phi = y - \eta_\delta \tag{88}$$

and the approximate expressions for the stream functions have been determined.

There is one assumption in the above derivation that has not been explicitly stated. The interface was assumed to be a streamline for the flow in the liquid phase when the limit as ρ_V/ρ_L approaches zero of Equation (84) was taken. However, there is a velocity component normal to the interface, otherwise the vapor layer could not grow along the plate. Therefore the interface is not really a

streamline, but if the density ratio is small the 'leakage' across the interface will be small.

The energy equation in the liquid was given by Equation (43) as

$$\frac{\partial \phi}{\partial y}\frac{\partial \theta}{\partial x} - \frac{\partial \phi}{\partial x}\frac{\partial \theta}{\partial y} = \frac{1}{Pe}\left[\frac{\partial^2 \theta}{\partial y^2} + \frac{PrU_\infty^2}{C_{P_L}\Delta T}\left(\frac{\partial^2 \phi}{\partial y^2}\right)^2\right] \quad . \tag{89}$$

But $\phi = y - \eta_\delta$, and taking the limit as Pe approaches infinity,

$$\frac{\partial \theta}{\partial x} + \frac{d\eta_\delta}{dx}\frac{\partial \theta}{\partial y} = 0 \quad . \tag{90}$$

The solution to Equation (90) as obtained by separation of variables is

$$\theta = C\, e^{\kappa(\eta_\delta - y)} \quad , \tag{91}$$

where C and κ are constants. The boundary condition Equation (66) is trivially satisfied and Equation (65) gives C = 1 Thus

$$\theta = e^{\kappa(\eta_\delta - y)} \quad , \tag{92}$$

where κ is as yet undetermined. An expression for the local Nusselt number can now be determined by substituting the approximate solutions for ψ and θ into Equation (73). The result is

$$Nu_x = \frac{Pe}{\Delta T}\frac{\rho_V}{\rho_L}\frac{\lambda}{C_{P_L}}\left[\frac{1}{2}\frac{\partial \eta_\delta}{\partial x}\right] + \kappa \quad . \tag{93}$$

Here κ represents the contribution to the overall local Nusselt number due to the effect of the liquid conducting heat away from the vapor layer. If it is assumed that the liquid conduction effect is small, then κ can be taken as zero. Solving for ΔT,

$$\Delta T = \frac{Pe}{Nu_x} \frac{\rho_V}{\rho_L} \frac{\lambda}{C_{P_L}} \left(\frac{1}{2} \frac{\partial \eta_\delta}{\partial x}\right) \tag{94}$$

The term $\left(\frac{1}{2} \frac{d\eta_\delta}{dx}\right)$ is the nondimensional volume flow rate per unit area across the interface. This corresponds directly to the term $\frac{C_Q}{C_A}$ in the equation for the entrainment theory. Thus by comparing Equations (13) and (94), one can see that this approximate solution to the conservation equations produces an expression similar to that employed in the entrainment theory.

3.5 Nusselt Number Estimate from a Turbulent Boundary Layer Model

In the entrainment theory development, an empirical relation was assumed for the Nusselt number using the relevant dimensionless parameters. In this section a theoretical estimation of the Nusselt number is made by applying a cavity model proposed by Brennen [30]. This cavity model has been successfully used by Billet and Weir [26-27] to account for gas diffusion effects on ventilated cavities.

Following the procedure outlined by Brennen [30], the flow over a cavity wall is represented by flow over a flat plate. As shown in Figure 39, the $\tilde{x}$-axis is placed in the direction of the flow, the $\tilde{y}$-axis is perpendicular to the flow, and the turbulent boundary

layer has an approximate origin near the cavity formation point. Initially, the velocity and temperature profiles in the liquid are different, however, it is assumed that the profiles will be similar at the end of the cavity provided that the turbulent Prandtl number is nearly unity. This change in the temperature profile is caused by the flux of heat into the cavity.

The difference between the temperature profile at any position $\tilde{x}$ and the initially uniform temperature profile represents a loss of heat from the boundary layer which can be written as

$$\Delta\dot{q} = \rho_L \, C_{P_L} \int_0^\infty (T_\infty - T)\tilde{u} \, d\tilde{y} \quad . \tag{95}$$

Since the velocity and temperature profiles are assumed similar, they can be expressed as defect profiles in the form

$$\frac{U_\infty - \tilde{u}}{U_\infty - U_C} = \frac{T_\infty - T}{T_\infty - T_C} = f(y) \quad , \tag{96}$$

where U_C and T_C are the velocity and temperature at the cavity surface and U_∞ and T_∞ are the velocity and temperature outside of the boundary layer. Substituting Equation (96) into Equation (95) and evaluating at x = L gives the total heat flux into the cavity as

$$\dot{q} = \pi \, D_M \, \rho_L \, C_{P_L} \, U_\infty \, \Delta T \int_0^\infty f(\tilde{y}) \left[1 - \left(\frac{U_\infty - U_C}{U_\infty} \right) f(\tilde{y}) \right] d\tilde{y} \tag{97}$$

where D_M is a characteristic cavity size parameter for an axisymmetric cavity and $\Delta T = T_\infty - T_C$.

Since the cavity surface is assumed straight, the turbulent boundary layer has the same boundary conditions as half the wake flow behind a flat plate parallel to the free stream, provided that the ratio of momentum thickness (θ_m) to cavity length (L) is small. Then from Townsend [35], $f(\tilde{y})$ is a Gaussian function given as

$$f(\tilde{y}) = \exp\left[-\left(\frac{\pi}{2}\right)^{0.5} \frac{R_T'}{C_D} \frac{\tilde{y}^2}{(\tilde{x}-\tilde{x}_o)} D\right] , \qquad (98)$$

where the momentum thickness is assumed constant along the free streamline. In Equation (98), $\tilde{x}_o$ is the virtual origin of the turbulent boundary layer, R_T' is a constant representative of the large eddy structure, C_D is the drag coefficient, and D is a characteristic dimension of the body.

The value of the drag coefficient can be shown to be proportional to the momentum thickness at cavity formation (θ_m) and inversely proportional to the body size so that

$$C_D = \text{constant} \cdot \theta_m/D \ . \qquad (99)$$

The length of the turbulent boundary layer to the end of the cavity ($\tilde{x}-\tilde{x_o}$) can be approximated by the cavity length, which together with Equation (99) gives

$$f(\tilde{y}) = \exp\left[-\text{constant} \cdot \frac{\tilde{y}'}{L \cdot \theta_m}\right] \qquad (100)$$

Now, substituting Equation (100) into Equation (97) and neglecting terms of order $[f(\tilde{y})]^2$ yields

$$\dot{q} = \text{constant} \cdot D_M \rho_L C_{P_L} U_x \Delta T \int_0^x \exp\left[-\frac{\tilde{y}'}{L \cdot \theta_m}\right] dy \qquad (101)$$

Integration of this equation gives the result that

$$\dot{q} = \text{constant} \cdot D_M \rho_L C_{P_L} V_x \Delta T \sqrt{\theta_m \cdot L} \quad , \qquad (102)$$

where the momentum thickness (θ_m) and the characteristic diameter of the cavity (D_M) are to be evaluated for the particular model geometry, and the velocity outside the boundary layer is assumed equal to the free stream velocity. It can be noted that neglecting the higher order terms in this case is essentially the same approximation as produced in the laminar boundary layer development in Section 3.4. The liquid is assumed to have a constant velocity in the $\tilde{y}$-direction, but have an exponential variation in temperature. However, the temperature profiles are different for the two cases.

For the axisymmetric type bodies considered in this study, the characteristic cavity diameter (D_M) can be taken to be proportional to the model diameter (D) and the momentum thickness estimated from the flat plate laminar boundary layer expression

$$\theta_m = \frac{0.664\ \tilde{x}}{\left(\frac{V_\infty \cdot \tilde{x}}{\nu_L}\right)^{0.5}} \quad , \tag{103}$$

where the distance $\tilde{x}$ can be approximated by the model diameter. This gives an expression for the heat flux as

$$\dot{q} = \text{constant}\ \rho_L\ C_{P_L}\ \Delta T\ (L/D)^{0.5} D^{1.75} V_\infty^{0.75} \nu_L^{0.25} \quad . \tag{104}$$

Expressing this in terms of the Nusselt number,

$$Nu = \frac{\dot{q}D}{\Delta T A_W k_L} = \text{constant} \cdot \frac{D}{A_W k_L} \left\{ \rho_L\ C_{P_L}\ (L/D)^{0.5} D^{1.75} V_\infty^{0.75} \nu_L^{0.25} \right\}$$

or, in terms of dimensionless quantities

$$Nu = \frac{\text{constant}}{C_A} (L/D)^{0.5} \left(\frac{V_\infty \cdot D}{\nu_L}\right)^{0.75} \left(\frac{\nu_L}{\alpha_L}\right) \quad . \tag{105}$$

As determined by Billet, Hall, and Weir [24], the area coefficient (C_A) for the zero-caliber ogive can be expressed as

$$C_A = \text{constant} \cdot (L/D)^{1.19} \tag{106}$$

and for the quarter-caliber ogive,

$$C_A = \text{constant} \cdot (L/D)^{1.18} \quad . \tag{107}$$

Since these two expressions are almost identical, the theoretical estimate of the Nusselt number for either model is

$$Nu = \text{constant} \cdot (L/D)^{-0.68} Re^{0.75} \cdot Pr \qquad (108)$$

This expression will be compared to the empirical determination of the Nusselt number in Chapter IV

CHAPTER IV

EXPERIMENTAL DATA CORRELATIONS

4.1 Introduction

Correlation of experimental data is an important aspect of both the entrainment and the B-factor theories. In addition, correlation of experimental measurements of cavitation numbers, cavity geometry, and cavity flow coefficients help to simplify analysis of these data. In this chapter, the curve-fit method used to correlate the data in this study is presented, and the resulting empirical correlations are presented and discussed. Data correlations obtained by other investigators are also given for comparison.

4.2 Curve-Fit Method

In Chapter III, empirical relations for the various dimensionless cavity flow parameters were assumed to be of the general form

$$F = C \cdot G^{\alpha} \cdot H^{\beta} \cdot \ldots , \qquad (109)$$

where F is the quantity to be correlated, G, H, ... are the relevant scaling parameters, and C, α, β, ... are constants. Taking the natural logarithm of both sides yields

$$\ln F = \ln C + \alpha \ln G + \beta \ln H + \ldots \quad . \tag{110}$$

This equation is linear in terms of the logarithm of the parameters. The standard least-squares curve-fit method can be applied (see, for example, Becket and Hurt [36]) to solve for the unknowns C, α, β, ...

The procedure involves minimizing the sum of the squares of the difference between the experimental and calculated values of the logarithm of F, which can be expressed as

$$\sum_{1}^{N} (\ln\tilde{F} - \ln F)^2 = \Delta \quad , \tag{111}$$

where N is the number of data points and the tilda indicates experimental values. Substituting Equation (110) into Equation (111) yields

$$\sum_{1}^{N} (\ln F - C' - \alpha \ln G - \beta \ln H - \ldots)^2 = \Delta \quad , \tag{112}$$

where $C' = \ln C$. Now, to minimize the quantity Δ, the partial derivative is taken with respect to each unknown (C', α, β, ...) and set equal to zero. This yields a set of simultaneous equations which can be expressed as

$$C' N + \alpha[\sum_{1}^{N} (\ln G)] + \beta[\sum_{1}^{N} (\ln H)] + \ldots = \sum_{1}^{N} (\ln \tilde{F})$$

$$C'(\sum_{1}^{N} \ln G) + \alpha[\sum_{1}^{N} (\ln G)^2] + \beta[\sum_{1}^{N} (\ln G)(\ln H)] + \ldots = \sum_{1}^{N} (\ln \tilde{F})(\ln G)$$

and

$$C'(\sum_{1}^{N} \ln H) + \alpha[\sum_{1}^{N} (\ln G)(\ln H)] + \beta[\sum_{1}^{N} (\ln H)^2] + \ldots = \sum_{1}^{N} (\ln \tilde{F})(\ln H) \quad (113)$$

Equations (113) are a system of linear algebraic equations and are solved for the unknowns by standard matrix techniques. Then, since $C = e^{C'}$, all of the unknowns in the correlative expression, Equation (109), have been determined. This technique was used to determine all of the correlations used in this study.

4.3 Cavitation Numbers and Blockage Effects

Correlations of cavitation number (σ) as a function of dimensionless cavity length (L/D) were made for developed cavities on the zero- and quarter-caliber ogive test models. Biller, Holl and Weir [24] obtained data in the 30.5 cm water tunnel for model diameters of 1.27, 0.635, and 0.318 cm. For this test, the ratios of model diameter to test section diameter are quite small so that blockage effects are negligible. However, data obtained in this study were taken in the 3.8 cm tunnel for model diameters of 0.635

and 0.318 cm. This corresponds to model to test section diameter ratios (D/D_T) of 0.167 and 0.083. Thus, the blockage effects for these data are important. In addition, data were obtained by Hord [15] on the quarter-caliber ogive for a D/D_T equal to 0.308. Details of the analysis of the data obtained by Hord are given in Appendix B. The resulting data correlations in the form

$$\sigma = C_5 \, (L/D)^n \tag{114}$$

are given in Table III for the two model contours and various values of D/D_T.

The cavitation number correlations in Table III are plotted in Figure 40 for the zero-caliber ogive and in Figure 41 for the quarter-caliber ogive. The symbols on these figures indicate an average of at least 40 data points. Referring to the figures, it can be seen that as the model to test section diameter ratio increases, the cavitation number increases for a given dimensionless cavity length. Thus, blockage effects can significantly affect the cavitation number. In fact, the data by Hord [15] is so strongly affected by blockage that he assumed that the cavitation number was independent of dimensionless cavity length and grand averaged all of his data. However, the curve-fit of his data in this study does show a weak dependence on L/D as shown by the upper curve in Figure 41.

One method to correct measured cavitation numbers affected by blockage is to determine the blockage correction factor (N_B) defined as

$$N_B = \frac{\text{cavitation number}}{\text{unblocked cavitation number}} \quad . \tag{115}$$

Figure 42 gives the blockage correction factor as a function of dimensionless cavity length and model to test section diameter ratio for the two model contours. It can be seen from the figure that N_B increases with increasing L/D and D/D_T. The blockage correction factor also appears to be nearly independent of nose contour for the models considered. Expressions for N_B may be determined from the corresponding cavitation number correlations in Table III.

4 4 Entrainment Theory Correlations

As discussed in Chapter III, employment of the entrainment theory requires empirical correlations of the cavity area coefficient, cavity flow coefficient, and Nusselt number. The correlative expressions are given by Equations (15), (14), and (16) respectively.

The correlation of the cavity area coefficient was made from the data given by Billet, Holl, and Weir [24] for zero- and quarter-caliber ogives with model diameters of 1.27 and 0.635 cm for a range of velocities and dimensionless cavity lengths in water. These correlations are shown as the solid lines in Figures 9 and 10.

The correlations of flow coefficients were made from the data given by Billet and Weir [26-27] for zero- and quarter-caliber ogives with model diameters of 1.27, 0.635, and 0.318 cm for a range of velocities and cavity lengths in water. These correlations are shown as the solid lines in Figures 11-16.

Correlations of Nusselt numbers were made from maximum temperature depression data obtained in this study for zero- and quarter-caliber ogives with model diameters of 0.635 cm in water and model diameters of 0.635 and 0.318 cm in Freon 113, and data obtained by Fricks [18] for zero- and quarter-caliber ogives with model diameters of 0.318 cm in Freon 113. The ranges of velocity, temperature, and dimensionless cavity length employed in this study are given in Table II. In addition, a correlation for the Nusselt number was determined from the temperature depression data taken by Hord [15] on quarter-caliber ogives in nitrogen and hydrogen (see Appendix B).

The constants and exponents for all of the data correlations are given in Table IV. These include the correlations for the zero- and quarter-caliber ogive data obtained in this study, the correlations for the quarter-caliber ogive data obtained by Hord [15], and the theoretical Nusselt number relationship obtained in Chapter III. The pertinent equations are referenced in the table.

Once the correlations of the area coefficient, flow coefficient, and Nusselt number have been determined, an expression for the maximum temperature depression can be determined from Equation (13).

The resulting correlations in the form of Equation (17) are also given in Table IV and plotted as solid lines on Figures 30 to 32 for the zero-caliber ogives and Figures 33 to 35 for the quarter-caliber ogives.

Comparison of the correlative expressions can be made by referring to Table IV. The cavity area coefficient (C_A) for the two model contours have almost the same dependence on dimensionless cavity length (L/D), and C_A for the zero-caliber ogive is about twice that for the quarter-caliber ogive. The cavity flow coefficient (C_Q) correlations also have about the same dependence on L/D. However, the Reynolds number (Re) and the Froude number (Fr) exponents on the C_Q correlation for the quarter-caliber ogive are greater than for the zero-caliber ogive, reflecting the greater dependence of C_Q on velocity and model diameter for the more streamlined body.

Comparison of the three empirical Nusselt number (Nu) expressions indicates relatively good agreement except for the Prandtl number (Pr) exponent. The L/D exponents range from - 0.74 to - 1.35, the Re exponents from 1.00 to 1.39, and the Fr exponents from 0.24 to 0.56. All of these exponents have the same sign and are of the same order for like terms. However, the exponents on Pr vary greatly from 0.05 to 0.84. Thus, the role of the Prandtl number in the entrainment theory correlations is unclear.

The theoretical estimate of the Nusselt number derived in Chapter III is given in Table IV for comparison with the empirical correlations. It can be seen from the Table that the theoretical

exponents on L/D and Pr are slightly greater and the exponents on Re are slightly less than the range of exponents determined from the data. However, the overall agreement between theory and experiment is quite good.

Examining the maximum temperature depression (ΔT_{max}) correlations, it can be seen that the exponents all have similar signs for like terms, and they all agree qualitatively except for the Prandtl number exponents. Thus, although the ΔT_{max} data for the zero-caliber ogives shows a trend with velocity and model diameter which is opposite that of the quarter-caliber ogive data, the ΔT_{max} expressions are consistent when expressed in terms of dimensionless parameters in that the exponents on like terms have the same sign. In addition, referring to Figures 30 to 35, the empirical ΔT_{max} correlations are a good curve-fit to the experimental data, with the standard deviation being 0.25°C for the zero-caliber ogive and 0.07°C for the quarter-caliber ogive.

4.5 B-Factor Theory Correlations

Correlations of temperature depression data for developed cavities have been made by several investigators using the B-factor theory. A summary of the various correlations are given in Table V. As shown in the table, three different methods of calculating the B-factor have been used, and the correlations are expressed in the form of Equation (32).

The exponents on the liquid thermal diffusivity (α_L) vary widely from 3.52 to - 1.00 showing no consistent trends. This is similar to the problem with the Prandtl number exponents in the entrainment theory. The model diameter exponents are also inconsistent, but the only two experiments that varied model diameter had very different model geometries. The free stream velocity (V_∞), cavity length (L), and kinematic viscosity (ν_L) exponents are each fairly consistent. Direct comparison of the B-factor and entrainment theory correlations were not made due to the fact that different physical reasoning was used to develop the two theories, and different curve-fit methods were used to determine the exponents.

CHAPTER V

SUMMARY

5.1 Theoretical Considerations

The entrainment theory and the B-factor theory are semi-empirical methods to describe thermodynamic phenomena in developed cavitation. They have been successfully applied to correlate measured cavity temperature depression data. The entrainment theory, however, is a more physical approach derived from a simple energy balance that accounts for the cavity geometry, vapor mass flow rate, and heat transfer mechanisms. The entrainment theory can also be derived from an approximate solution to the equations of motion for a two phase, two-dimensional laminar boundary layer. A theoretical analysis of the cavity heat transfer mechanism based on a method proposed by Brennen [30] yields an expression for the Nusselt number which agrees in part with empirical results

5.2 Cavitation Numbers and Blockage

The cavitation number based on cavity pressure is an important parameter for describing developed cavities. The experimental data show that the cavitation number is solely a function of dimensionless cavity length and is independent of velocity, temperature, model diameter, and working fluid for a given model contour and model to

test section diameter ratio. The cavitation number, when based on a local pressure within the cavity, is nearly constant for the first 60% of the cavity, then decreases rapidly near the cavity closure point due to the increase in cavity pressure.

Blockage can have a significant effect on measured cavitation numbers. A good measure of tunnel blockage for axisymmetric flows is the ratio of model diameter to test section diameter. As the tunnel blockage increases, the cavitation number also increases for a given value of dimensionless cavity length. For severely blocked conditions, the cavitation number can appear to be independent of dimensionless cavity length. The blockage correction factor, defined as the ratio of the cavitation number with blockage to the unblocked cavitation number, is an effective means to correct for blockage effects in that it is nearly independent of nose contour. Empirical correlations of the cavitation number and the blockage correction factor as a function of dimensionless cavity length have been obtained.

5.3 Cavity Area and Flow Coefficients

The cavity area coefficient and cavity flow coefficient are two important dimensionless parameters employed in the entrainment theory. The area coefficient, a dimensionless representation of the cavity surface area, is determined from photographs of developed cavity profiles. The flow coefficient, a dimensionless

representation of the volume flow rate of vapor through the cavity, is determined by measuring the volume flow rate of gas needed to sustain a ventilated cavity.

The experimentally determined area coefficient is solely a function of dimensionless cavity length. For different model contours, the magnitude of the area coefficient changes, but its dependence on dimensionless cavity length remains nearly the same. The experimentally determined flow coefficient increases with increasing velocity, model diameter, and dimensionless cavity length. For different model contours, the dependence of the flow coefficient on dimensionless cavity length remains nearly the same, but its dependence on velocity and model diameter is greater for the more streamlined quarter-caliber ogive than for the zero-caliber ogive. Empirical correlations of the area and flow coefficients with the pertinent flow parameters have been determined.

5.4 Measured Temperature Depressions

Measurements of the difference between the free stream temperature and the cavity temperature were made for a variety of flow conditions. These data, along with data obtained by other investigators, provide a wealth of information concerning thermodynamic effects on developed cavitation.

The axial variation of temperature depressions within the cavity was found to be linear, with the maximum temperature depression occurring near the leading edge of the cavity. The

maximum temperature depression increases with increasing dimensionless cavity length and free stream temperature. However, the maximum temperature depression increases with increasing free stream velocity and model diameter for the quarter-caliber ogives, but has the opposite trend for the zero-caliber ogives. All ΔT_{max} data show consistent trends when analyzed in terms of Reynolds number, Prandtl number, Péclét number, Froude number, and dimensionless cavity length in the context of the entrainment theory because the signs of like terms are the same. The maximum temperature depression data have been used to determine Nusselt number relations for developed cavities, which, when employed with the entrainment theory, can be used to estimate cavity temperature depressions.

5.5 Recommendations for Further Study

Three basic problems concerning thermodynamic effects on developed cavitation need further study. First, the effect of model configuration on temperature depressions has not been adequately determined. Additional experimental data is needed to extend the application of the entrainment theory to additional two and three dimensional bodies.

Second, an extension of present theories should be attempted that would account for the effects of model geometry on the cavity heat transfer mechanisms. In addition, more extensive and general theoretical analyses of thermodynamic effects should be conducted

Third, the role of the fluid property terms, especially the Prandtl number and/or thermal diffusivity, in the thermodynamics of developed cavities remains unclear. Further experimentation is needed over a wider range of temperatures in many different fluids to further define the effects of fluid property variations. Also, attempts should be made to determine if vapor fluid properties other than vapor density have an effect on the cavity temperature depression.

REFERENCES

1. Stahl, H. A. and Stepanoff, A. J., "Thermodynamic Aspects of Cavitation in Centrifugal Pumps," Trans. ASME, Vol. 78, 1956.

2. Fisher, R. C., Discussion of "A Survey of Modern Centrifugal Pump Practice for Oilfield and Oil Refining Services," by N. Tetlow, Proc. Inst. Mech. Engrs., Vol. 152, 1945.

3. Jacobs, R. B., "Prediction of Symptoms of Cavitation," J. Res., Nat. Bur. Stand. (U.S.), Vol. 65C, No. 3, 1961.

4. Acosta, A. J. and Hollander, A., "Remarks on Cavitation in Turbomachines," Hydromechanics Laboratory, California Institute of Technology, Report 79.3, October 1959.

5. Salemann, V., "Cavitation and NPSH Requirements of Various Liquids," Trans. ASME, Series D, Journal of Basic Engineering, Vol. 81, 1959.

6. Spraker, W. A., "The Effects of Fluid Properties on Cavitation in Centrifugal Pumps," Trans. ASME, Journal of Engineering for Power, Vol. 87, No. 3, 1965.

7. Hammitt, F. G., "Observation of Cavitation Scale and Thermodynamic Effects in Stationary and Rotating Components," Trans. ASME, Series D, Journal of Basic Engineering, Vol. 85, 1963.

8. Ruggeri, R. S. and Gelder, T. F., "Cavitation and Effective Liquid Tension of Nitrogen in a Tunnel Venturi," NASA TN D-2088, 1964.

9. Gelder, T. F., Ruggeri, R. S., and Moore, R. D., "Cavitation Similarity Considerations Based on Measured Pressure and Temperature Depressions in Cavitated Regions of Freon 114," NASA TN D-3509, 1966.

10. Moore, R. D. and Ruggeri, R. S., "Prediction of Thermodynamic Effects of Developed Cavitation Based on Liquid-Nitrogen and Freon 114 Data in Scaled Venturis," NASA TN D-4899, 1968.

11. Hord, J., Edmonds, D. K., and Millhiser, D. R., "Thermodynamic Depressions Within Cavities and Cavitation Inception in Liquid Hydrogen and Liquid Nitrogen," NASA CR-72286 and NBS Report 9705, 1968.

12. Hord, J. and Voth, R. O., "Tabulated Values of Cavitation B-Factor for Helium, H_2, N_2, F_2, O_2, Refrigerant 114, and H_2O," NBS TN 397, 1971.

13. Hord, J., Anderson, L. M., and Hall, W. J., "Cavitation in Liquid Cryogens, Volume I--Venturi," NASA CR-2054, 1972.

14. Hord, J., "Cavitation in Liquid Cryogens, Volume II--Hydrofoil," NASA CR-2156, Jan. 1973.

15. Hord, J., "Cavitation in Liquid Cryogens, Volume III--Ogives," NASA CR-2242, May 1973.

16. Hord, J., "Cavitation in Liquid Cryogens, Volume IV--Combined Correlations for Venturi, Hydrofoil, Ogives, and Pumps," NASA CR-2448, 1974.

17. Billet, M. L., "Thermodynamic Effects on Developed Cavitation in Water and Freon 113," M.S. Thesis, The Pennsylvania State University, March 1970.

18. Fricks, E. E., "The Influence of Temperature, Velocity, Size, and Boundary Form on the Thermodynamic Effect in Developed Cavitation in Freon 113," M.S. Thesis, The Pennsylvania State University, March 1974.

19. Holl, J. W. and Kornhauser, A. K., "Thermodynamic Effects on Desinent Cavitation on Hemispherical Nosed Bodies in Water at Temperatures from 80 Deg F to 260 Deg F," Trans. ASME, Series D, Journal of Basic Engineering, March 1970.

20. Holl, J. W. and Treaster, A. L., "Cavitation Hysteresis," Trans. ASME, Journal of Basic Engineering, March 1966.

21. Seidel, G. S., "An Investigation of Thermodynamic Effects on Cavitation in Water from 80°F to 180°F on Hemispherical-Nosed Bodies," M.S. Thesis, The Pennsylvania State University, June 1966

22. Holl, J. W., "Cavitation Research Facilities at the Ordnance Research Laboratory of The Pennsylvania State University," presented at the Symposium on Cavitation Research Facilities and Techniques, Fluids Engineering Conference, ASME, Philadelphia, Pennsylvania, May 18-20, 1964.

23. Lehman, A. F., "The Garfield Thomas Water Tunnel," Ordnance Research Laboratory, The Pennsylvania State University, Serial No. NOrd 16597-56.

24. Billet, M. L., Holl, J. W., and Weir, D. S., "Geometric Description of Developed Cavities on Zero and Quarter Caliber Ogive Bodies," Applied Research Laboratory Technical Memorandum, File No. TM 74-136, May 6, 1974.

25. Waid, R. L., "Cavity Shapes for Circular Disks at Angles of Attack," Pasadena, California, Hydrodynamics Laboratory, California Institute of Technology, Report E-73.4, 1957.

26. Billet, M. L. and Weir, D. S., "The Effect of Gas Diffusion on the Flow Coefficient for a Ventilated Cavity," submitted to the Symposium on Cavity Flows, Joint Conference of the Fluids Engineering and Lubrication Divisions, ASME, Minneapolis, Minnesota, May 5-7, 1975.

27. Billet, M. L. and Weir, D. S., "The Effect of Gas Diffusion and Vaporization on the Entrainment Coefficient for a Ventilated Cavity," Applied Research Laboratory Technical Memorandum, File No. TM 74-15, Jan. 24, 1974.

28. Buddenbaum, L. E., "Thermodynamic Effects on Developed Cavitation on Zero-Caliber-Ogives in Water at Temperatures from 80°F to 260°F," M. Engr. Report, The Pennsylvania State University, March 1968.

29. Holl, J. W., "An Effect of Air Content on the Occurrence of Cavitation," Trans. ASME, Journal of Basic Engineering, Vol. 82, No. 4, 1960.

30. Brennen, C., "The Dynamic Balances of Dissolved Air and Heat in Natural Cavity Flows," Journal of Fluid Mechanics, Vol. 37, Part I, 1969.

31. Hammitt, F. G., "Effects of Gas Content Upon Cavitation Inception, Performance, and Damage," University of Michigan Report No. UMICH 01357-21-I, 1971.

32. Holl, J. W. and Wislicenus, G. F., "Scale Effects on Cavitation," Trans. ASME, Series D, Journal of Basic Engineering, Vol. 83, 1961.

33. Acosta, A. J. and Parkin, B. R., Discussion of "Scale Effects on Cavitation," by J. W. Holl and G. F. Wislicenus, Trans. ASME, Series D, Journal of Basic Engineering, Vol. 83, 1961.

34. Reichardt, H., "The Laws of Cavitation Bubbles at Axially Symmetrical Bodies in a Flow," MAP Reports and Translations, Report No. 776, Aug. 15, 1956.

35. Townsend, A. A., The Structure of Turbulent Shear Flow, Cambridge University Press, 1956.

36. Becket, R. and Hurt, J., Numerical Calculations and Algorithms, McGraw-Hill Book Company, New York, 1967.

37. Keenan, J. H. and Keyes, F. G., Thermodynamic Properties of Steam, John Wiley and Sons, Inc., New York, 1936.

38. Benning, A. F. and McHarness, R. C., "The Thermodynamic Properties of 'Freon-113' (CCL_2F-$CCLF_2$)," E. I. du Pont de Nemours and Company, Wilmington, Delaware, 1938.

39. Downing, R. C., "Transport Properties of 'Freon' Fluorocarbons," E. I. du Pont de Nemours and Company, Wilmington, Delaware, 1967.

40. "Thermodynamic Properties of Freon 114 Refrigerant," E. I. du Pont de Nemours and Company, Wilmington, Delaware, 1966.

41. McCarty, R. D. and Weber, L. A., "Thermophysical Properties of Parahydrogen from the Freezing Liquid Line to 5000 R for Pressures to 10,000 psia," NBS TN 617, 1972.

42. Jacobsen, R. T., Stewart, R. B., McCarty, R. D., and Hanley, H. J. M., "Thermophysical Properties of Nitrogen from the Fusion Line to 3500 R (1944 K) for Pressures to 150,000 psia (10342 × 10^5 N/m^2)," NBS TN 648, 1973.

APPENDIX A

THERMOCOUPLE FABRICATION AND INSTALLATION PROCEDURE

Cavity temperatures were measured with copper-constantan thermocouples installed in the cavity temperature models. Three thermocouples were constructed from 0.010 cm diameter wire stock with a 0.00025 cm polyurethane coating. To form the thermocouple bead, the insulation was carefully stripped away from one end of the wires and the copper and constantan wires twisted together. The wires were then welded with a helium atmosphere arc-welder which formed the bead. The bead was reinforced with a small amount of epoxy cement and the leads coated with enamel paint to prevent shorts.

The thermocouples were then strung through the thermocouple ports and out the rear of the test model. Each set of leads was laid through 26-gauge teflon tubing that extended into the model for added protection. The thermocouples were positioned in the ports such that the beads protruded just above the model surface. The remaining space in the port was filled with epoxy cement to secure the bead in position. The teflon tubes holding the thermocouple leads were anchored to the rear of the model using General Electric RTV compound. The model was then inserted into the sting-mount

with the tubing running through one of the stings. Finally, the tubing with the thermocouple leads inside was anchored inside the sting with epoxy.

The model was then installed in the tunnel, with the leads exiting through the tunnel wall. The three thermocouples were each connected in series with the free stream thermocouple, and the procedure completed.

APPENDIX B

ANALYSIS OF THE DATA OBTAINED BY J. HORD

Extensive data of measured pressure and temperature depressions for developed cavities on quarter-caliber ogives were made by Hord [15]. These data were obtained in liquid hydrogen and liquid nitrogen for model diameters of 0.533, 0.907, and 1.067 cm for a variety of flow conditions. The data are presented in tabular form at the end of his report, making it easy to analyze. The thermophysical properties of liquid hydrogen and nitrogen are available from the National Bureau of Standards in References [41] and [42].

To determine the cavitation number as a function of dimensionless cavity length, the cavity pressure measured at the leading edge pressure port, free stream pressure, and free stream velocity were used. The empirical correlation was then determined by curve-fitting the resulting data. Three different model diameters were tested, but only one value of model to test section diameter ratio was tested since three scaled test sections were used.

The entrainment theory was also applied to the temperature depression data. Due to the large volume of data, linear extrapolations to the leading edge of the cavity were not made.

The temperature depression measured at the leading edge thermocouple was considered to be the maximum temperature depression. The Nusselt number correlation was then determined using these maximum temperature depression data and the flow coefficient and area coefficient relations obtained in this study.

TABLE I

SUMMARY OF TEST MODELS USED IN THIS INVESTIGATION

Model	Purpose	Diameter (cm)	Number of Pressure Ports	Number of Thermocouple Ports
Zero-Caliber Ogive	Ventilated Cavity Measurements	0.318	1	0
		0.635	1	0
		1.27	1	0
	Cavity Pressure Measurements	0.318	3	0
		0.635	3	0
	Cavity Temperature and Pressure Measurements	0.318	0	3
		0.635	1	3
Quarter-Caliber Ogive	Ventilated Cavity Measurements	0.318	1	0
		0.635	1	0
		1.27	1	0
	Cavity Pressure Measurements	0.318	3	0
		0.635	3	0
	Cavity Temperature and Pressure Measurements	0.318	0	3
		0.635	1	3

TABLE II

AVAILABLE EXPERIMENTAL DATA OF THERMODYNAMIC EFFECTS ON DEVELOPED CAVITATION

Model	Fluid	Investigators	Model Diameters (cm)	Range of Parameters	L/D	T_∞ (°K)	$\frac{\rho_V}{\rho_L}$	V_∞ (m/sec)	ΔT (°K)
Venturi	Hydrogen	Hord, et. al. (1972)	2.48	Min.	0.8	19.9	1.7×10^{-2}	30.1	0.2
				Max.	3.6	23.0	3.9×10^{-2}	59.1	2.7
	Hydrogen	Hord, et. al. (1968)	2.48	Min.	1.3	20.3	1.9×10^{-2}	33.8	1.1
				Max.	3.3	22.8	3.7×10^{-2}	62.5	4.6
	Nitrogen	Hord, et. al. (1968)	2.48	Min.	3.3	78.4	6.1×10^{-3}	10.7	0.4
				Max.	3.3	89.5	1.9×10^{-2}	22.6	4.9
	Hydrogen	Moore & Ruggeri (1968)	2.48, 3.50	Min.	1.0	20.3	1.9×10^{-2}	33.5	1.4
				Max.	2.6	23.3	4.2×10^{-2}	62.5	3.1
	Freon-114	Moore & Ruggeri (1968)	2.48, 3.50	Min.	0.2	255.6	2.1×10^{-3}	19.0	0.3
				Max.	2.7	303.2	1.3×10^{-2}	50.0	5.8
	Nitrogen	Ruggeri & Gelder (1964)	3.50	Min.	1.1	78.0	6.0×10^{-3}	6.2	0.6
				Max.	3.3	79.3	7.0×10^{-3}	14.1	1.7
	Freon-114	Gelder, et. al. (1966)	3.50	Min.	0.3	259.0	2.4×10^{-3}	5.8	1.5
				Max.	2.3	300.0	1.2×10^{-2}	13.4	5.8
Hydrotoil	Hydrogen	Hord (Jan. 1973)	0.792	Min.	1.1	20.3	1.9×10^{-2}	32.4	0.8
				Max.	5.4	23.0	3.9×10^{-2}	66.8	3.9
	Nitrogen	Hord (Jan. 1973)	0.792	Min.	1.4	76.3	5.1×10^{-3}	7.4	0.5
				Max.	6.4	88.8	1.8×10^{-2}	24.4	3.3

TABLE II (CONT.)

AVAILABLE EXPERIMENTAL DATA OF THERMODYNAMIC EFFECTS ON DEVELOPED CAVITATION

Model	Fluid	Investigators	Model Diameters (cm)	Range of Parameters	L/D	T_∞ (°K)	$\frac{\rho_V}{\rho_L}$	V_∞ (m/sec)	ΔT (°K)
Quarter-Caliber Ogive	Hydrogen	Hord (May 1973)	0.533, 0.907 1.07	Min.	1.0	20.3	1.9×10^{-2}	35.5	0.4
				Max.	4.6	23.1	4.0×10^{-2}	92.5	2.0
	Nitrogen	Hord (May 1973)	0.533, 0.907 1.07	Min.	0.8	76.5	5.2×10^{-3}	8.8	0.4
				Max.	7.2	91.8	2.4×10^{-2}	34.4	2.7
	Freon-113	This Study	0.318, 0.635	Min.	2.0	313.2	4.6×10^{-3}	19.5	1.4
				Max.	7.0	367.7	1.9×10^{-2}	36.6	8.9
	Water	This Study	0.635	Min.	2.0	338.2	1.7×10^{-4}	19.5	0.1
				Max.	5.0	394.2	1.2×10^{-3}	36.6	1.1
Zero-Caliber Ogive	Freon-113	This Study	0.318, 0.635	Min.	2.0	311.2	4.3×10^{-3}	19.5	0.5
				Max.	7.0	367.2	1.9×10^{-2}	36.6	4.1
	Water	This Study	0.635	Min.	2.0	336.2	1.5×10^{-4}	19.5	0.0
				Max.	5.0	394.7	1.2×10^{-3}	36.6	0.7

TABLE III

CAVITATION NUMBER CORRELATIONS
(Equation 114)

	Fluid	Zero-Caliber Ogive		Quarter-Caliber Ogive	
		Constant	L/D Exponent	Constant	L/D Exponent
Unblocked*	Water	0.751	- 0.75	0.484	- 0.69
$\frac{D}{D_I}$ = 0.083	Freon 113	0.505	- 0.45	0.405	- 0.51
$\frac{D}{D_I}$ = 0.167	Water Freon 113	0.625	- 0.38	0.419	- 0.29
$\frac{D}{D_I}$ = 0.308**	Hydrogen Nitrogen	-----	-----	0.607	- 0.16

*Data from Billet, Holl, and Weir (1974)

**Data from Hord (May 1973)

TABLE IV

CONSTANTS AND EXPONENTS FOR ENTRAINMENT THEORY CORRELATIONS

Model	Quantity	Equation Number	Constant	L/D Exponent	Re Exponent	Fr Exponent	Pr Exponent
Zero-Caliber Ogive	C_A	(15)	4.59	1.19	-------	--------	--------
	C_Q	(14)	0.424×10^{-2}	0.69	0.16	0.13	--------
	Nu	(16)	0.103×10^{-3}	-1.35	1.39	0.25	0.84
	ΔT_{max}	(17)	8.97	0.85	-1.23	-0.11	-0.84
Quarter-Caliber Ogive	C_A	(15)	2.06	1.18	--------	--------	--------
	C_Q	(14)	0.320×10^{-4}	0.74	0.46	0.26	--------
	Nu	(16)	0.546×10^{-2}	-0.74	1.00	0.34	0.49
	ΔT_{max}	(17)	0.284×10^{-2}	0.30	-0.54	-0.08	-0.49
Quarter-Caliber Ogive*	Nu	(16)	0.375×10^{-2}	-0.84	1.02	0.56	0.05
	ΔT_{max}	(17)	0.414×10^{-2}	0.40	-0.56	-0.30	-0.05
Zero- & Quarter-Caliber Ogive**	Nu	(103)	----------	-0.68	0.75	--------	1.00

*Correlation using ΔT data from Herd (May 1973) and C_Q and C_A data from this study

**Derived from turbulent boundary layer cavity model

EXPONENTS FOR B-FACTOR THEORY CORRELATIONS

Model	Fluids	Investigators	γ_1 Exponent	V_∞ Exponent	L Exponent	$\bar{\gamma}_1$ Exponent	D Exponent
	Freon-114	Gelder, et. al.* (1966)	- 0.5	0.85	0.16	--------	--------
	Hydrogen	Bord, et. al.* (1968)	3.52	0.554	0.348	--------	--------
Venturi	Nitrogen	Bord, et. al.* (1968)	1.22	0.492	--------	--------	--------
	Hydrogen Freon-114	Moore & Ruggeri** (1968)	- 1.0	0.8	0.3	--------	- 0.1
	Hydrogen	Bord, et. al.*** (1972)	1.92	0.74	0.34	--------	--------
Hydrofoil	Hydrogen Nitrogen	Bord*** (Jan. 1973)	- 0.8	0.64	0.45	1.03	--------
Quarter Caliber Ogive	Hydrogen Nitrogen	Bord*** (May 1973)	- 0.32	0.21	0.34	0.84	0.60

Equation (32).

*B-factor calculated from Equation (26).

**B-factor calculated from Equation (21).

***B-factor calculated from Equation (29).

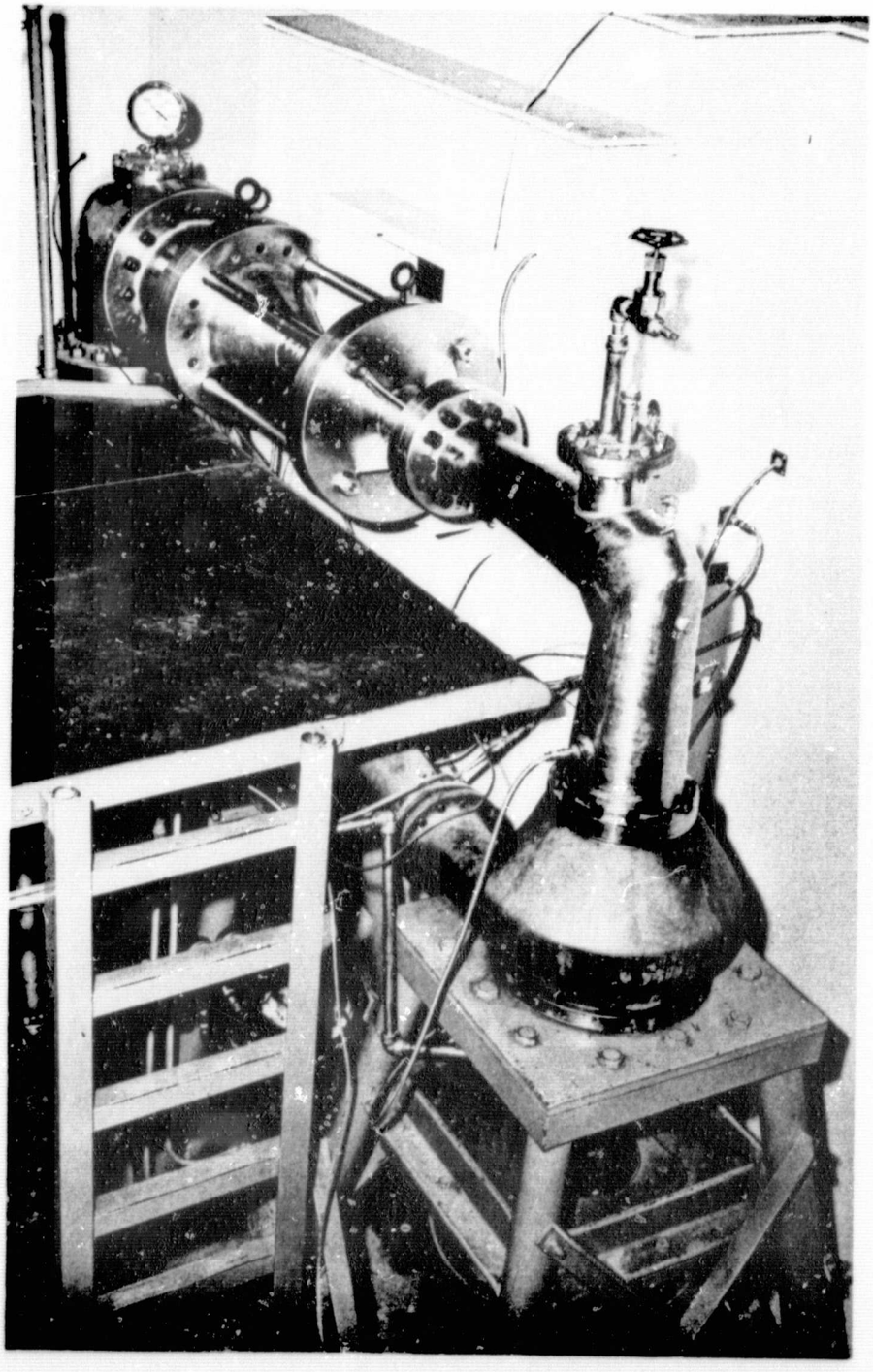

Figure 1: Photograph of 3.8 cm Ultra-High-Speed Cavitation Tunnel

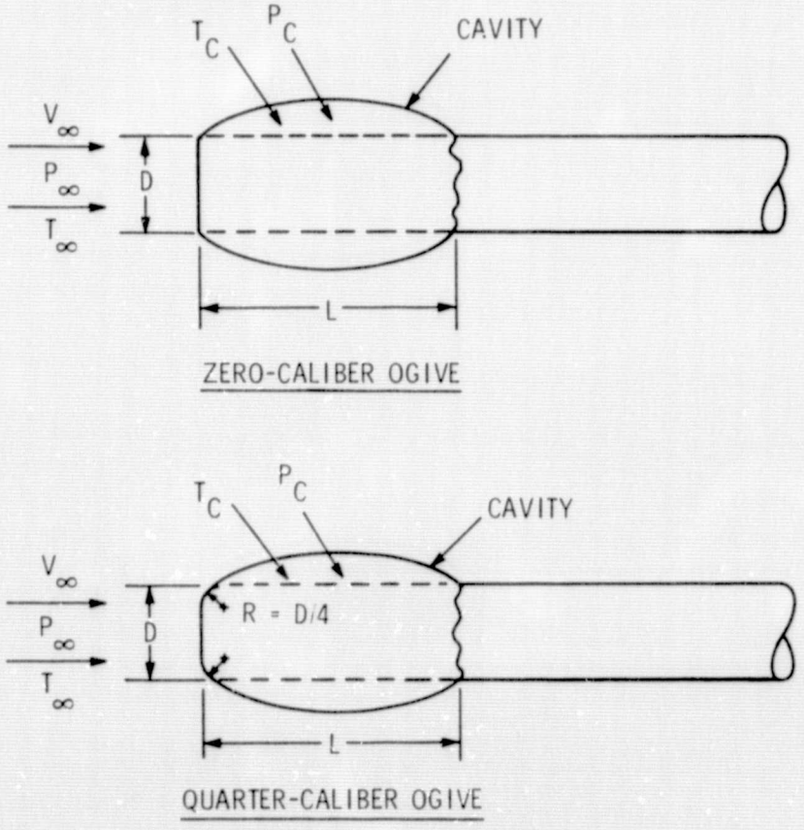

Figure 2: Description of the Nose Contour of Ogive Test Models

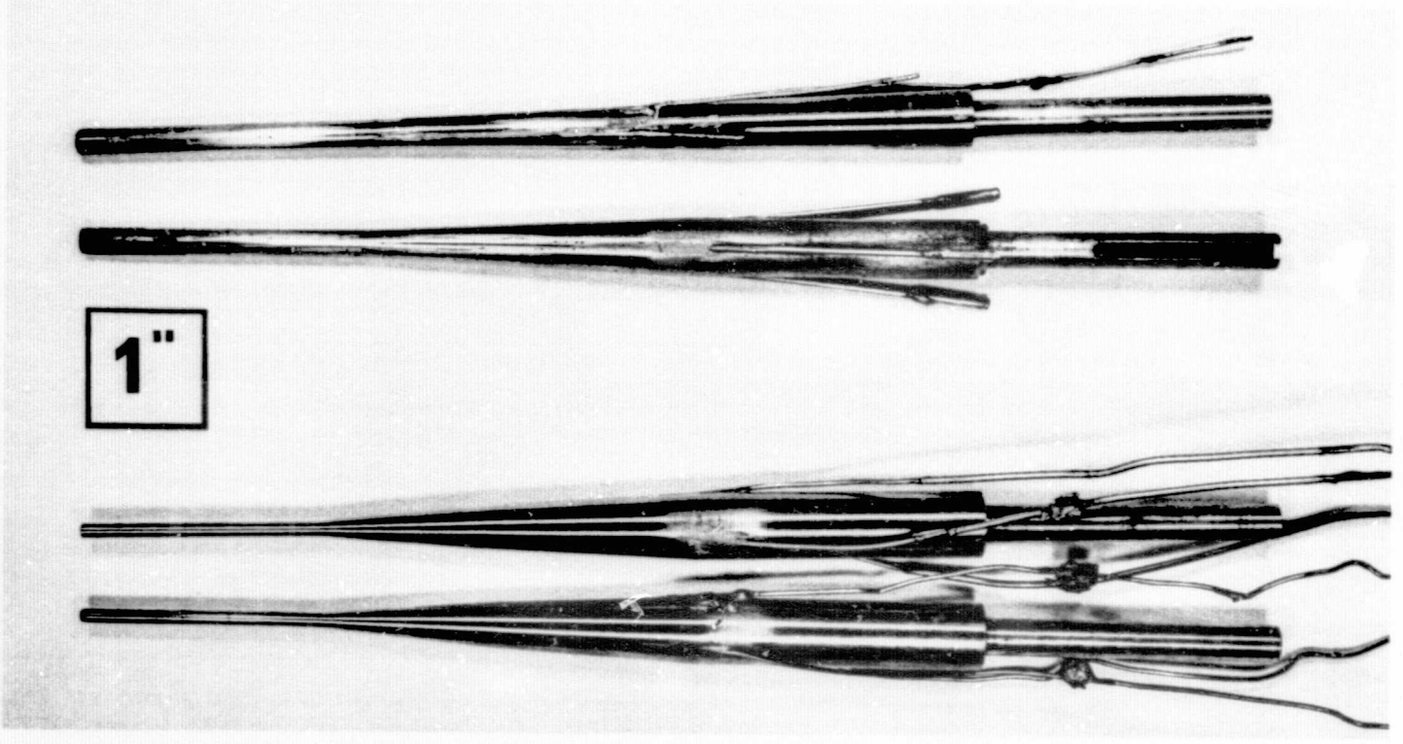

Figure 3: Photograph of Test Models for Cavity Pressure Measurements

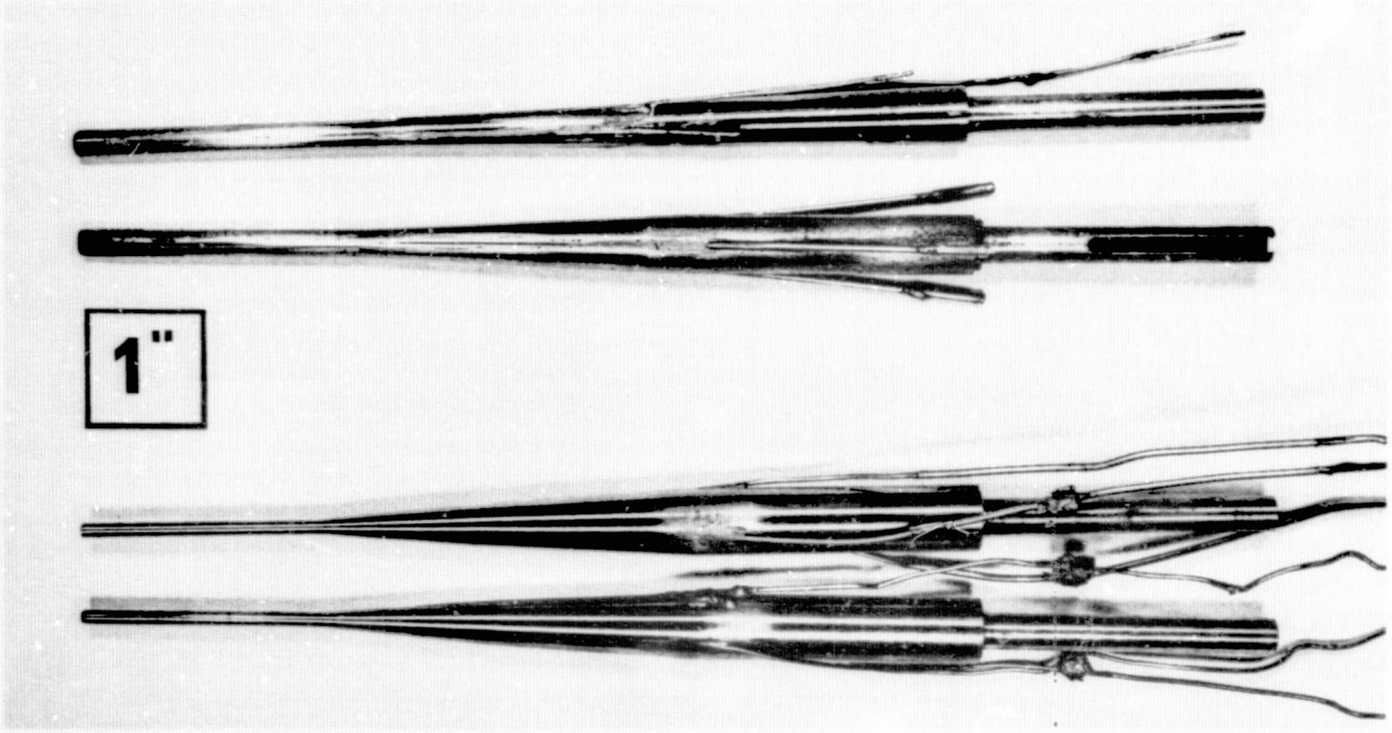

Figure 3: Photograph of Test Models for Cavity Pressure Measurements

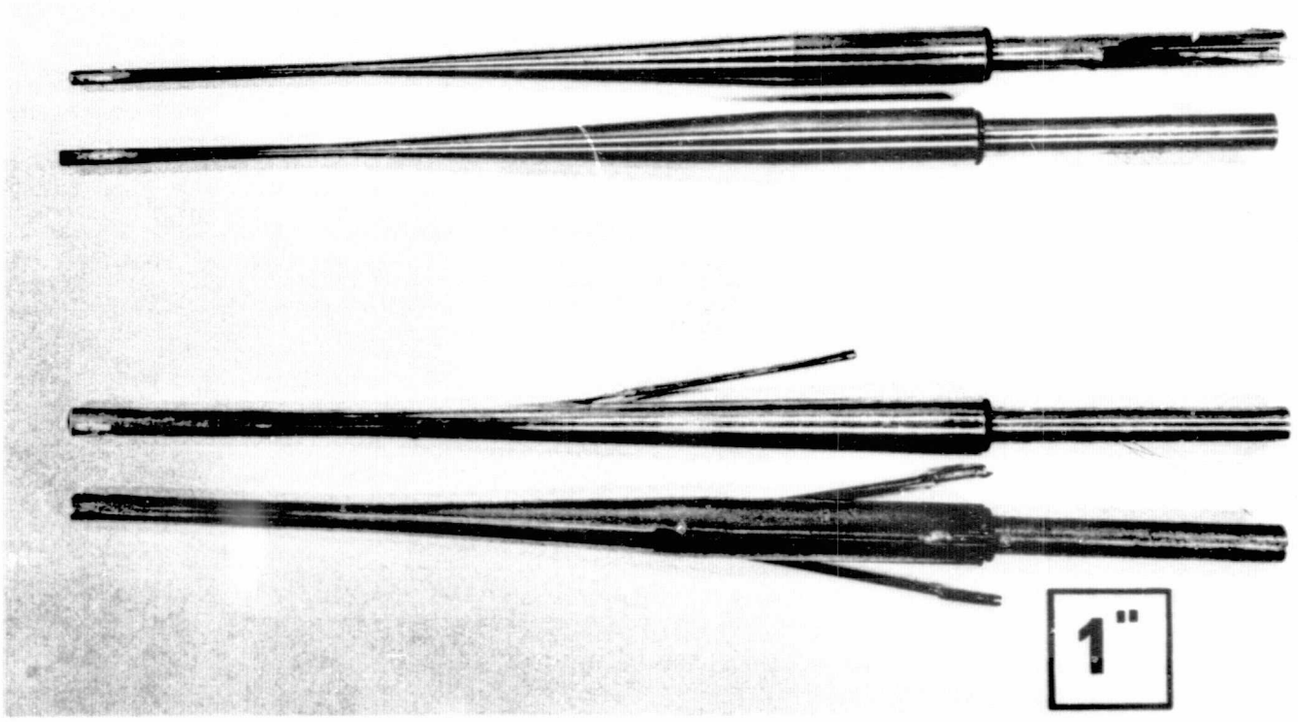

Figure 4: Photograph of Test Models for Cavity Temperature Measurements

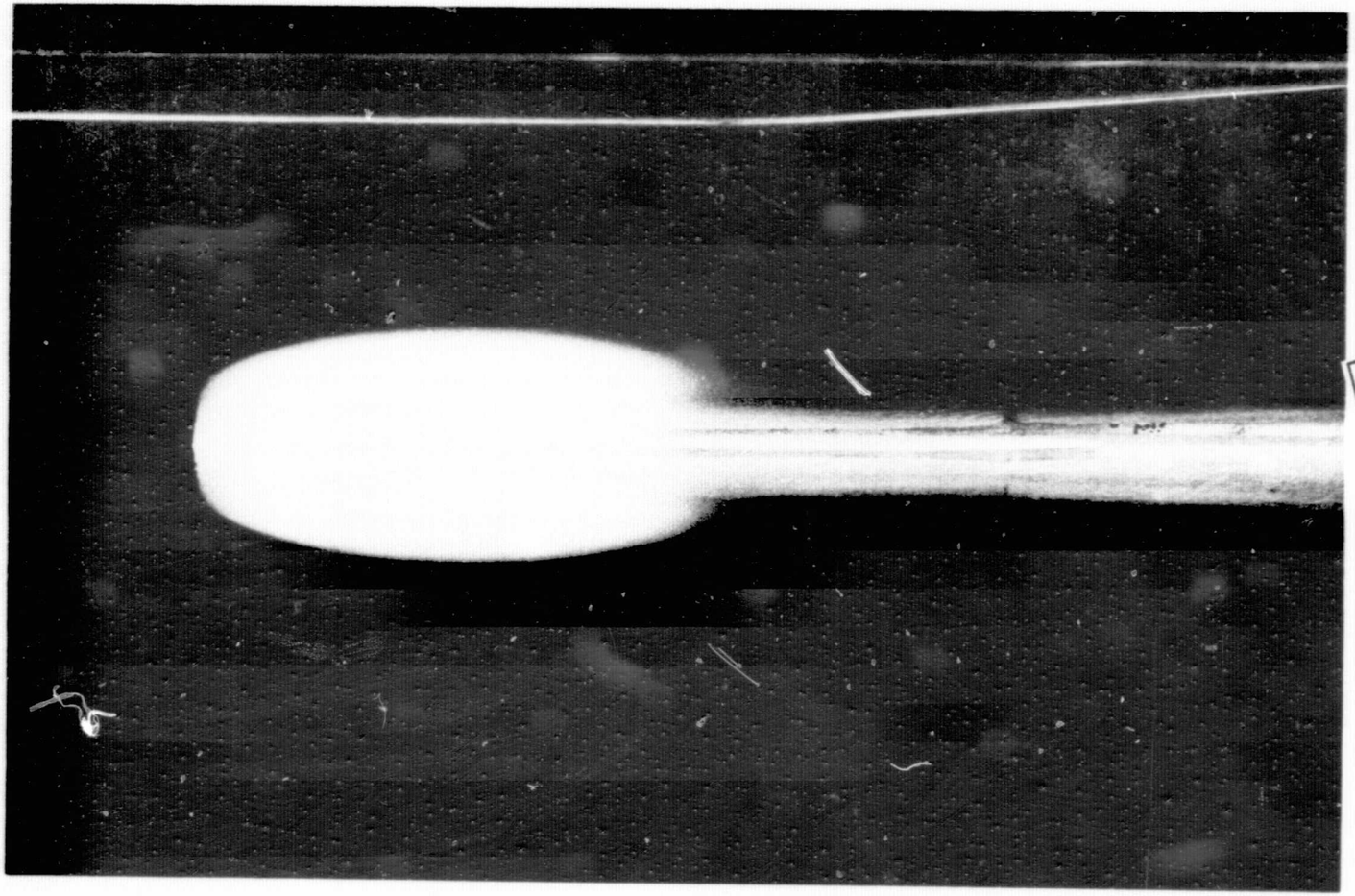

Figure 5: Photograph of a Developed Cavity on a Zero-Caliber Ogive in Water (D = 0.635 cm, V_∞ = 19.5 m/sec, and L/D = 5)

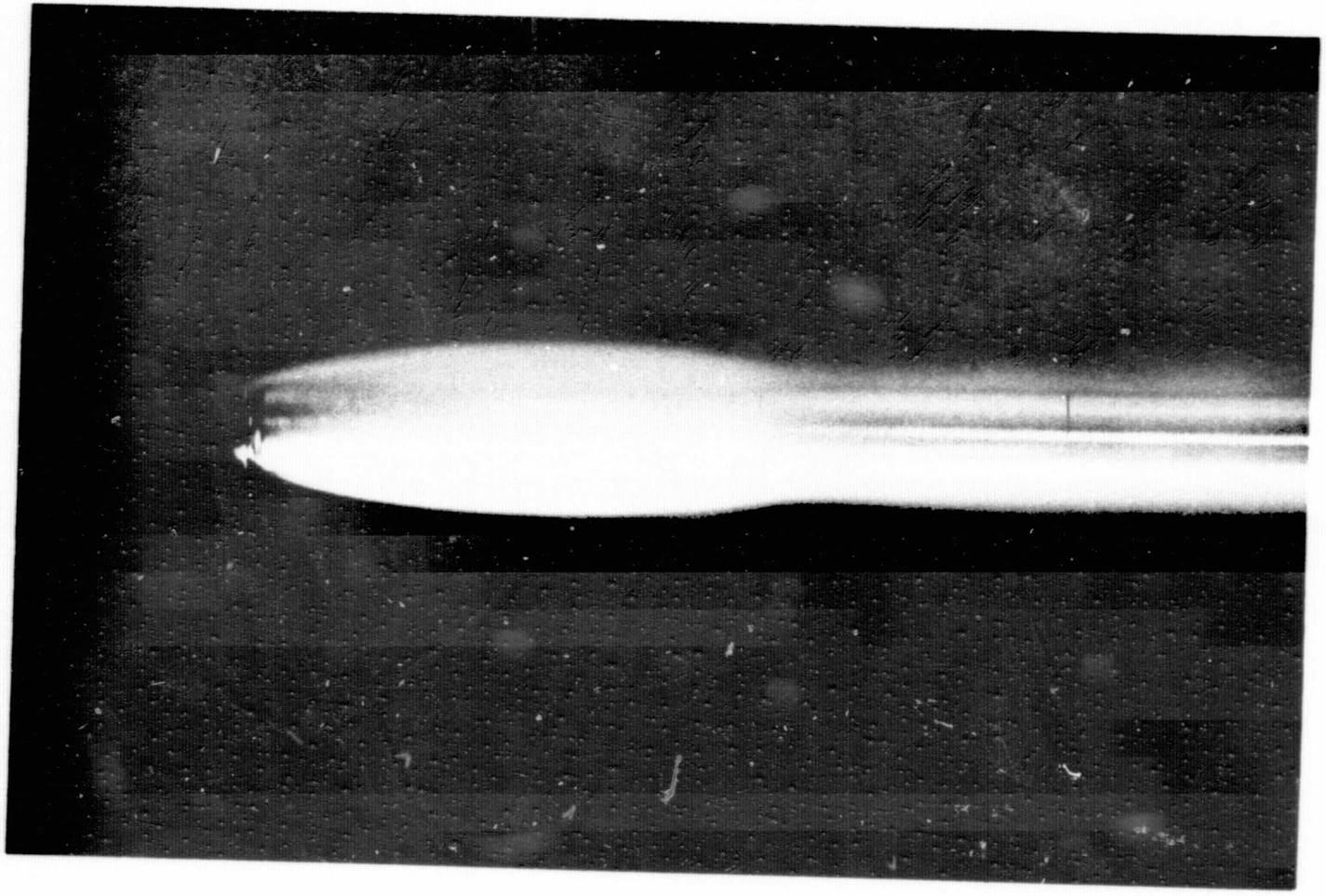

Figure 6: Photograph of a Developed Cavity on a Quarter-Caliber Ogive in Water (D = 0.635 cm, V_∞ = 19.5 m/sec, and L/D = 5)

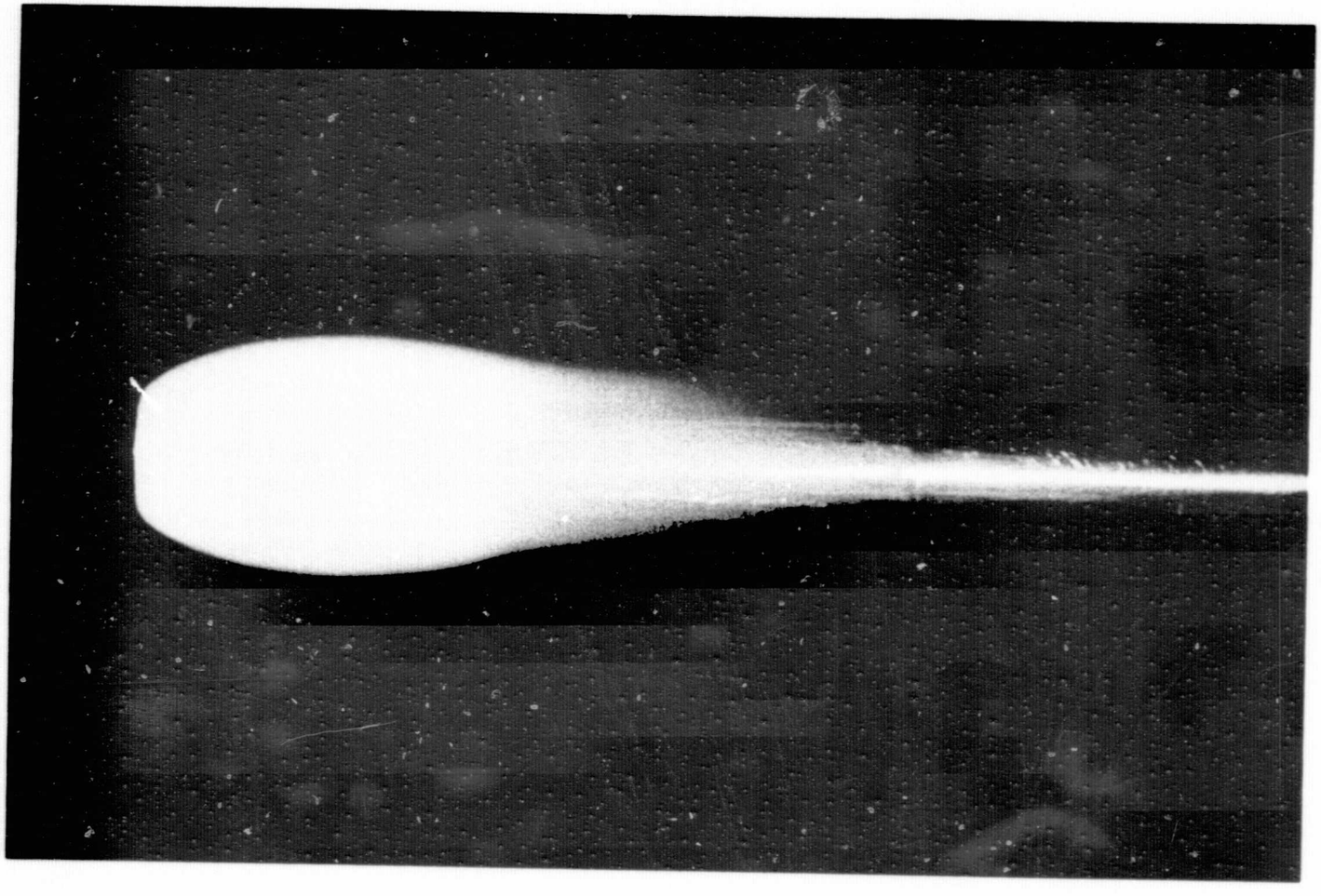

Figure 7: Photograph of a Developed Cavity on a Zero-Caliber Ogive in Freon 113 (D = 0.635 cm, V_∞ = 19.5 m/sec, and L/D = 5)

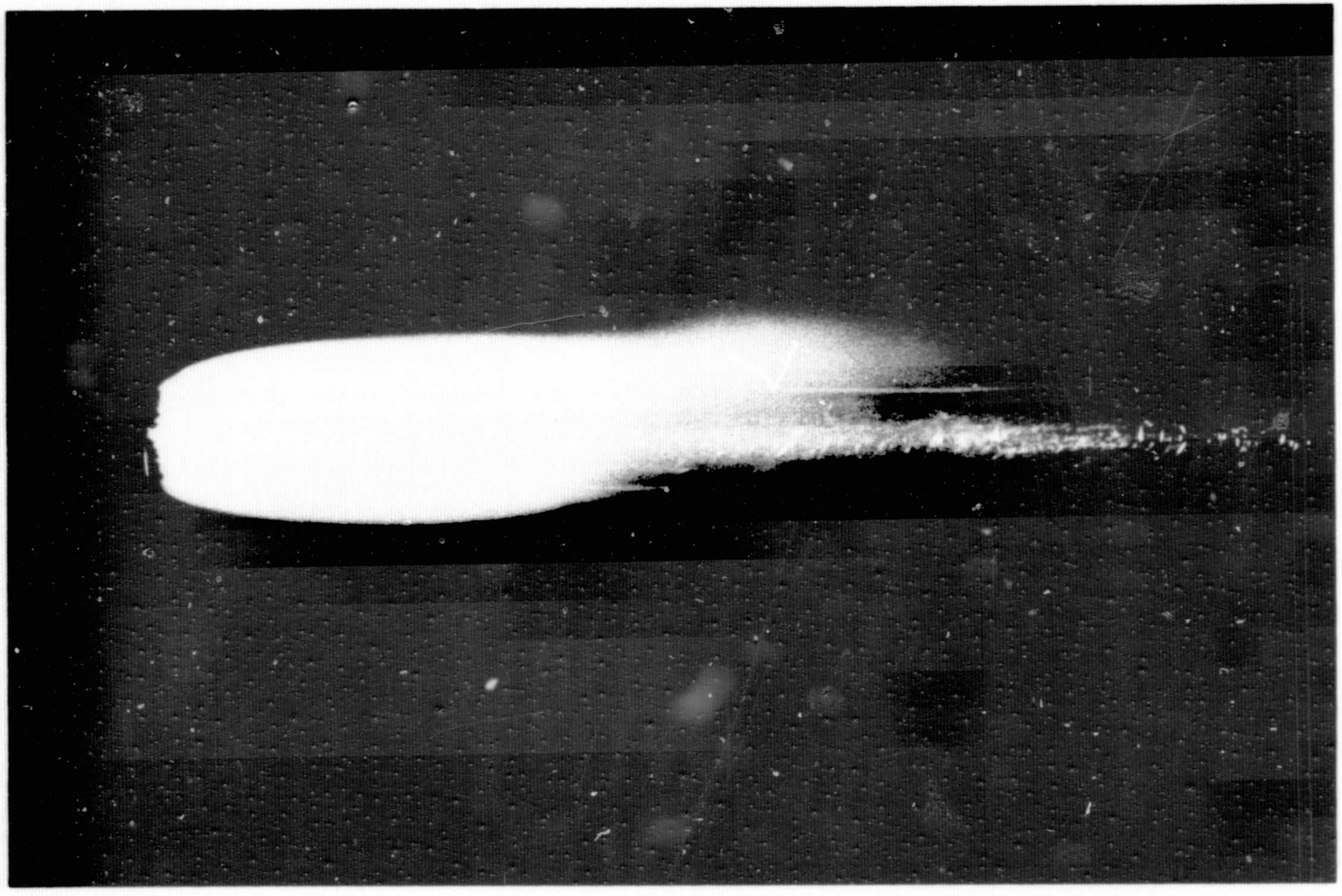

Figure 8: Photograph of a Developed Cavity on a Quarter-Caliber Ogive in Freon 113 (D = 0.635 cm, V_∞ = 19.5 m/sec, and L/D = 5)

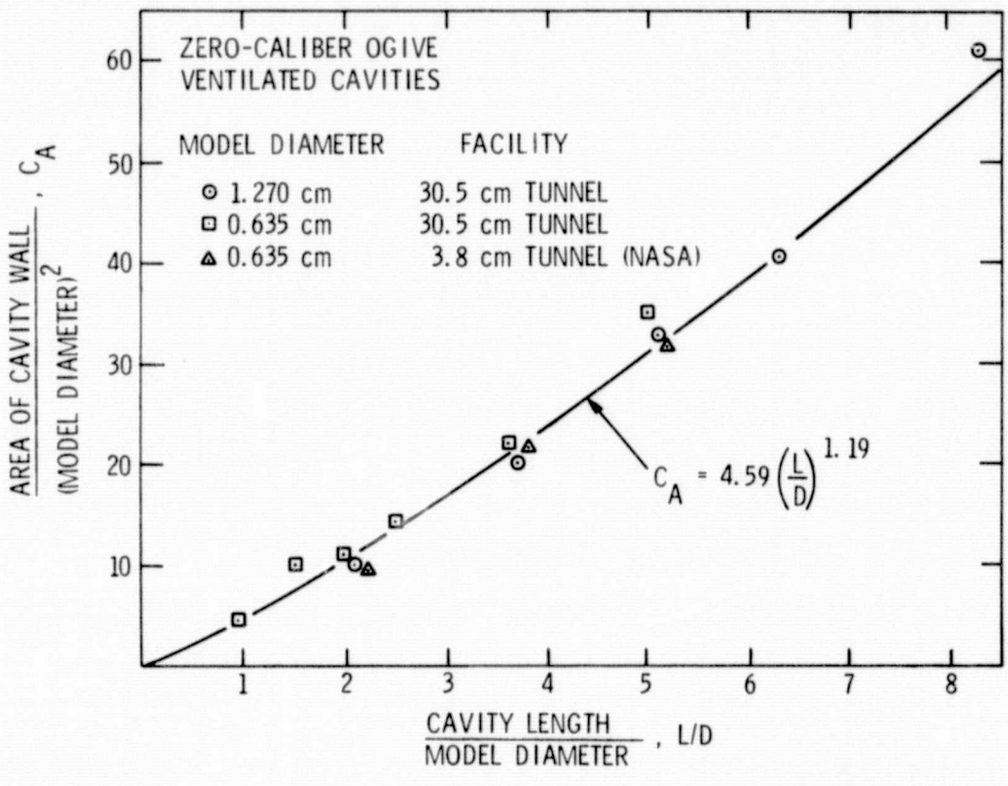

Figure 9: Area Coefficient Versus Dimensionless Cavity Length for the Zero-Caliber Ogives

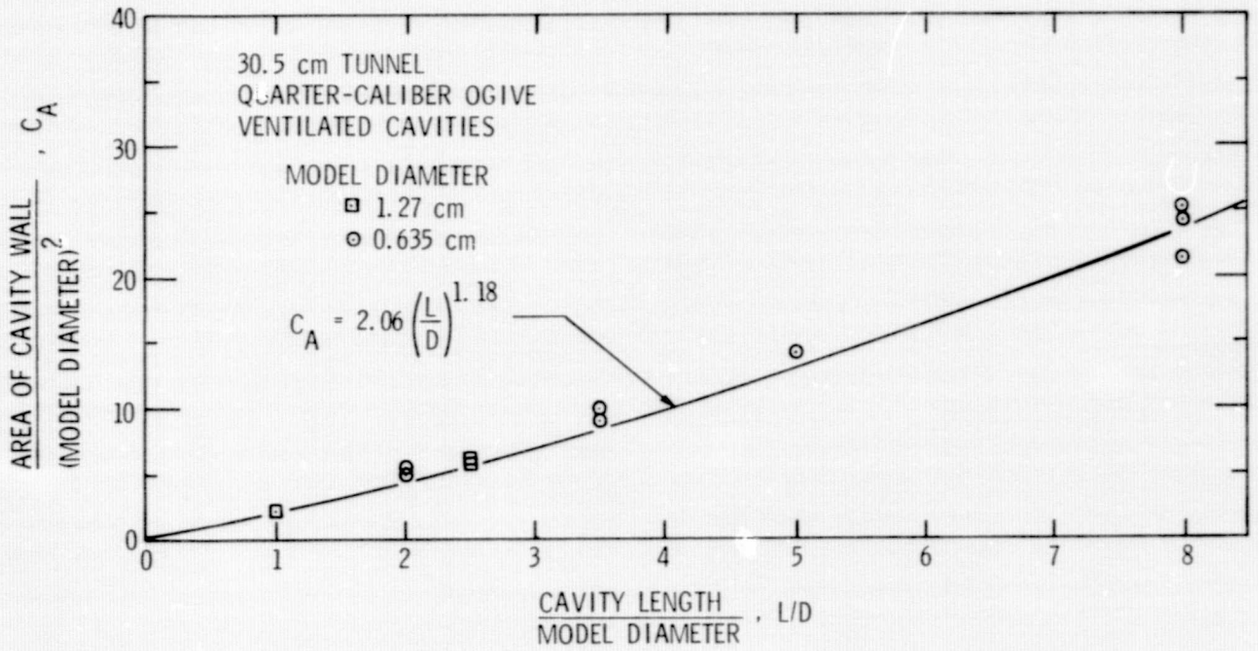

Figure 10: Area Coefficient Versus Dimensionless Cavity Length for the Quarter-Caliber Ogives

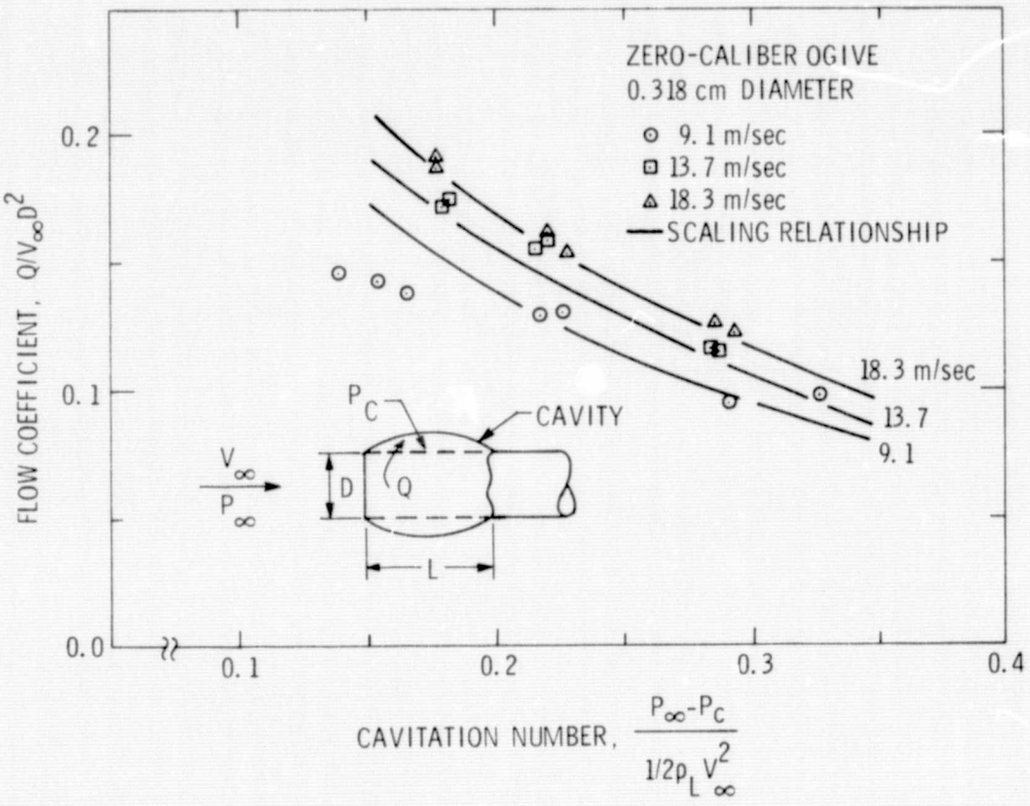

Figure 11: Flow Coefficient Versus Cavitation Number for the 0.318 cm Diameter Zero-Caliber Ogive

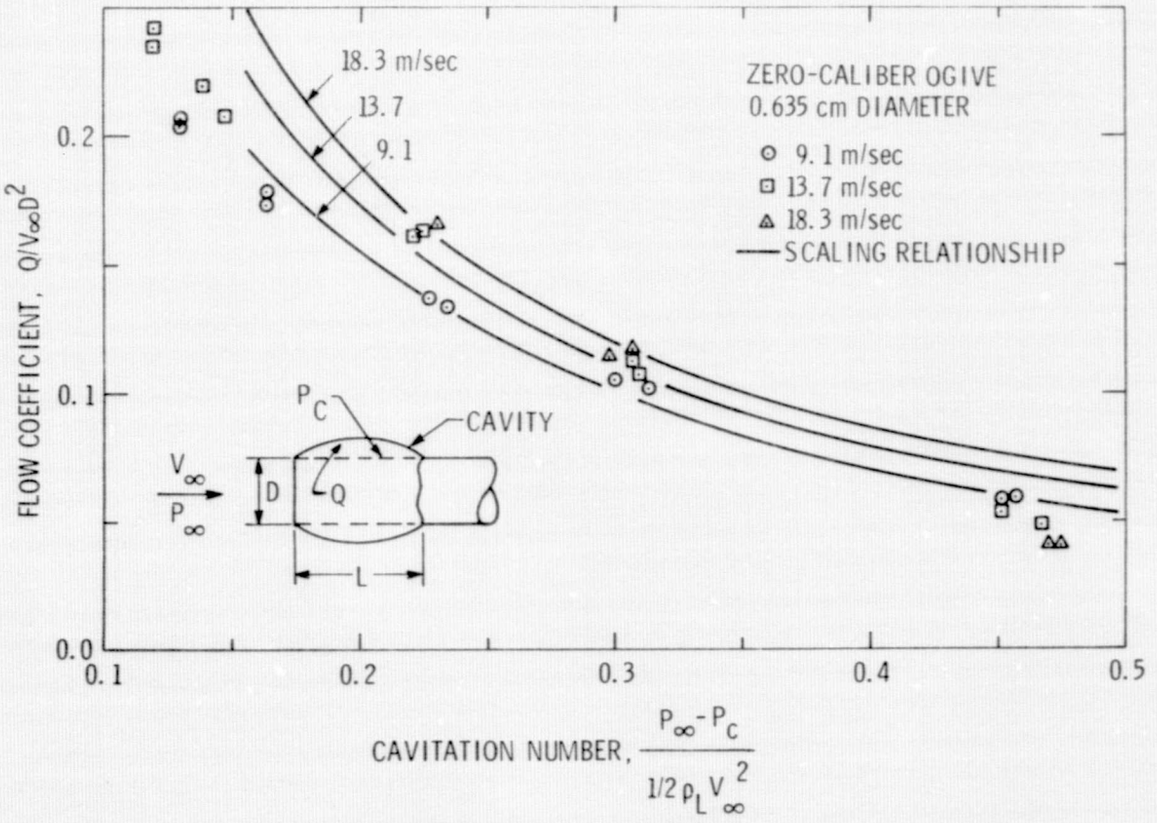

Figure 12: Flow Coefficient Versus Cavitation Number for the 0.635 cm Diameter Zero-Caliber Ogive

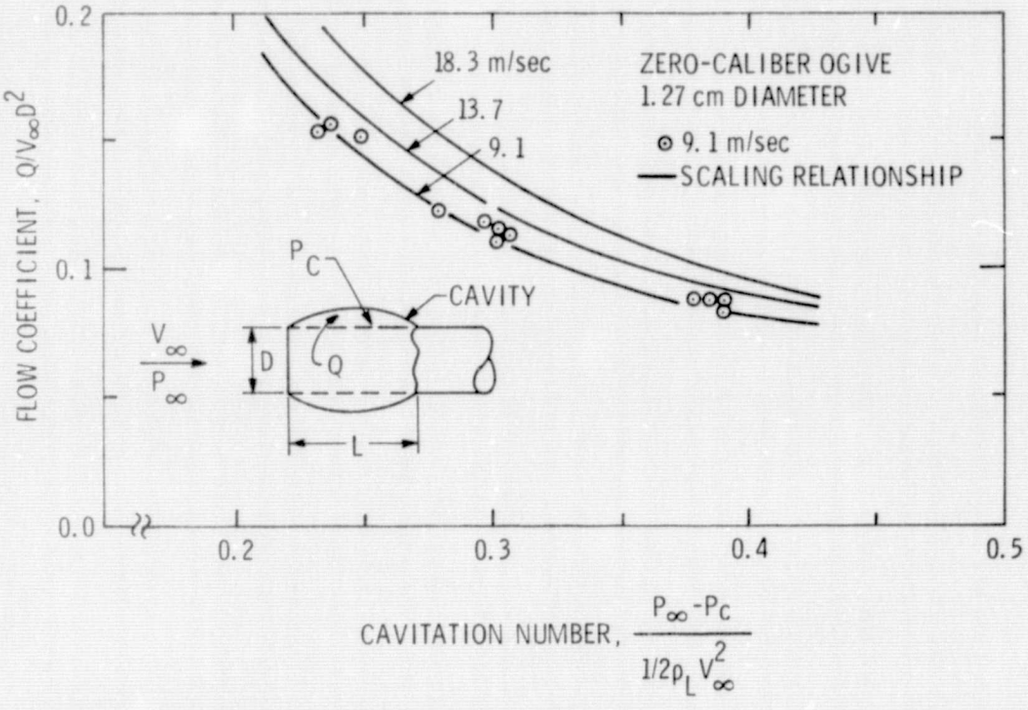

Figure 13: Flow Coefficient Versus Cavitation Number for the 1.27 cm Diameter Zero-Caliber Ogive

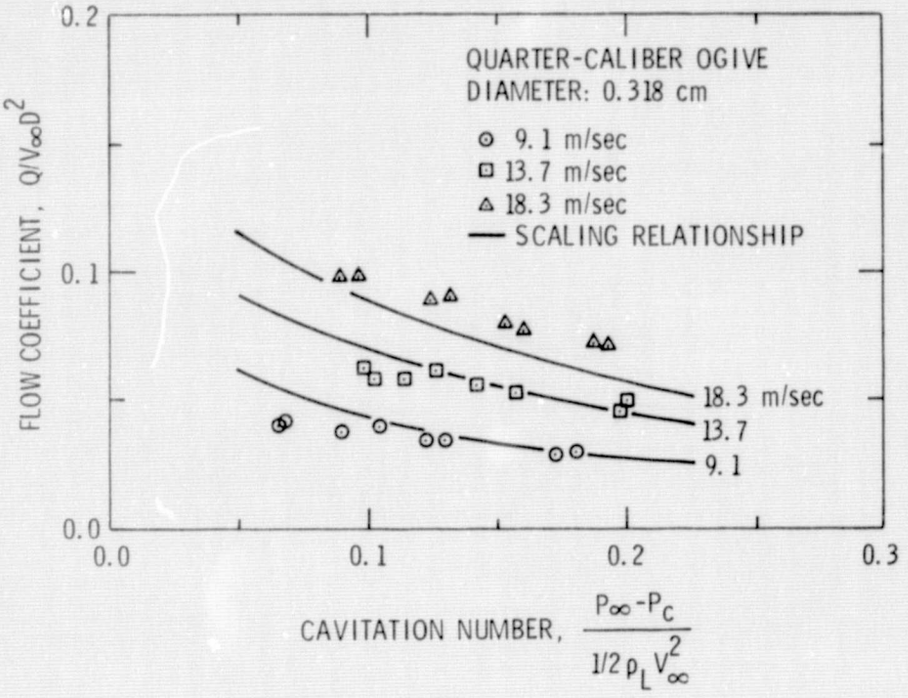

Figure 14: Flow Coefficient Versus Cavitation Number for the 0.318 cm Diameter Quarter-Caliber Ogive

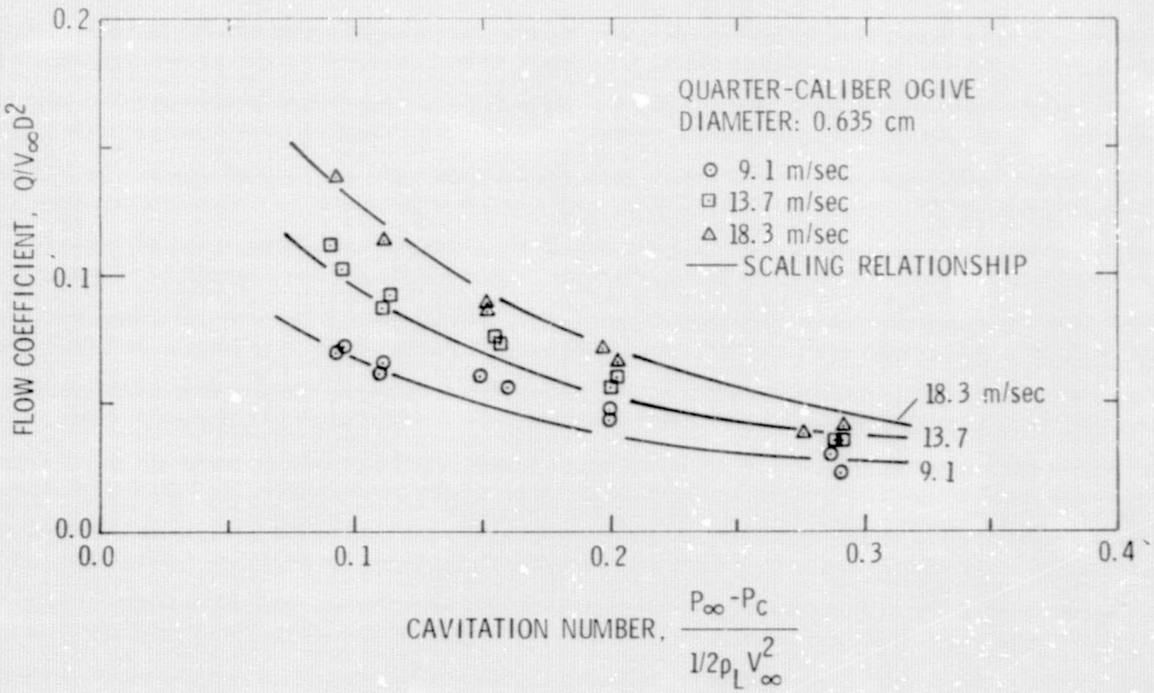

Figure 15: Flow Coefficient Versus Cavitation Number for the 0.635 cm Diameter Quarter-Caliber Ogive

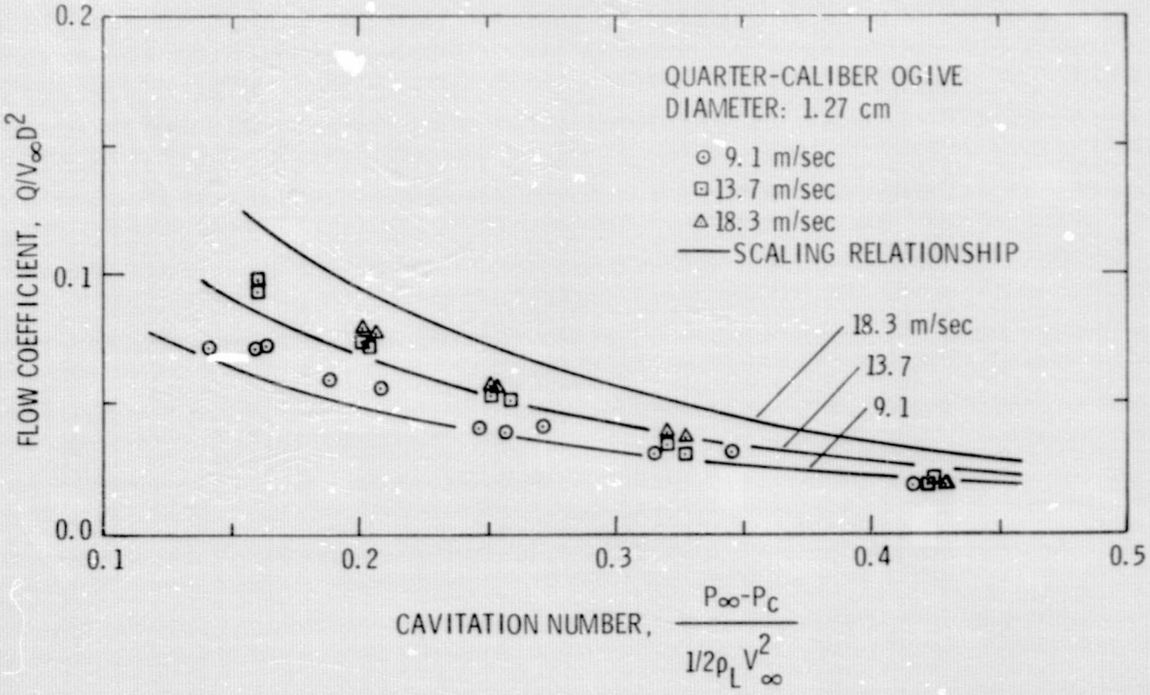

Figure 16: Flow Coefficient Versus Cavitation Number for the 1.27 cm Diameter Quarter-Caliber Ogive

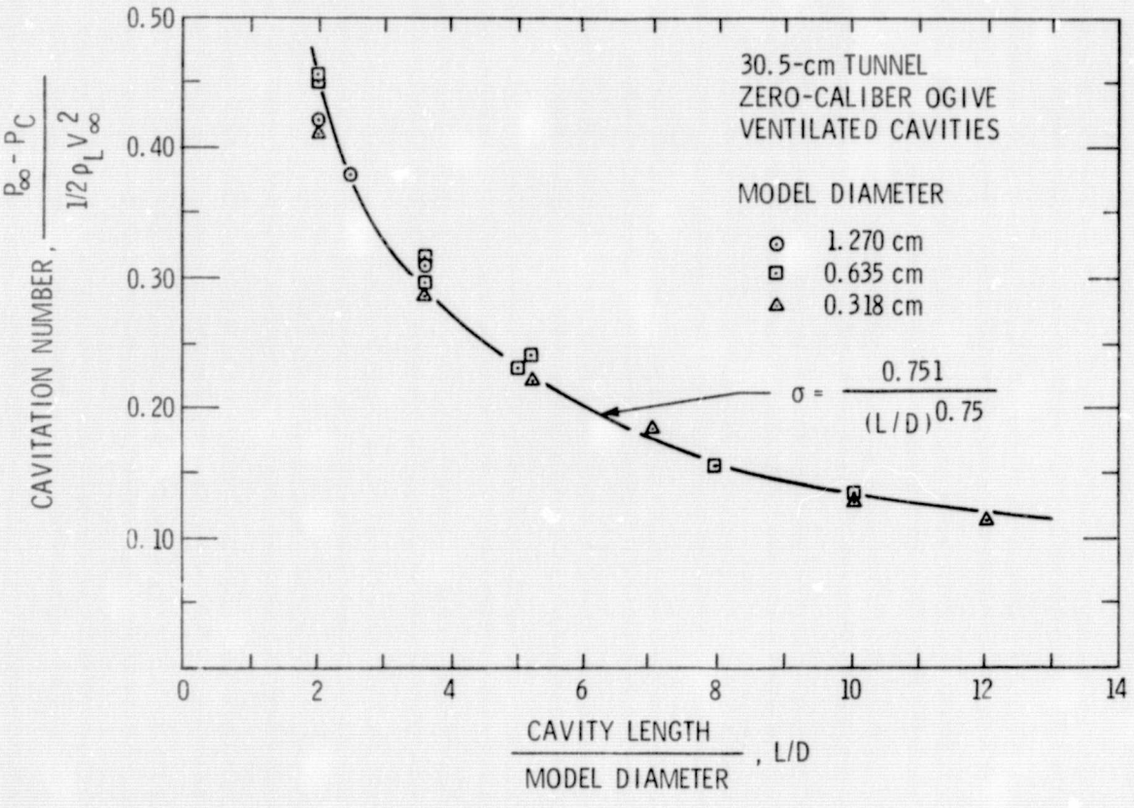

Figure 17: Cavitation Number Versus Dimensionless Cavity Length for the Zero-Caliber Ogives in the 30.5 cm Water Tunnel (No Blockage)

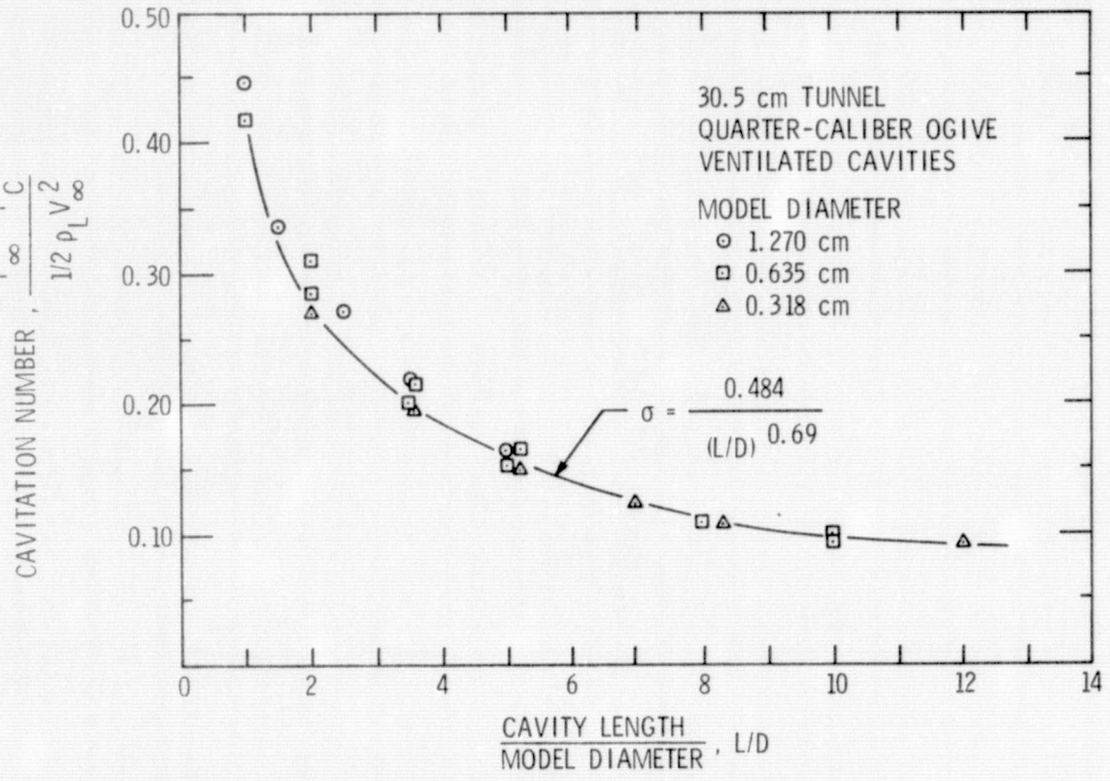

Figure 18: Cavitation Number Versus Dimensionless Cavity Length for the Quarter-Caliber Ogives in the 30.5 cm Water Tunnel (No Blockage)

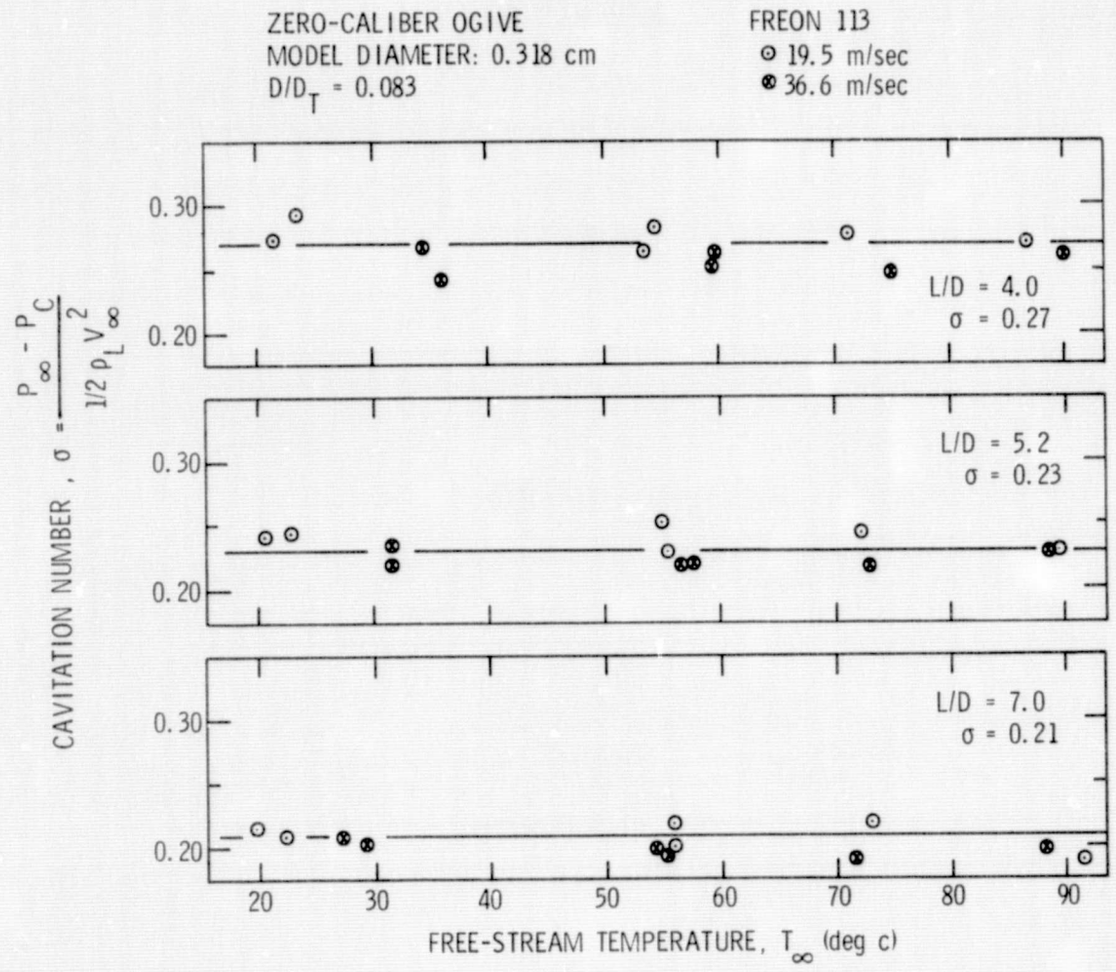

Figure 19: Cavitation Number Versus Free Stream Temperature for the 0.318 cm Diameter Zero-Caliber Ogive in the 3.8 cm Tunnel ($D/D_T = 0.083$)

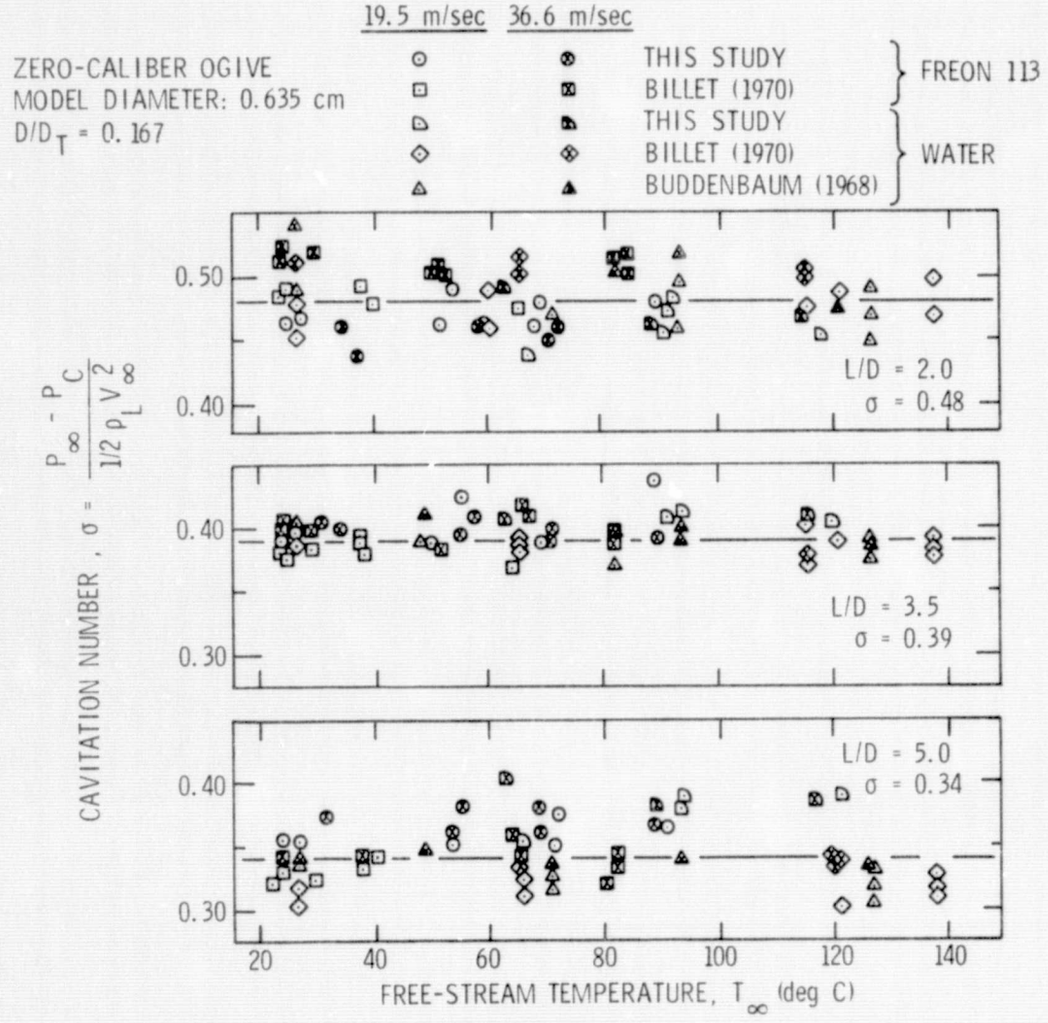

Figure 20: Cavitation Number Versus Free Stream Temperature for the 0.635 cm Diameter Zero-Caliber Ogive in the 3.8 cm Tunnel ($D/D_T = 0.167$)

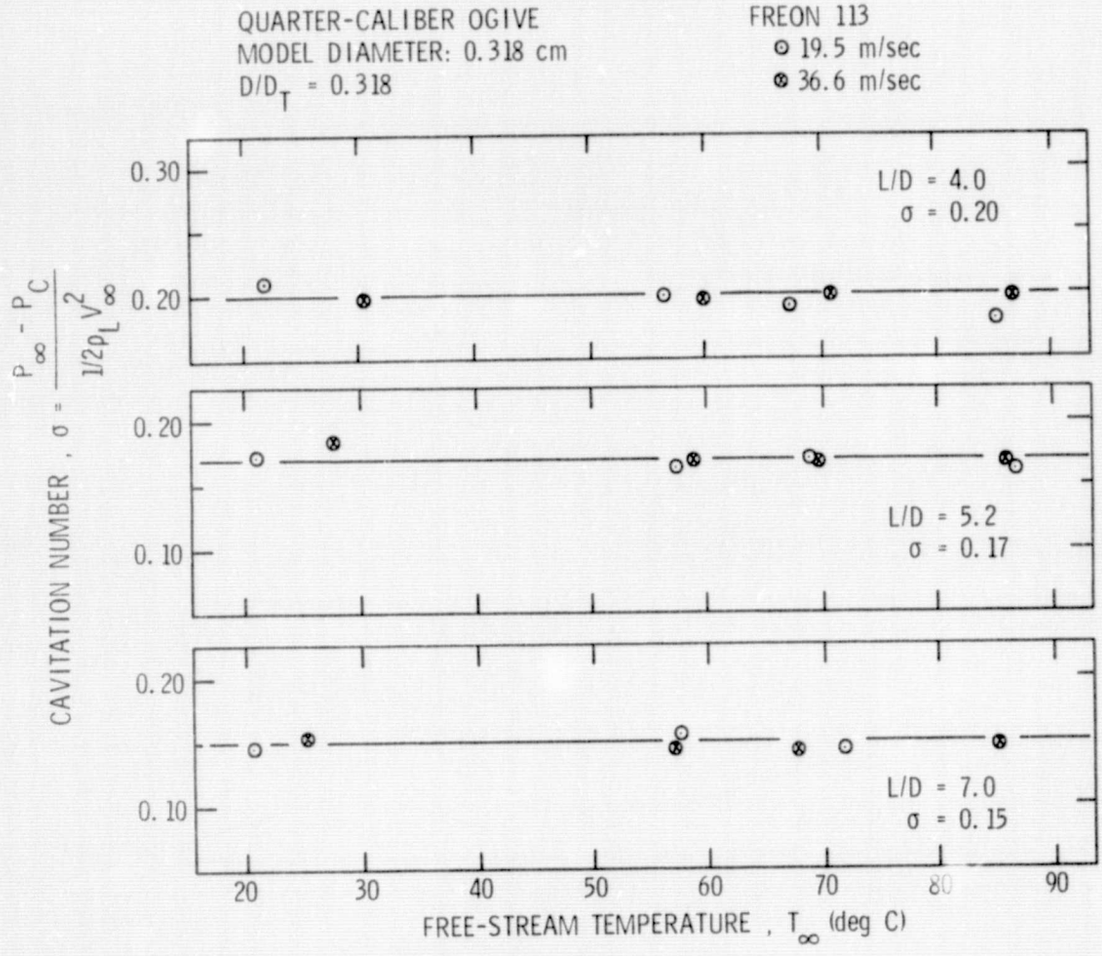

Figure 21: Cavitation Number Versus Free Stream Temperature for the 0.318 cm Diameter Quarter-Caliber Ogive in the 3.8 cm Tunnel ($D/D_T = 0.083$)

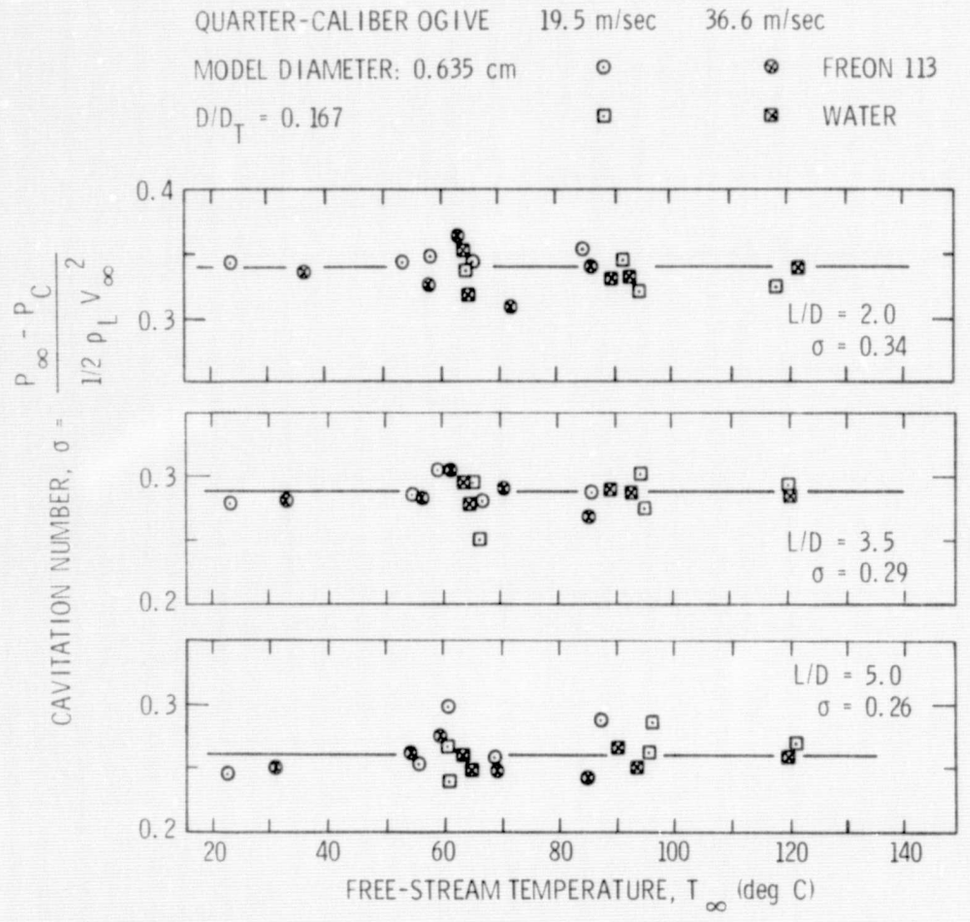

Figure 22: Cavitation Number Versus Free Stream Temperature for the 0.635 cm Diameter Quarter-Caliber Ogive in the 3.8 cm Tunnel ($D/D_T = 0.167$)

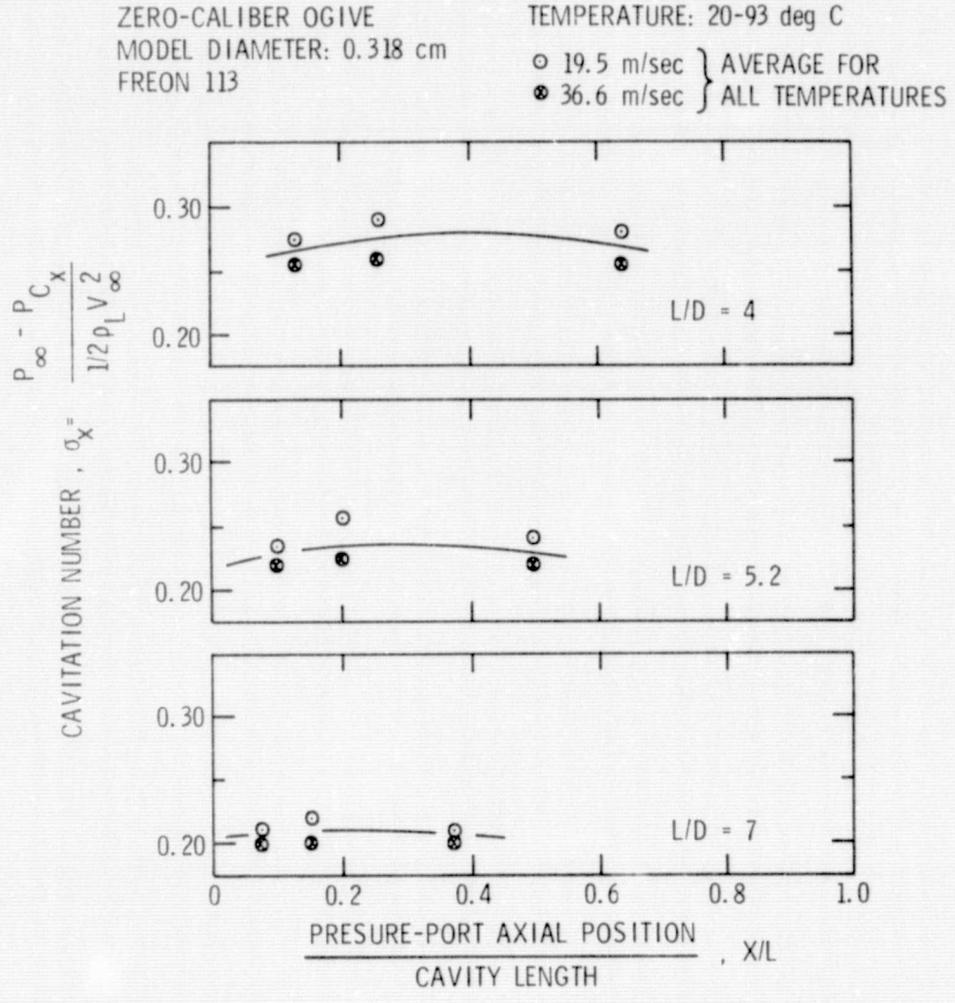

Figure 23: Cavitation Number Versus Dimensionless Axial Position for the 0.318 cm Diameter Zero-Caliber Ogive in the 3.8 cm Tunnel

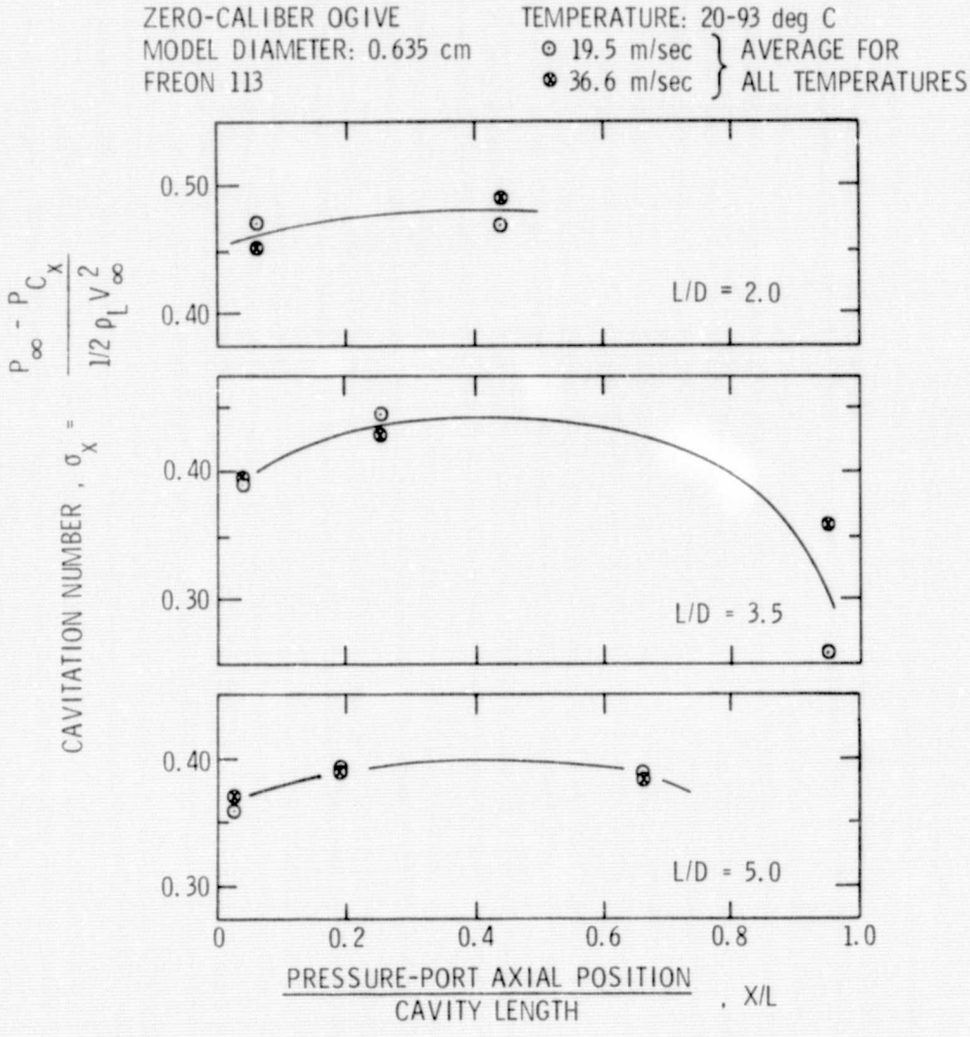

Figure 24: Cavitation Number Versus Dimensionless Axial Position for the 0.635 cm Diameter Zero-Caliber Ogive in the 3.8 cm Tunnel

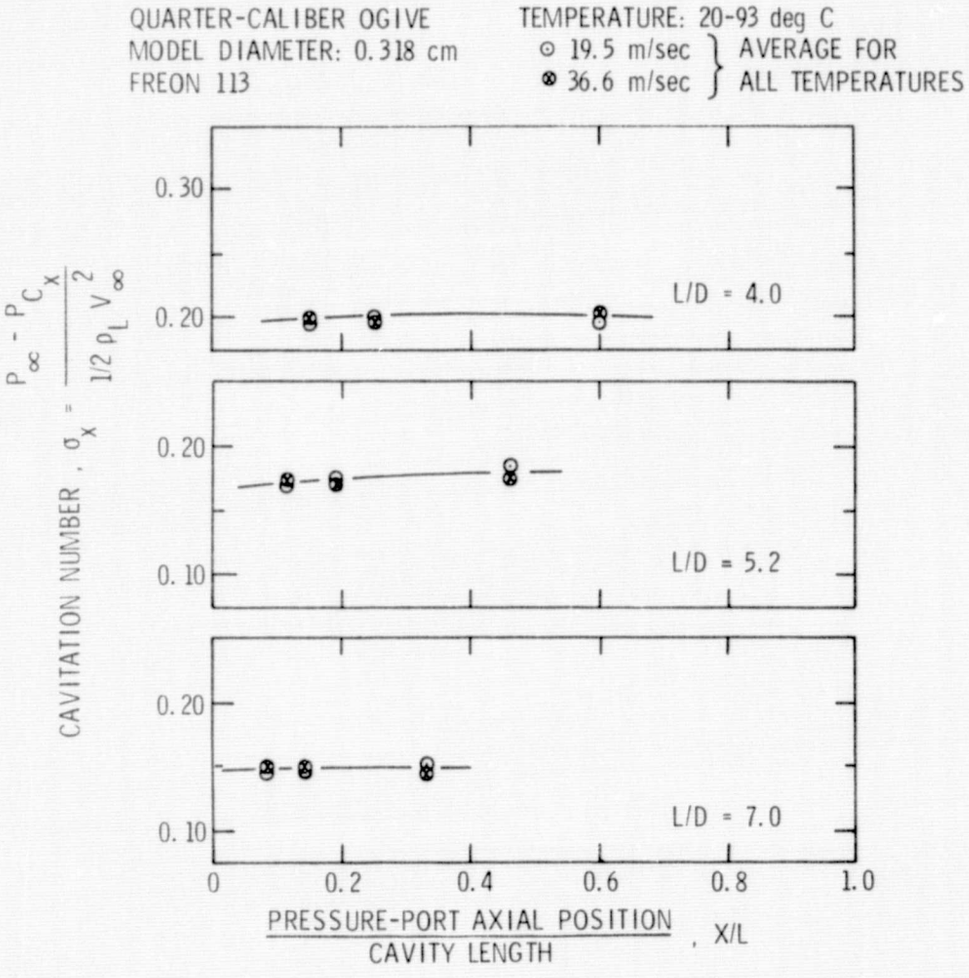

Figure 25: Cavitation Number Versus Dimensionless Axial Position for the 0.318 cm Diameter Quarter-Caliber Ogive in the 3.8 cm Tunnel

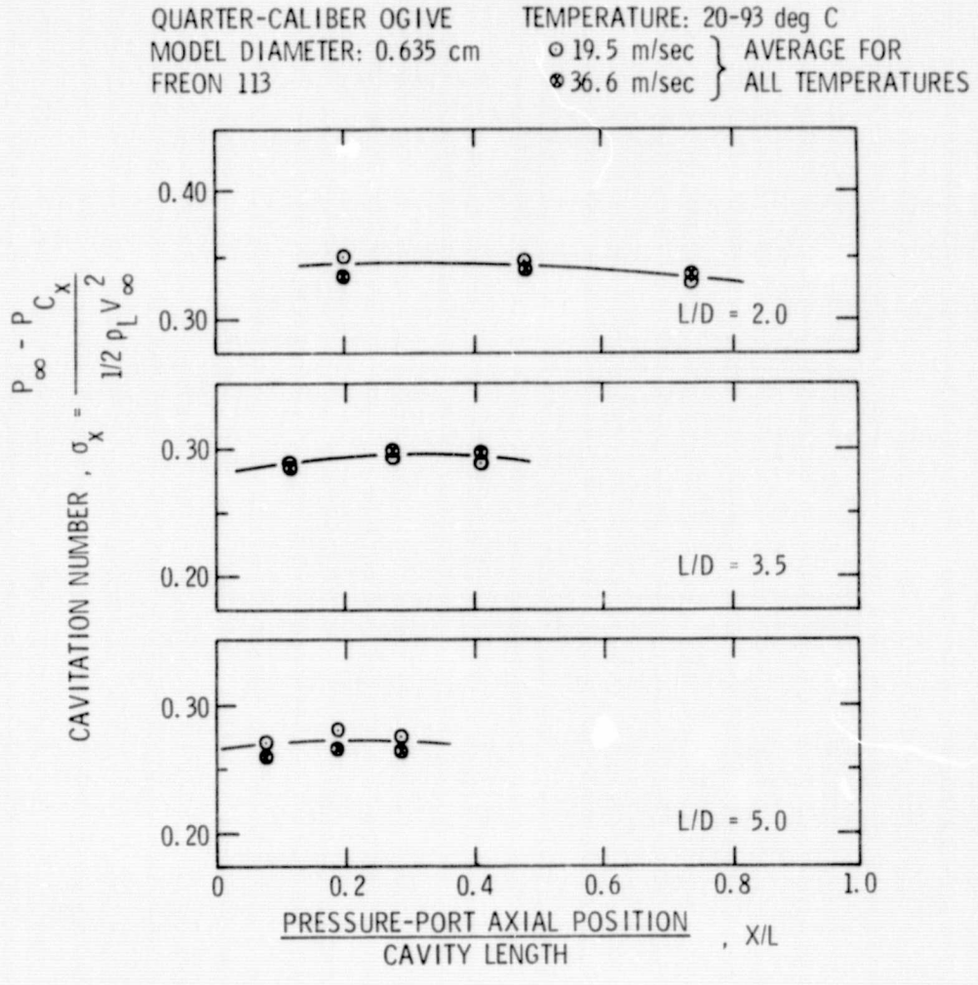

Figure 26: Cavitation Number Versus Dimensionless Axial Position for the 0.635 cm Diameter Quarter-Caliber Ogive in the 3.8 cm Tunnel

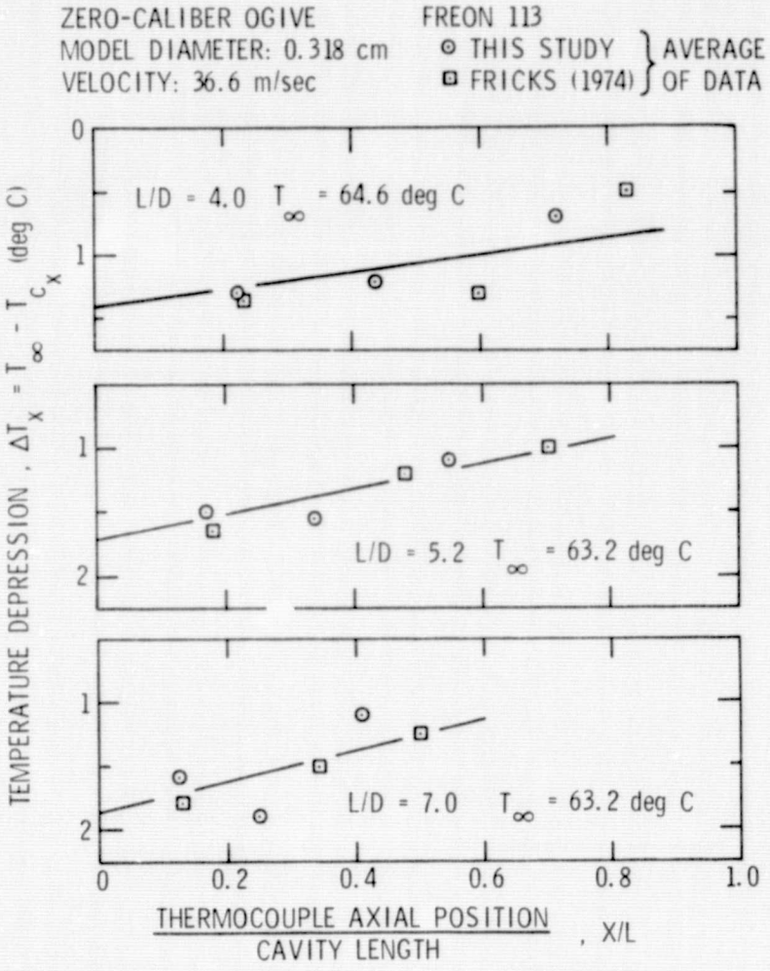

Figure 27: Typical Temperature Depression Versus Dimensionless Axial Position Data for the 0.318 cm Diameter Zero-Caliber Ogive in Freon 113

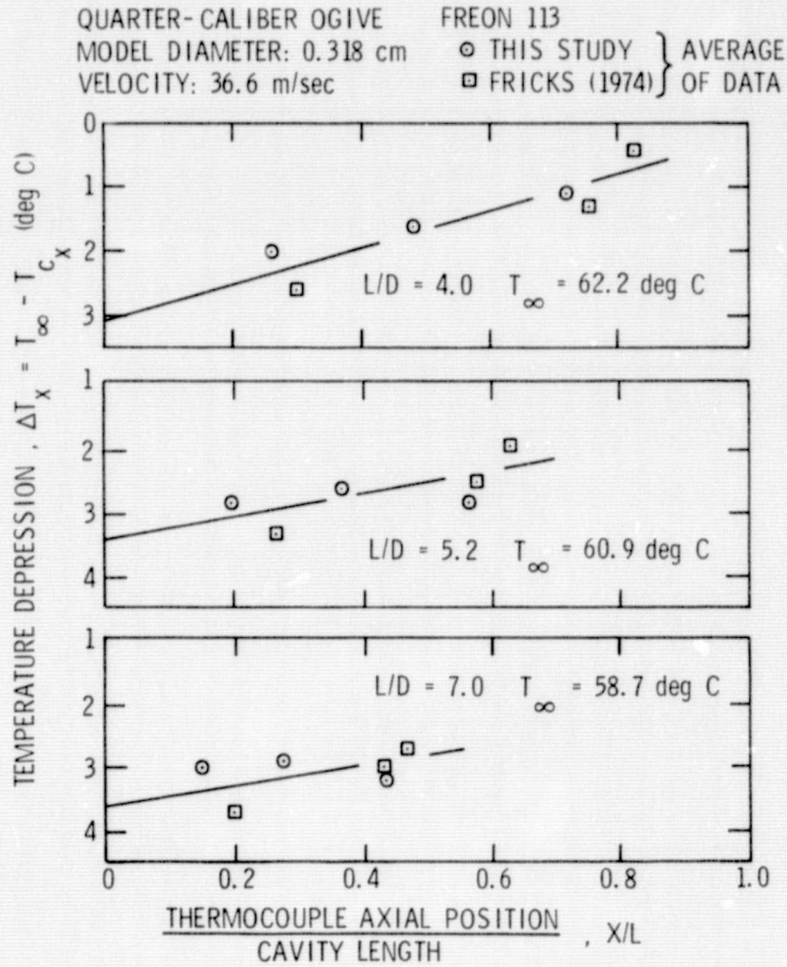

Figure 28: Typical Temperature Depression Versus Dimensionless Axial Position Data for the 0.318 cm Diameter Quarter-Caliber Ogive in Freon 113

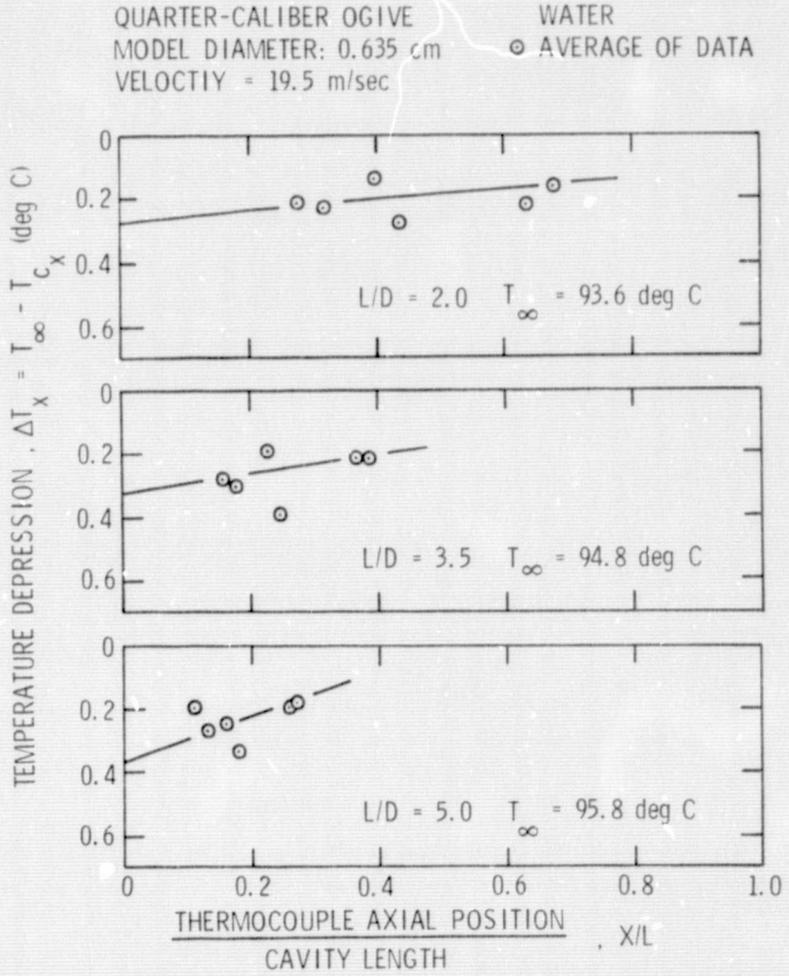

Figure 29: Typical Temperature Depression Versus Dimensionless Axial Position Data for the 0.635 cm Diameter Quarter-Caliber Ogive in Water

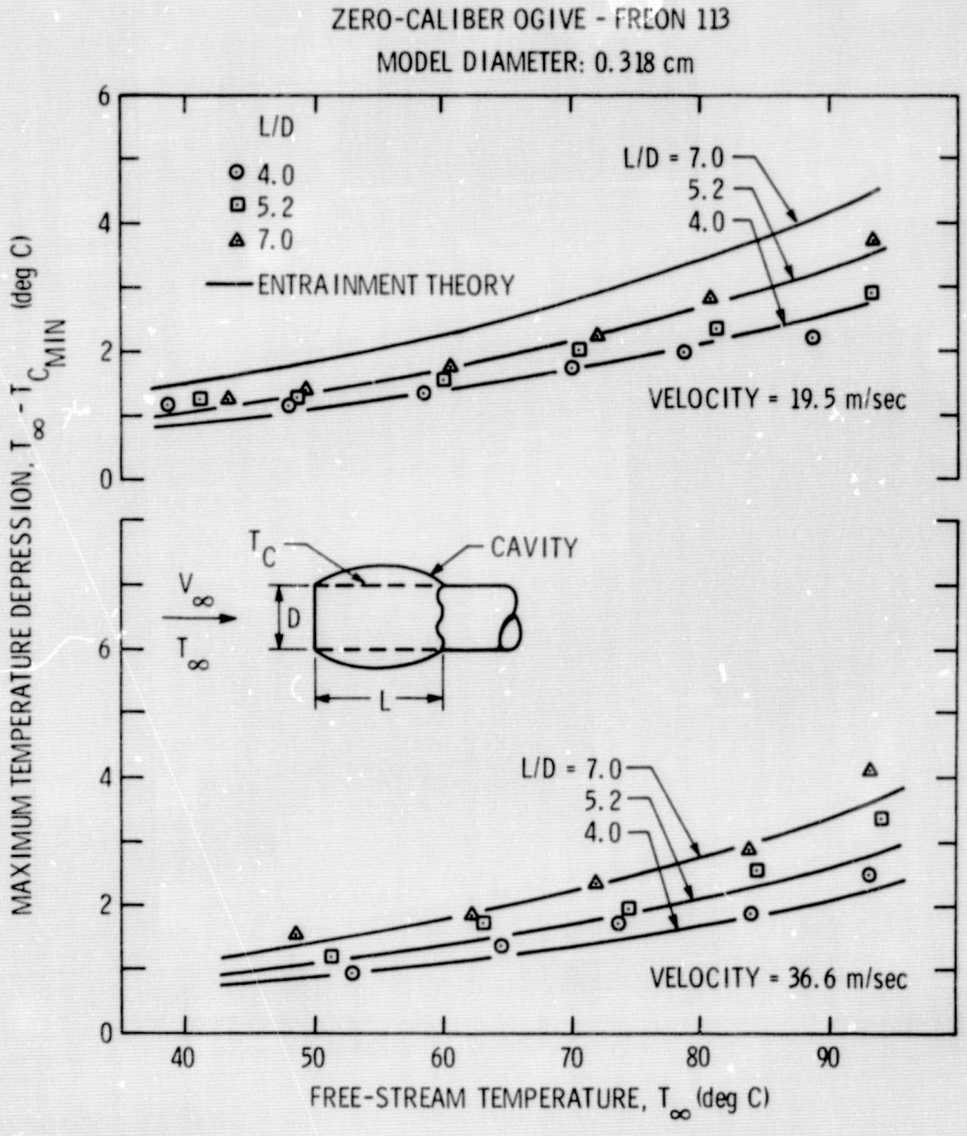

Figure 30: Maximum Temperature Depression Versus Free Stream Temperature for the 0.318 cm Diameter Zero-Caliber Ogive in Freon 113

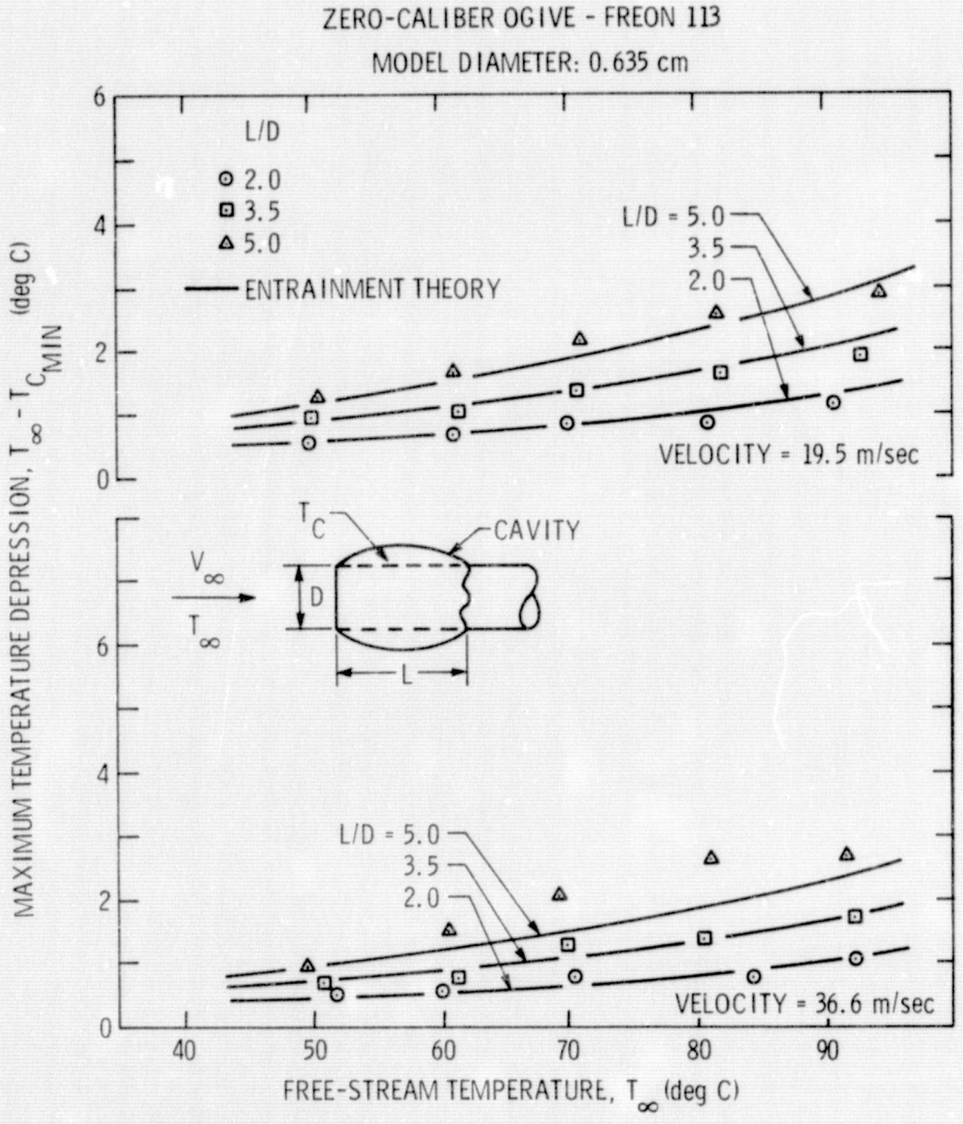

Figure 31: Maximum Temperature Depression Versus Free Stream Temperature for the 0.635 cm Diameter Zero-Caliber Ogive in Freon 113

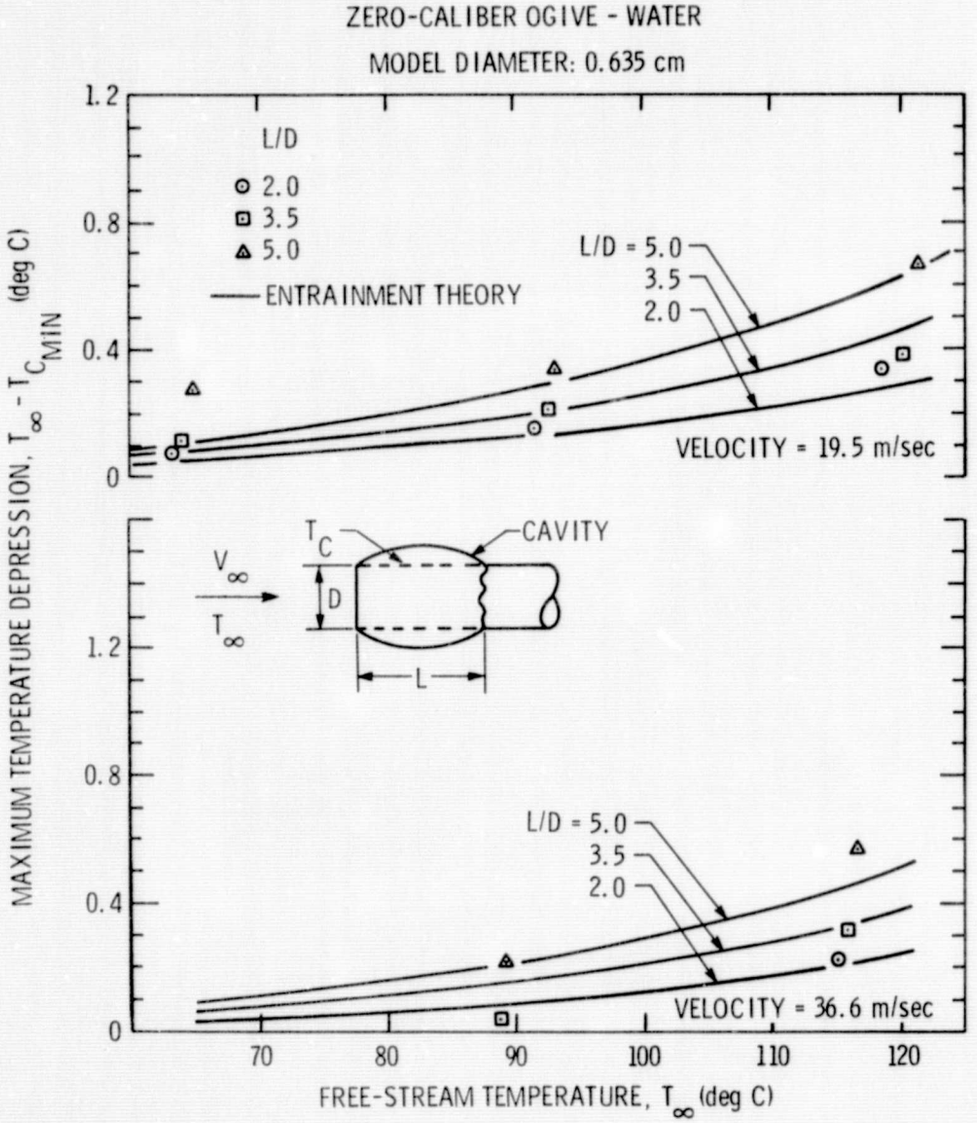

Figure 32: Maximum Temperature Depression Versus Free Stream Temperature for the 0.635 cm Diameter Zero-Caliber Ogive in Water

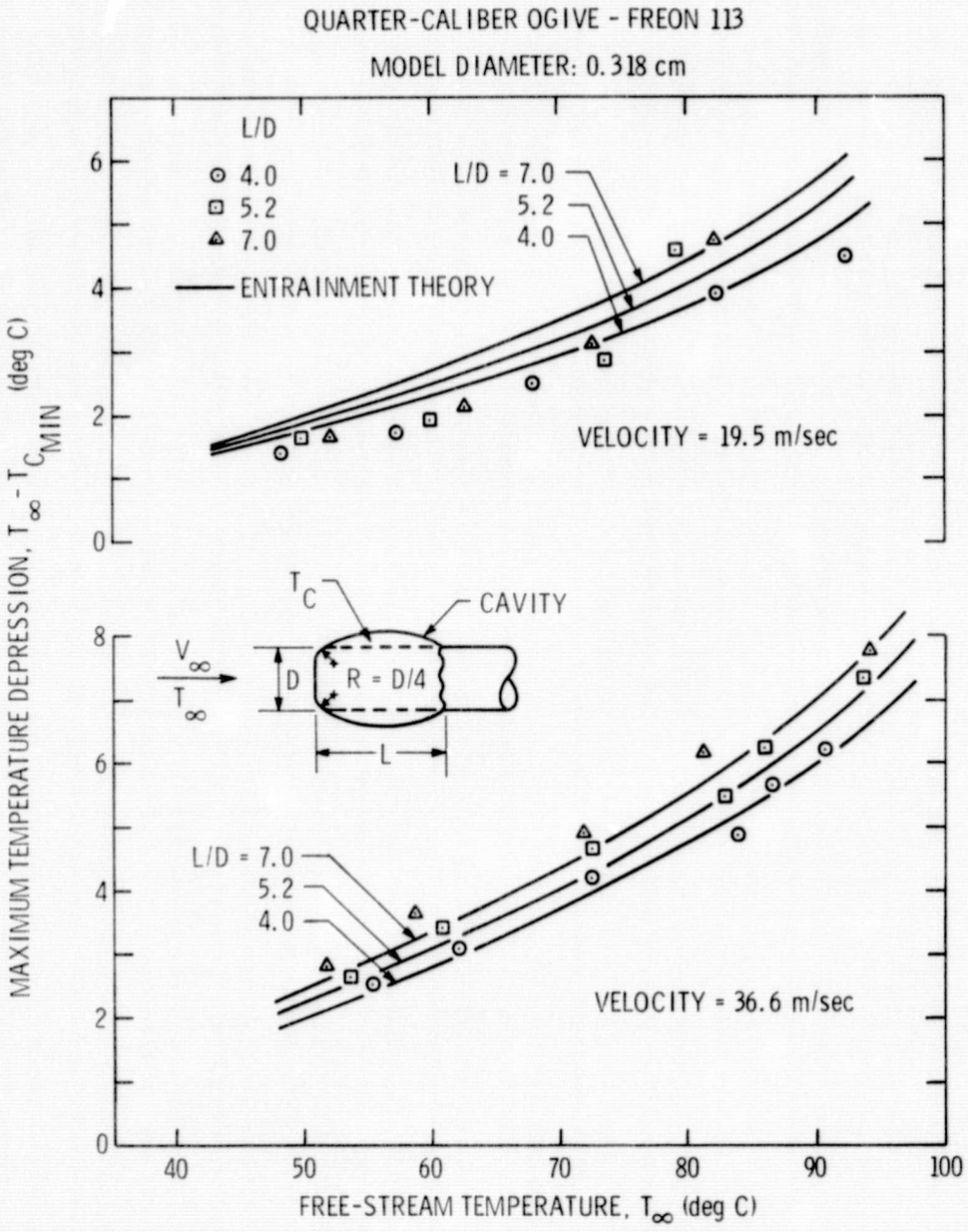

Figure 33: Maximum Temperature Depression Versus Free Stream Temperature for the 0.318 cm Diameter Quarter-Caliber Ogive in Freon 113

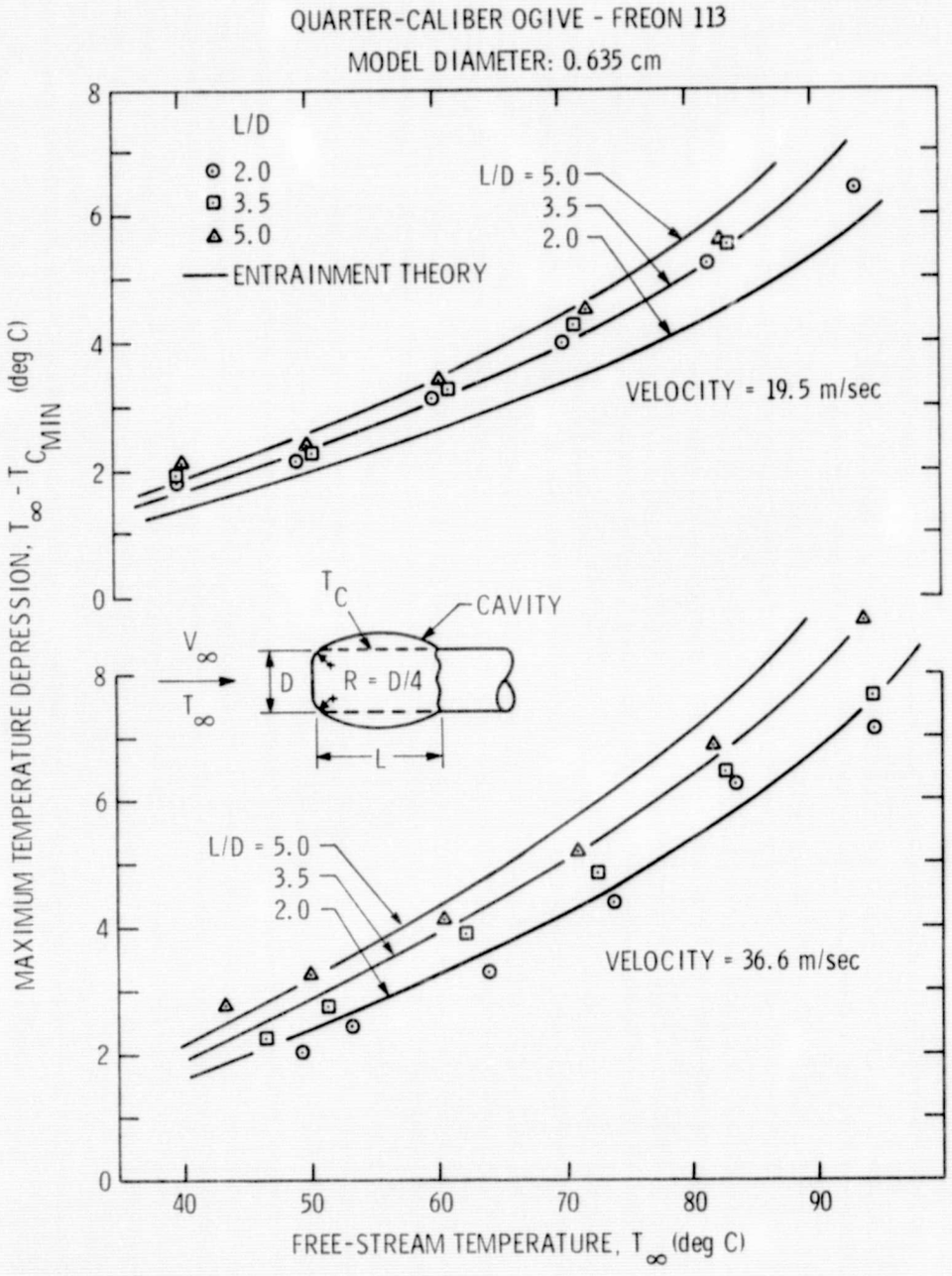

Figure 34: Maximum Temperature Depression Versus Free Stream Temperature for the 0.635 cm Diameter Quarter-Caliber Ogive in Freon 113

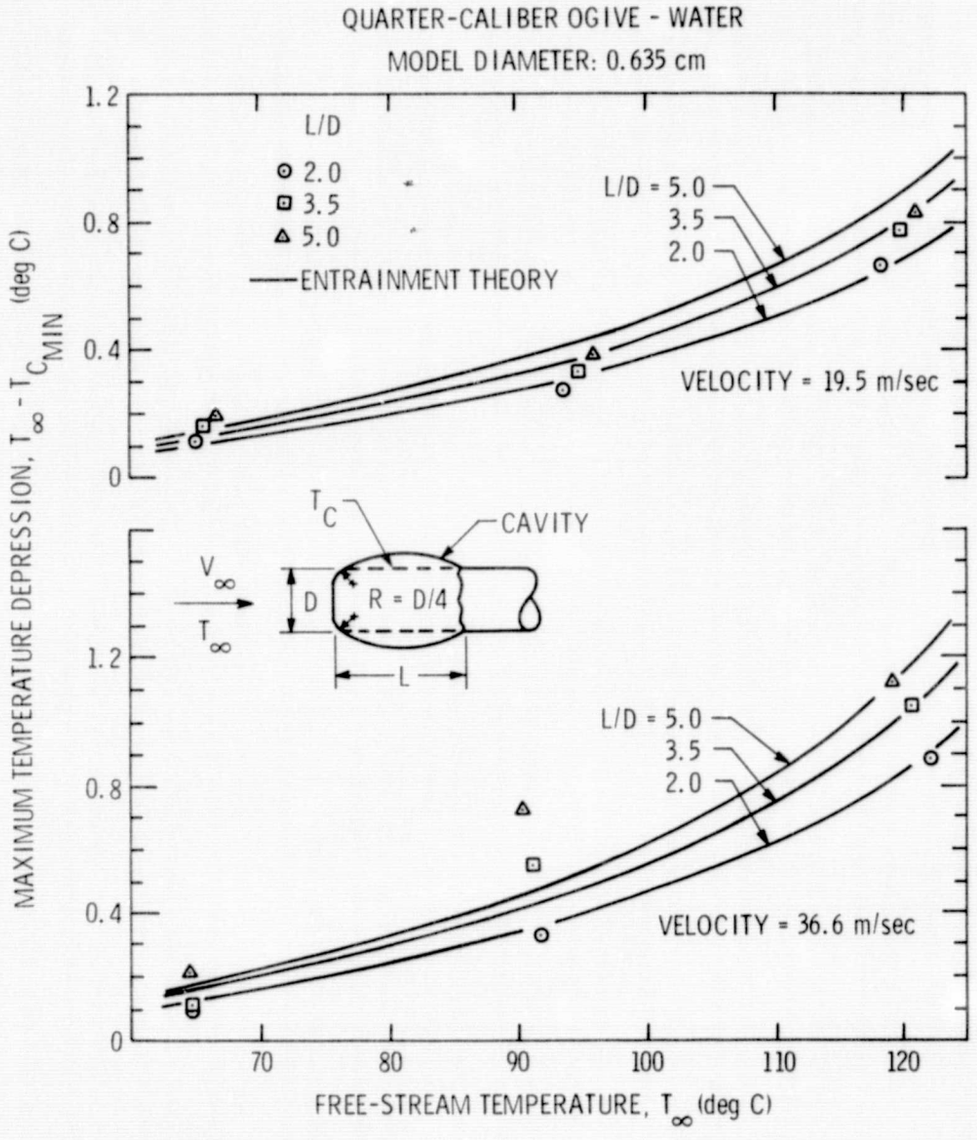

Figure 35: Maximum Temperature Depression Versus Free Stream Temperature for the 0.635 cm Diameter Quarter-Caliber Ogive in Water

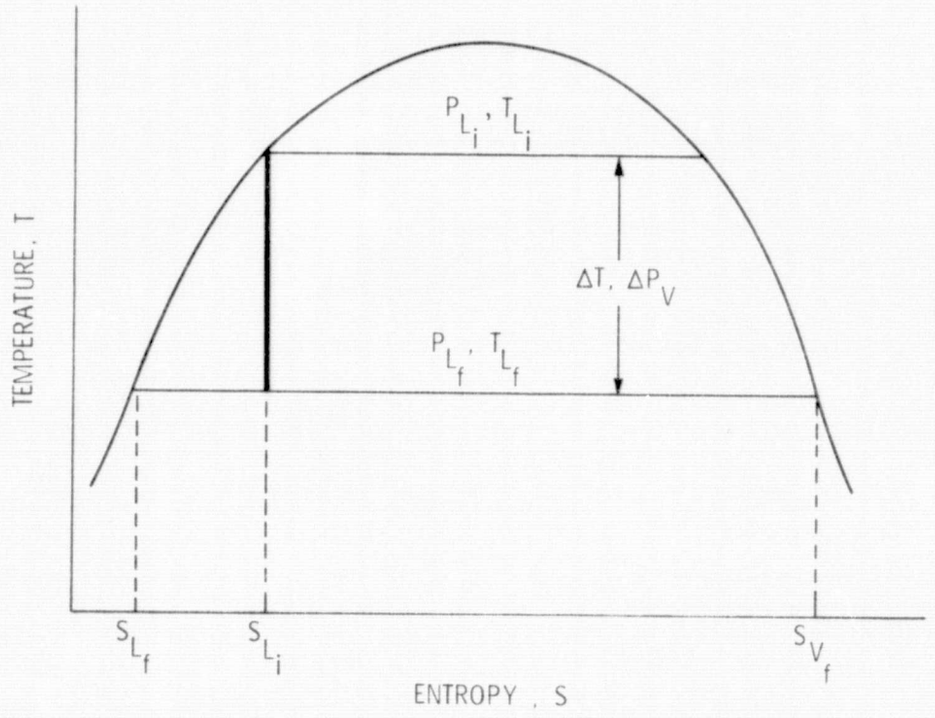

Figure 36: Temperature Versus Entropy Diagram for Calculation of B Factor

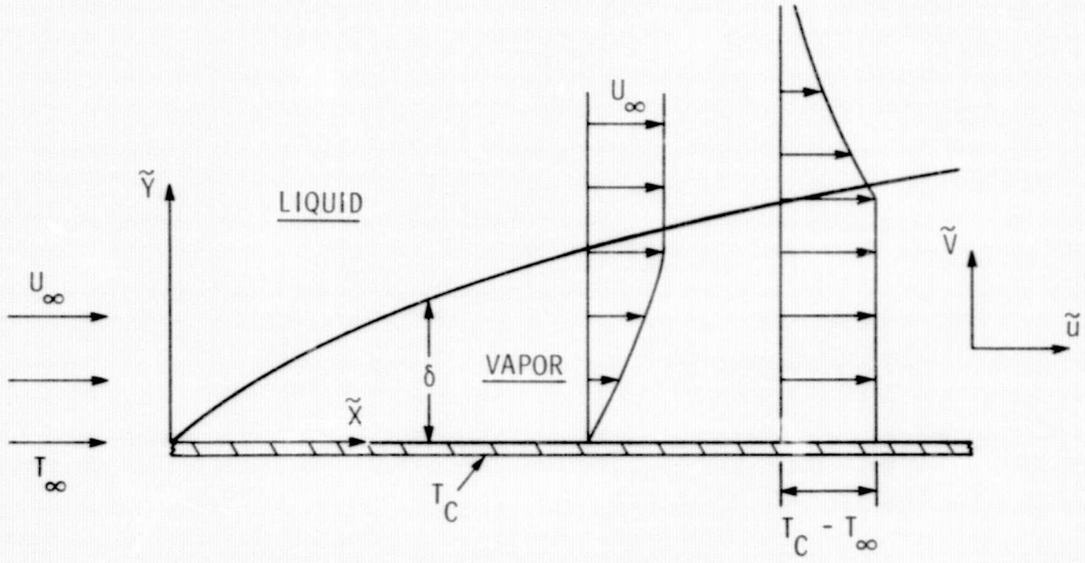

Figure 37: Two-Phase Laminar Boundary Layer Model

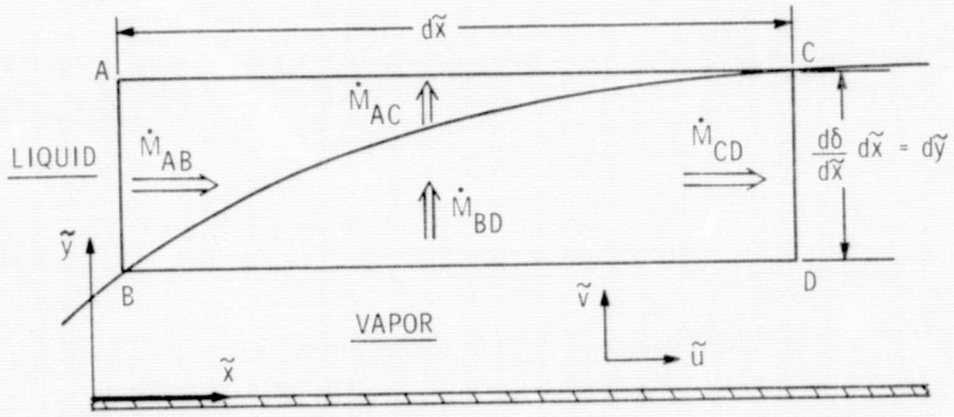

Figure 38: Control Volume for Interface Mass Conservation Development

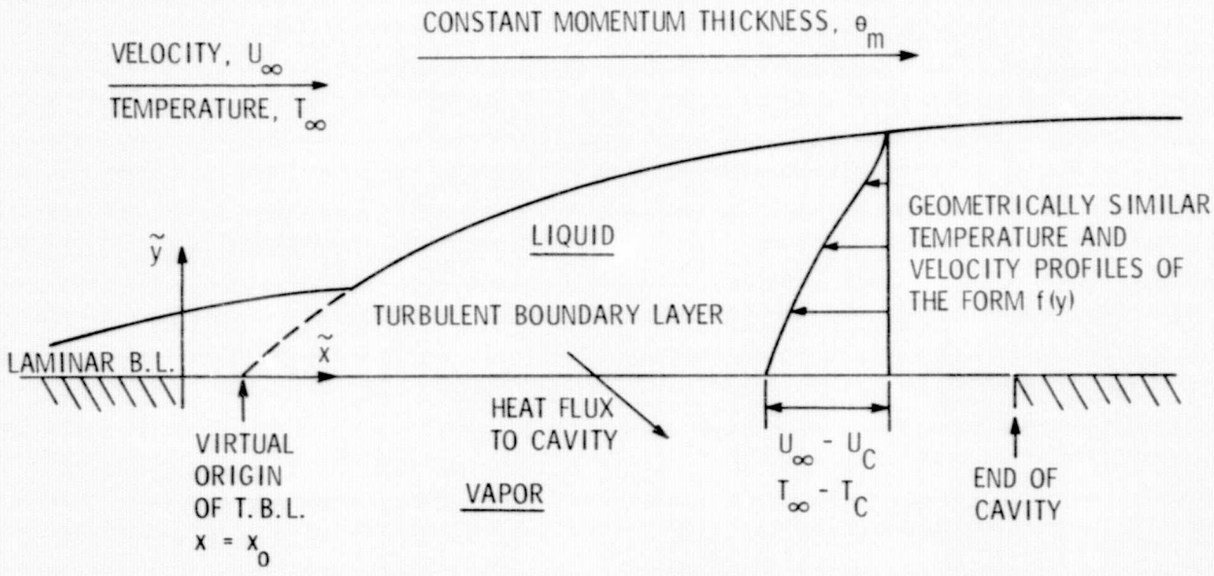

Figure 39: Turbulent Boundary Layer Heat Transfer Model

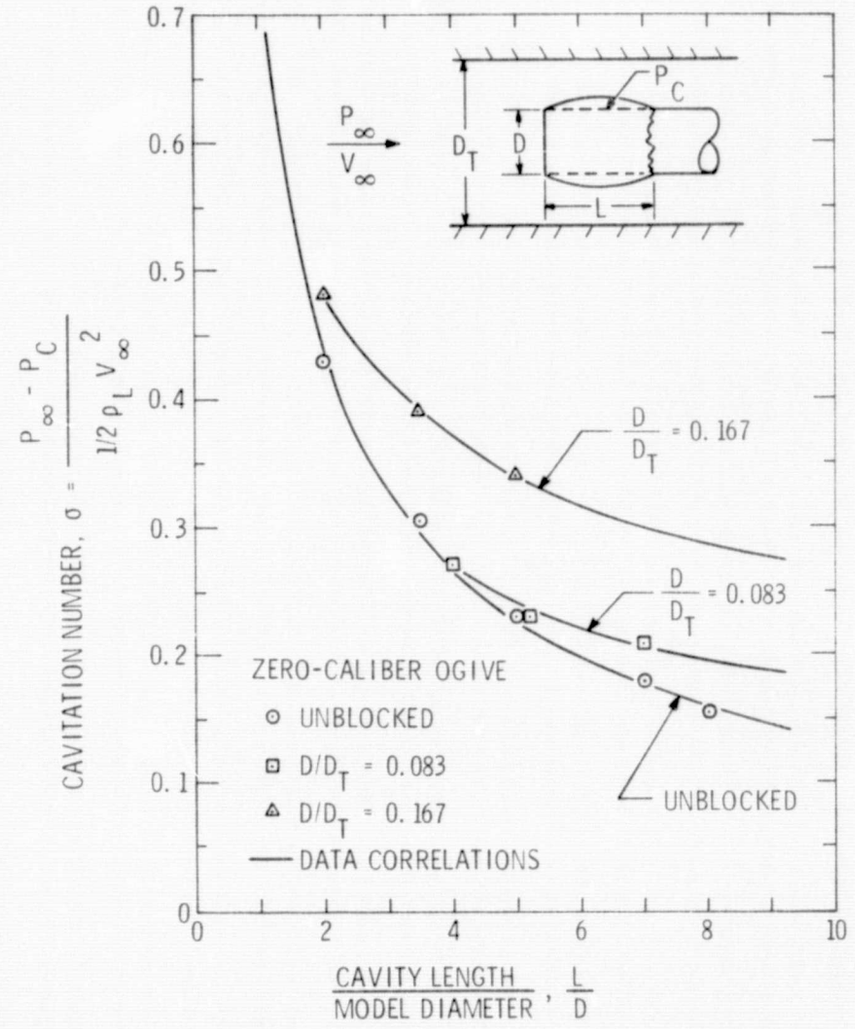

Figure 40: Cavitation Number Versus Dimensionless Cavity Length for the Zero-Caliber Ogives in Blocked and Unblocked Conditions

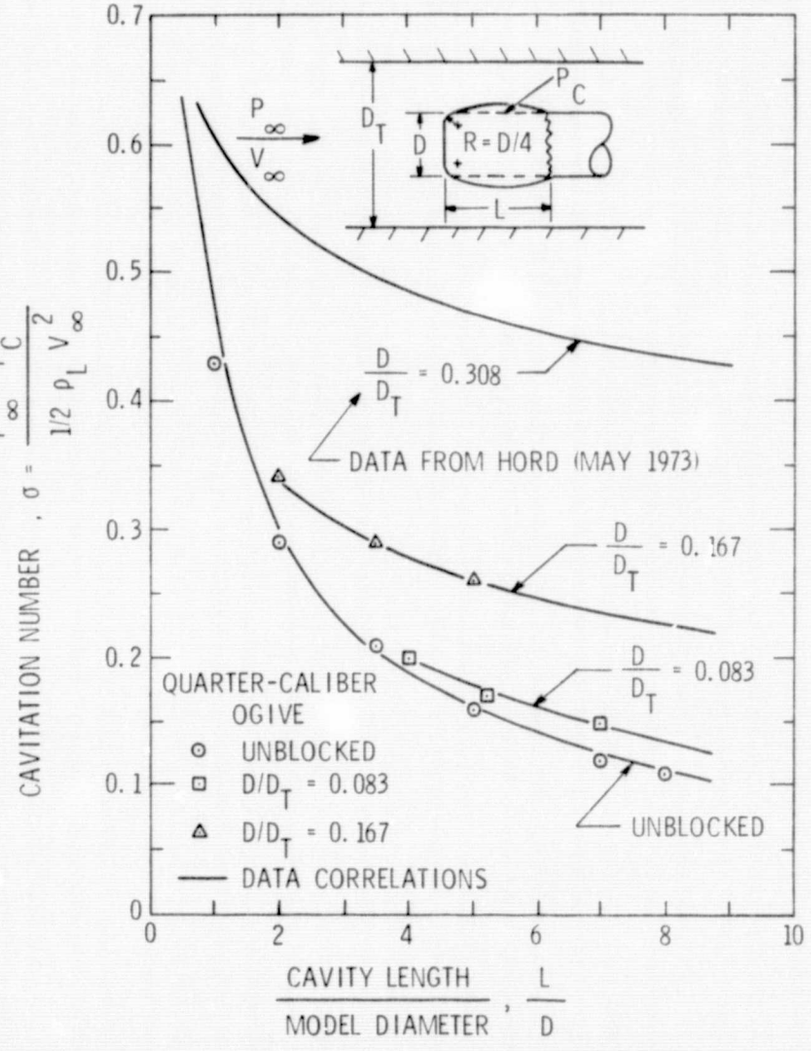

Figure 41: Cavitation Number Versus Dimensionless Cavity Length for the Quarter-Caliber Ogives in Blocked and Unblocked Conditions

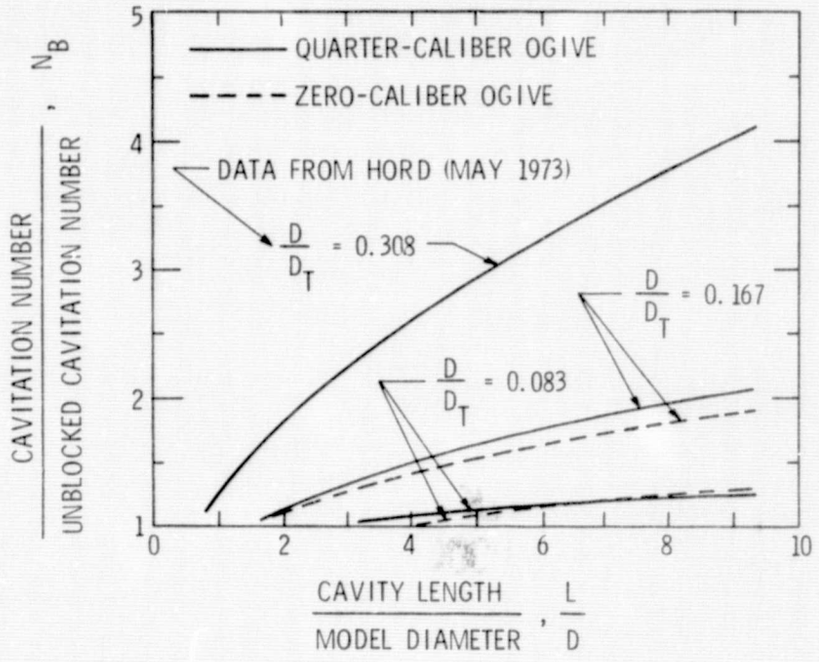

Figure 42: Blockage Correction Factor Versus Dimensionless Cavity Length for the Zero- and Quarter-Caliber Ogives